2021

Link Scheduling in Wireless Powered Internet of Things Networks

Ying Liu
University of Wollongong

Link Scheduling in Wireless Powered Internet of Things Networks

A thesis submitted in partial fulfilment of the requirements for the award of the degree

Doctor of Philosophy

from

UNIVERSITY OF WOLLONGONG

by

Ying Liu

Bachelor of Engineering (Telecommunications)

Master by Research (Telecommunications)

School of Electrical, Computer and Telecommunications Engineering

March 2021

Statement of Originality

I, Ying Liu, declare that this thesis, submitted in partial fulfilment of the requirements for the award of Doctor of Philosophy, in the School of Electrical, Computer and Telecommunications Engineering, University of Wollongong, is wholly my own work unless otherwise referenced or acknowledged. The document has not been submitted for qualifications at any other academic institutions.

Signed

Ying Liu

March 15, 2021

Abstract

Internet of Things (IoT) networks rely on devices with sensors and/or actuators to monitor critical targets/objects, and to control/manage an environment. Example devices include smart sensors and wearable devices that facilitate pandemic control, and management of smart homes and cities. In these applications, devices are required to sense their environment and forward sensed data or samples to a fusion centre for processing. Apart from that, these devices are likely to be powered by energy sources such as solar or Radio Frequency (RF) signals.

The amount of RF energy harvested by a sensor device is time varying due to random channel gains. This in turn affects their transmit power during uplink data transmissions to a Hybrid Access Point (HAP). Hence, the amount of harvested RF energy has an impact on the sum-rate at a HAP. In addition, the sum-rate is also affected by the number of devices that transmit in a given time slot. In this respect, this thesis considers a HAP that is equipped with a Successive Interference Cancellation (SIC) radio. In addition, the HAP assigns one or more uplinks data transmission slots to these devices. In this regard, an important and challenging problem is to determine an uplink transmission schedule that maximises the throughput at the HAP. Moreover, a key consideration is that the HAP has imperfect Channel State Information (CSI). To this end, this thesis aims to develop an algorithm to cope with unknown channel gain that allows the HAP to learn the best

transmission schedule.

Another approach to maximise sum-rate is to take advantage of ambient backscattering, which allows a device to carry out communication with negligible energy cost. Consequently, it is able to utilise its energy to collect more data or transmit at a higher power when it uses conventional active RF transmissions. To this end, this thesis considers a novel problem whereby sensor devices use ambient backscatter communications (AmBC) to maximise the number of samples uploaded to a HAP. Sensor devices are able to cooperate with each other. For example, a sensor device with large data but low energy can backscatter data to its neighbour device that has high energy but little data. Its neighbour device then uploads data directly to the HAP. Therefore, sensor devices have different operation modes, such as backscatter transmission, backscatter reception and active data uploading, in each time slot. This thesis aims to determine the operation mode of each device in each time slot in order to maximise the total amount of uploaded samples.

Lastly, this thesis outlines a study on data collection in a *multi-hop* RF-charging network with batteryless IoT devices, so called tags. These tags forward data via Tag-to-Tag (T2T) communications to a gateway. The aim is for the gateway to collect the maximum amount of data from tags over a given time frame. To do so, this thesis jointly optimises sensing, link scheduling and routing. In particular, it optimises the time used by tags to collect data and data transmission, which involves solving an NP-hard link scheduling problem.

Acknowledgments

First, I would like to express my deepest gratitude to my supervisor, Associate Professor Kwan-Wu Chin. He has guided me patiently throughout my research work, starting from research direction, problem selection to paper writing. His immense knowledge, serious attitude and dedicated work attitude have given me more power and spirit to excel in doing research. At the same time, his humorous, easy-going and decent personality make me feel that we are more like friends rather than as a supervisor. He has inspired me to become a university lecturer and a researcher. He is a great mentor to me and a true model of a scholar.

Second, I am also pleased to say thank you to A/Prof. Qinghua Guo and Prof. Jiangtao Xi, who were my supervisors during my Master by Research degree. The research experience in their team has built the foundation of my research career. It would not have been possible to conduct my PhD research without their precious guidance and support.

Third, during my PhD years, I have many good memories of time spent with my friends at the University of Wollongong. They are Dr Tianle Liu, Dr Yishun Wang, Dr Dawei Gao, Dr Yuanyuan Zhang, Miss Yawen Zheng and other lab mates in building B39-201. I will always remember the insightful research discussions in our office, interesting chats during coffee breaks and funny games in the weekends. I wish them all the best with their research, work and life.

Lastly, I am grateful to my parents and my husband Dr Changlin Yang for their great support and love throughout my life. They are always caring, motivate me and encourage me to accomplish my personal goals.

Contents

List of Figures

List of Tables

Abbreviations

AGV	Automatic Guided Vehicle
AmBC	Ambient Backscatter Communication
AWGN	Additive White Gaussian Noise
AP	Access Point
BER	Bit Error Rate
BIP	Binary Integer Programming
BS	Base Stations
BTTN	Backscattering Tag-to-Tag Network
CDMA	Code-Division Multiple Access
CSI	Channel State Information
D2D	Device-to-Device
DDPG	Deep Deterministic Policy Gradient
DWP	Double Weighted Protocol
EHD	Energy Harvesting Device
HAP	Hybrid Access Point
HST	Harvest-Sample-Transmi
ILP	Integer Linear Programming
IoT	Internet of Things
LCD	Low Complexity Decoding

LP	Linear Programming
M2M	Machine-to-Machine
MAC	Medium Access Control
Max-L	Maximum Link Scheduling
MILP	Mixed Integer Linear Program
MIMO	Multiple-Input Multiple-Output
MINLP	Mixed Integer Non-Linear Program
NOMA	Non-Orthogonal Multiple Access
OLCMR	Optimal Link Cost Multipath Routing
OMA	Orthogonal Multiple Access
RF	Radio Frequency
RFID	RF IDentification
SIC	Successive Interference Cancellation
SINR	Signal-to-Interference-plus-Noise Ratio
SISO	Single-Input and Single-Output
T2T	Tag-to-Tag
TDMA	Time Division Multiple Access
WPCN	Wireless Power Communication Network
WPT	Wireless Power Transfer
WSN	Wireless Sensor Network

Chapter 1

Introduction

The Internet of Things (IoT) enables anywhere anytime communications between humans and devices. It facilitates efficient information sharing and collaboration between people and things. At the same time, it reduces the cost of labor as monitoring and control of an environment can be carried out via devices with sensors and actuators. For example, in a forest alert monitoring system [1], sensor devices acquire information such as temperature, humidity, solar radiation, and barometric pressure. Another example is the piglet monitoring system in [2], which requires multiple devices, each with a different sensor, to respond whenever a piglet is being crushed by its sow. Actuators are then used to save a piglet during such a crushing event. In these examples, sensor devices continuously or periodically generate samples of their environmental conditions.

A fundamental issue is the limited energy on devices, which bounds their operational lifetime and the amount of data collected by an IoT system. This issue has led to a large of body of research into energy efficient operation or management [3, 4], energy harvesting technologies [5], and energy harvesting sensor networks [6, 7].

Another issue is optimizing uplink communications from devices to a gateway or fusion centre. That is, a gateway must be able to collect samples from devices quickly in order to optimise a given performance objective such as sum-rate [8, 9].

In this respect, a fundamental problem is scheduling one or more transmissions to the gateway.

To address the aforementioned issues, this thesis considers two recent research directions that aim to overcome the energy limitation of sensor devices. Specifically, Radio Frequency (RF) wireless power transfer [10] and backscatter communications [11]. As for the second issue, this thesis considers Non-Orthogonal Multiple Access (NOMA) with Successive Interference Cancellation [12]. These approaches are detailed in the following sections.

1.1 Wireless powered communications networks

Wireless Power Transfer (WPT) or wireless charging refers to the transmission of electrical energy from a power source to an electrical load without the use of wires or cables [13]. In general, WPT consists of two categories: near and far field. For near field or non-radiative technologies, power is transferred by magnetic fields using inductive coupling between coils of wires or via magnetic fields using resonance coupling [14]. In far field or radiative technologies, power is transferred via electromagnetic radiation or RF signals. Advantageously, RF signals are capable of powering a large number of devices distributed over a wide area. Also, far-field WPT does not require alignment between a transmitter and a receiver, which makes it possible to power mobile devices. Moreover, it has a wider and longer energy transfer range. However, it has low energy conversion efficiency especially when the harvested RF energy is small [15].

WPT also has the following advantages [14–17]:

- **Eco-friendly**: WPT allows devices to operate without a battery. Consequently, consumers will not dispose billions of battery chargers every year. As these discarded chargers sit in landfills, they leak heavy metals such as mercury and lead; both of which are harmful to the environment.

- **Safety**: WPT eliminates charging ports and improves charging safety. In particular, cables may age and cause severe hazards due to the generated electric spark during power transmission. On the other hand, WPT allows electric devices to be sealed completely. This improves production durability as these devices are water-proof and dust-proof; an example is the charger for electric toothbrushes and electric razors.

- **Flexibility**: wireless charging provides a more flexible way to charge devices located in difficult to reach locations. For example, active implantable medical devices such as left ventricular assist devices, cardiac pacemakers, and implantable cardioverter defibrillators [18]. Apart from that, WPT allows easy charging of heavy electric vehicles such as magnetic-levitating trains [19, 20], industrial Automatic Guided Vehicle (AGV) [21] or electric buses [22].

- **User-friendly**: WPT improves user experience. It simplifies anywhere anytime charging and removes hassle associated with cables. In addition, consumers can use a standardised wireless charging pad, e.g., one that supports the Qi wireless standard [23], for all their devices.

- **Innovation**: WPT technologies motivate advances in next-generation smart home and smart city applications. For example, future networks, e.g., 5G, will require a dense deployment of Access Points (APs) or Base Stations (BSs) to ensure high capacity. A key problem is powering these APs or BSs. Hence, solar-powered APs/BSs are of interest to operators [7, 24].

To date, the applications of WPT range from low-power consumer electronics to high-power electrical vehicles. Table 1.1 shows some commercial examples. A major incentive of WPT technology is to develop wireless charging systems for smart phones and portable computers. It is worth noting that in February 2017, Apple Inc., joined the Wireless Power Consortium, and hence, Apple iPhone 8 or later, as well as AirPods models can be wirelessly charged by any Qi-certified charger.

Table 1.1: WPT applications and some existing or future products

Applications		**Existing or Future Products**
Charger for consumer electronics	Mobile electronics	Apple iWatch, wireless keyboard and mouse, Qi charging pad; WiTricity WT8800 wireless transmitters [25]; Powermat charging ring [26]; IKEA furniture with an embedded Qi wireless charging pad and in-car charging.
	Household appliances	Inductive toothbrush [27, 28], wireless charging razors, Philips wireless charging headphone, inductive charging vacuum cleaners, Haier wireless TV and kitchen appliances.
Medical devices	Active implantable medical devices or portable medical instruments	Ventricular assist devices; pacemakers; defibrillators; left ventricular assist device; implantable therapies; Neurostimulator devices; handheld medical instruments and power tools, medical carts carrying computers and other diagnostic instruments.
Industrial	Demanding and mission critical industrial environments	Industrial Automatic Guided Vehicle (AGV) [21], slip rings and portable operator terminals and underwater vehicles.
Automotive	Electrical vehicles	Wireless charging pad or charging station for electrical cars such as Rolls-Royce, Audi, Nissan, Toyota, Mitsubishi, magnetic-levitating trains [19, 20], high power electric buses [22]; on-road charging of electrical vehicles [29].
Sensor nodes	Wireless Sensor Network (WSN)	Environmental monitoring such as temperature, moisture, and light [30], replenishing sensors embedded in concrete and powering ground sensors using UAVs [3, 31]; RFID and barcode readers [32].

Apple Inc., has also been granted a patent that uses Wi-Fi signal, i.e., 2.4 GHz and 5 GHz, to charge devices [33]. Another major development is the wireless charging of electric vehicles, such as cars, buses and trains, which have long been a promising option for sustainable transportation. To date, people have witnessed the development and commercialization of a charging pad such as WiTricity Drive 11 or charging stations such as Plugless charging stations for electrical vehicles. In addition, researchers are planning to place charging points/areas on roadways to achieve dynamic charging [34–36]. An example is South Korea's on-line electric vehicle project, whereby several buses operating around the country can be charged wirelessly [37]. Apart from that, the European Union funded the Unplugged project [38]. Its aim is to study how a smart inductive charging infrastructure can facilitate full electric vehicle integration in urban road systems while improving customer acceptance and perceived practicality.

1.1.1 Network Architectures

An RF signal is capable of carrying both information and power [10]. This fact has led to a practical architecture called Wireless Powered Communications Networks (WPCNs) [39]. A WPCN operates using the called the *harvest-then-transmit* protocol [39]. That is, IoT devices first receive a charge. They then use their harvested energy to drive their load; e.g., data transmissions. Figure 1.1 demonstrates two basic network architectures of WPCNs. As shown in Figure 1.1a, energy node and information receiver are located separately. The energy node transmits RF energy to charge devices A and B for some time period in the downlink. Then these devices use their harvested energy to transmit data to the information receiver in the uplink. Figure 1.1b shows a different architecture where the energy node and information receiver are co-located and integrated as a Hybrid Access Point (HAP). Compared to a separated WPCN system, the HAP functions as a centralised controller to coordinate energy and information transmissions in a co-located WPCN. In the downlink,

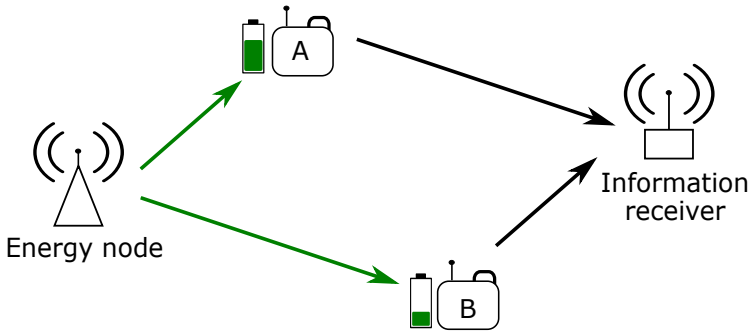

(a) A separated system

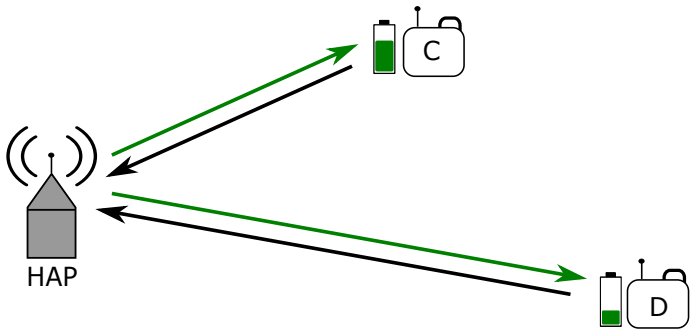

(b) A co-located system

Figure 1.1: Basic RF-charging network architectures: (a) separated energy transmitter (Tx) and information receiver (Rx), and (b) co-located energy Tx and information Rx. The green and black arrows represent downlink energy transfer and uplink information transmission, respectively.

the HAP broadcasts RF energy to charge energy harvesting devices. It then assigns an uplink data transmission slot to each device for data collection.

1.2 Backscatter Communications

A promising technology to address communications and energy efficiency problems in low-power IoT systems such as wireless powered sensor networks is backscattering [40]. Generally, in backscatter communications, a transmitter can transmit data to a receiver by reflecting incident RF signals rather than using its radio to generate RF transmissions [40]. For example, in two-state modulation, a transmitter can adjust its antenna impedance to an absorbing state and a reflecting state [40]. In the absorbing state, the transmitter absorbs incident RF signals to represent bit zero. Then in the reflecting state, it reflects incident RF signals to represent bit one. At

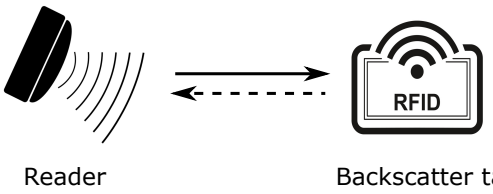

(a) Monostatic backscatter

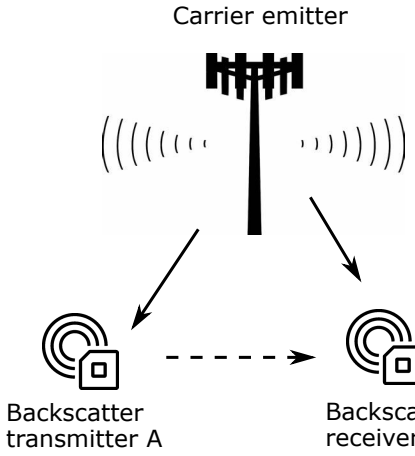

(b) Bistatic backscatter

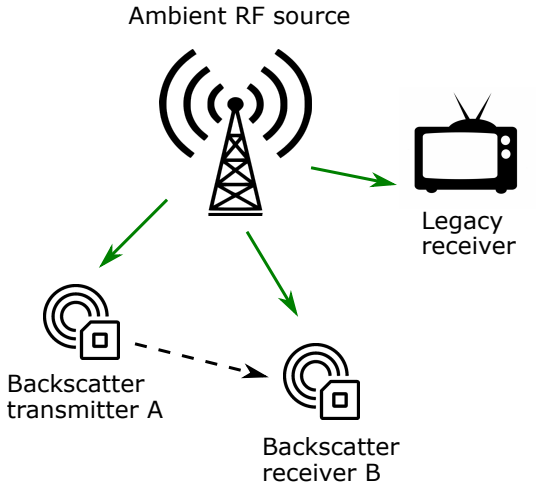

(c) Ambient backscatter

Figure 1.2: Three types of backscatter communications systems: (a) monostatic backscatter, (b) bistatic backscatter and (c) ambient backscatter. The black and green arrows represent continuous carrier signals and ambient RF signals, respectively. The dashed arrows represent backscattered signals.

the receiver, a backscatter demodulator then extracts the transmitted bit from the mixed modulated signal by leveraging the difference in data rates; see [11] and [41] for further information.

Backscatter communication systems can be classified into three categories based on the types of RF source and network architectures, namely, monostatic backscatter communications systems, bistatic backscatter communications systems and ambient backscatter communications systems as shown in Figure 1.2. A particular form of monostatic backscatter is RFID. As shown in Figure 1.2a, the system consists of an RFID tag and a reader. The reader emits an RF signal, which is then reflected or encoded by the RFID tag. Advantageously, tags do not have to store any energy and can be equipped with sensing capabilities [42]. However, note that RF source and backscatter receiver are co-located in an RFID reader. Hence, self interference

occurs between transmit and receive antennas in RFID readers, which degrades communications performance.

Another backscatter communications system is bistatic backscatter communications systems, see Figure 1.2b. A bistatic backscatter communications system usually has one carrier emitter which broadcasts unmodulated RF signals to multiple backscatter devices. By reflecting the incident RF signal, a backscatter transmitter is able to transmit a backscattered signal to a backscatter receiver. A major difference between bistatic and monostatic backscatter is that the RF source and backscatter receiver are separated. Therefore, bistatic backscatter communication avoids the doubly near-far problem of monostatic backscatter communications. This is because a backscatter transmitter can utilise RF signals from a nearby carrier emitter to backscatter data. Both monostatic and bistatic backscatter technologies require an un-modulated carrier signal. However, the deployment of dedicated carrier emitters increases network cost and power consumption.

Given the previous limitations, Ambient Backscattering Communication (AmBC) [11] is now of interest. It exploits existing RF signals such as television, Wi-Fi and cellular signals as a carrier signal. Advantageously, AmBC has low transmission cost that is in the orders of 1μW [41], which makes AmBC an attractive technology for use in sensing systems. A basic AmBC system is shown in Figure 1.2c, which relies on television signals. A nearby backscatter transmitter exploits these television signals to transmit its data to a backscatter receiver. Compared to monostatic and bistatic backscatter communications, AmBC does not require dedicated frequency spectrum or RF source, which has a lower cost and less energy consumption. Moreover, ambient RF source is usually more powerful, which has a larger coverage and allows multi-hop backscatter communications among backscatter nodes.

To date, there is some research on integrating backscatter communications with WPCNs systems [43]. For example, there is usually one ambient RF source, one or multiple IoT devices and one gateway in a backscatter assisted WPCNs. The devices can be either passive tags that only transmit data via backscattering or

hybrid devices that transmit data in both active and backscatter modes. They harvest energy from the RF source to power their circuit and data transmissions. In addition, the RF source also generates an excitation signal to enable backscattering from devices to the gateway. Furthermore, as demonstrated in [44], backscatter tags support Tag-to-Tag (T2T) communications. This is particularly useful as the backscatter communication range is limited, and thus requires tags to communicate via multi-hop communications in order to forward their data to a gateway.

1.3 Non-Orthogonal Multiple Access with Successive Interference Cancellation

NOMA is a multi-user access technology that is used in fifth generation (5G) wireless communications. Its aim is to improve the performance of existing Orthogonal Multiple Access (OMA) systems. Briefly, when using OMA, users transmit to a sink simultaneously using different time slots, frequencies or codes. However, the work in [45] shows that OMA is not able to theoretically guarantee the maximum sum-rate, and that the maximum number of users is bounded by the said resources. To this end, NOMA is proposed in [46] to address these limitations whereby in the same time slot, a transmitter is able to transmit different signals to multiple distinct receivers. Conversely, a receiver is able to receive from different transmitters. As shown in [47], NOMA has a number of advantages over OMA. Firstly, it is able to achieve the optimal channel capacity in both uplink and downlink additive white Gaussian noise (AWGN) channels. Moreover, it can theoretically support more users by using non-orthogonal resource allocation.

There are two types of NOMA [12]: code domain multiplexing and power domain multiplexing. Code domain multiplexing is similar with Code-Division Multiple Access (CDMA), where users are assigned a distinct code. On the other hand, in power domain multiplexing, users employ different power levels according to their

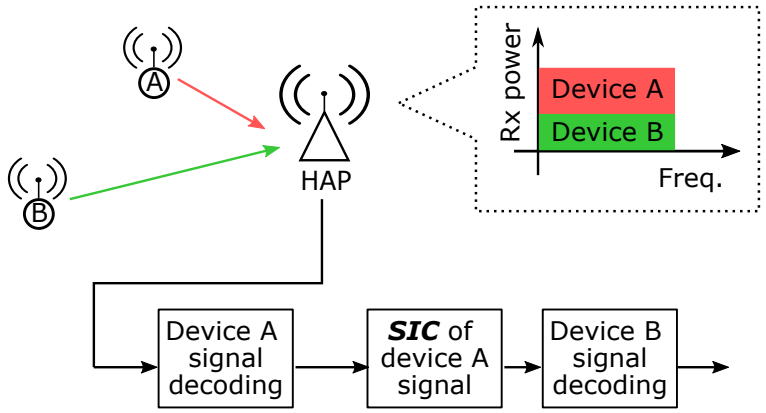

Figure 1.3: Uplink NOMA with SIC. The red and green arrows represent uplink data transmission from device A and B, respectively. The red and green blocks in the inset represent the received signal from device A and B, respectively.

channel conditions. Then, SIC is used to separate the transmission from each user.

SIC allows a receiver to decode multiple signals or transmissions if these signals meet a given set of Signal-to-Interference-plus-Noise Ratio (SINR) conditions. In particular, given a composite signal, the HAP decodes the signal from one device by treating signals from other devices as interference. If the SINR of the decoding signal meets a given threshold, then decoding is a success. The decoded signal is then subtracted from the composite signal. The process is then repeated for the resulting composite signal until all signals are decoded or any decoding signal does not meet the SINR threshold. Figure 1.3 shows a basic form of NOMA with SIC. The HAP first decodes signal from device A, which has stronger received power. It then subtracts the decoded signal and proceeds to decode the signal from device B.

To further explain the SIC process, consider a simple example with two simultaneous transmissions l_1 and l_2. Assume the received power of l_1 and l_2 at the HAP is $\gamma_1 = 0.2$ W and $\gamma_2 = 0.4$ W, and the ambient noise power is $\sigma_0^2 = 0.1$ W. If the required SINR threshold β is 1 dB, then both transmissions can be successfully decoded since the SINR Γ_1 and Γ_2 are larger than β, i.e., $\Gamma_2 = \frac{0.4}{0.1+0.2} = 1.33 \quad (1.25\text{ dB})$ and $\Gamma_1 = \frac{0.2}{0.1} = 2 \quad (3\text{ dB})$. However, if the required SINR threshold β is 1.5 dB, then both transmissions are unsuccessful. This is because the SINR Γ_2 of the stronger transmission l_2 is smaller than β, thus it cannot be decoded and subtracted suc-

cessfully, which leads to decoding failure of the weaker transmission l_1. Note that if a transmission fails to meet its SINR constraint, then the signal and subsequent transmissions are considered unsuccessful.

1.4 Research Statement

This thesis has three research aims: (i) deriving the optimal uplink transmission scheduling for a NOMA-based WPCN with imperfect CSI, (ii) maximizing the number of samples collected in an AmBC assisted WPCN, and (iii) optimising the links scheduled for data collection in multi-hop backscatter IoT wireless networks.

1.4.1 Uplink transmission scheduling in NOMA based WPCN with imperfect CSI

The first aim considers a multiple access WPCN where all devices are equipped with a rechargeable battery of finite capacity. At each time slot, the HAP first replenishes all devices via downlink RF energy transfer with a fixed power. Then devices transmit data packets to the HAP in the uplink using their harvested energy. In order to ensure collision free uplink transmissions and to improve channel capacity, the HAP is equipped with SIC capability. The main problem is to determine the set of transmitting devices in each time slot. Equivalently, this thesis aims to design a link scheduler that maximises the number of links that meet SIC constraints in each time slot. The key challenges include: (1) random channel gains, which cause the received power at the HAP and devices to vary. This affects decoding as well as the amount of received energy at each time slot. It is worth noting that this thesis considers imperfect CSI, and thus both the HAP and devices do not have exact channel gain information, and (2) devices have a finite battery size, meaning any energy that exceeds this size will be lost.

1.4.2 Data collection in AmBC assisted WPCNs

The second aim is to optimise the number of samples uploaded to a HAP in AmBC-assisted cooperative WPCNs. Hybrid devices have the ability to transmit data via their conventional radio or use AmBC from external RF sources such as those from a television and cellular tower. A HAP first supplies energy to charge these devices. Using their harvested RF energy, devices then collect one or more samples and transmit these samples to the HAP. A unique feature of the said WPCN is that devices have the option of transmitting their sample(s) directly to the HAP using their conventional radio, which incurs non-negligible energy cost, or take advantage of AmBC to relay data to another device. Therefore, hybrid devices have the following operation modes in each time slot: (a) sampling, (b) data upload to the HAP via their conventional radio, (c) transmit samples via AmBC to a neighbour, or (d) receive data via AmBC from a neighbour. Note that feature (c) and (d) mean any device can become a relay if doing so helps increase the number of samples that arrive at the HAP in future time slots.

The main research aim is to maximise the number of samples uploaded by AmBC-capable devices over multiple slots. In particular, this thesis addresses a link scheduling problem to optimise the operation mode of each hybrid device in each time slot. There are several challenges: (1) the amount of sampling data at each device is determined by its sampling frequency as well as the number of samples received from its neighbours via AmBC in previous time slots, (2) unlike prior works that assume fixed relays, this problem involves selecting hybrid devices to function as relays, and (3) it is important to consider interference among AmBC links when forwarding data.

1.4.3 Data collection in multi-hop backscatter IoT wireless networks

The last aim is to investigate link scheduling for data collection in multi-hop backscatter IoT networks. The system supports T2T communications, which helps to overcome the limited backscatter communications range, and thus requires tags to communicate via multi-hop communications in order to forward their data to a gateway. A HAP transmits a carrier signal that is then leveraged by tags to power their sensing circuit and T2T communications with a gateway. Specifically, tags first use the HAP's RF signals to operate their sensors. After that, they backscatter the HAP's RF signal to forward sampled data directly to the gateway or another tag. Note that passive tags do not have a battery/capacitor, meaning they can only carry out tasks when the HAP emits a signal.

Given the said network, this thesis aims to optimise its sensing and data transmission period in order to maximise the total samples collected by the gateway subject to *all* samples arriving at the gateway within a given time frame. The major challenge is to jointly determine the number of samples to collect and the links to activate in each time slot, where interfering links must be scheduled to transmit at different time slots. In this respect, a key consideration is that the transmit power of each tag is different, resulting in asymmetric communication links. Therefore, it is very important to consider the neighbours of each tag when scheduling links.

1.5 Contributions

1.5.1 Uplinks Schedulers for RF-Energy Harvesting Networks with Imperfect CSI

First, this thesis addresses a novel uplinks transmission scheduling problem in a wireless powered IoT network. This problem is significant as future IoT systems will require the HAP to collect data from energy harvesting devices quickly. Criti-

cally, this thesis considers a challenging but practical aspect: imperfect CSI. In this respect, this thesis presents two novel solutions. First, given a collection of transmission schedules, it outlines a discrete optimization solution that allows a HAP to pick the best transmission schedule. This thesis also outlines a heuristic approach that does not require the HAP to have the aforementioned collection of transmission schedules. Instead, the HAP constructs a schedule iteratively by greedily shifting transmissions of energy harvesting devices from a slot to another slot in the hope of shortening the schedule length.

The results show that the schedules derived from discrete optimization and the heuristic approach always have a higher throughput than Time Division Multiple Access (TDMA) with one device per slot and Frame Slotted Aloha. Moreover, this thesis reveals that the proposed heuristic approach is able to derive a schedule for networks with a large number of devices.

1.5.2 Link Scheduling in Backscatter-Assisted Wireless Powered Sensor Networks

This thesis then studies a novel problem that aims to maximise the number of uploaded samples by devices in wireless powered IoTs networks. To do so, it takes advantage of AmBC to help sensor devices conserve energy, and thus leaving them with more energy to collect samples. This thesis outlines a novel Mixed Integer Linear Program (MILP) for determining the operation mode of each device in each time slot. Its objective is to maximise the amount of samples collected over a given time horizon. It also presents a heuristic approach that allows the HAP to efficiently schedule the operation mode of each device in large scale IoT networks. It uses two weights that correspond to a device's preference as to whether it should transmit via its conventional radio or AmBC.

Lastly, this thesis contains a mathematical analysis that compares the total uploaded data in cases with and without AmBC. The analysis shows that equipping

devices with AmBC does lead to more samples at the HAP. It shows rigorously that even when all devices have sufficient energy, there exists a real value n, which is the number of devices gathering backscattered data from neighbours, whereby a AmBC-assisted system uploads more samples than one without AmBC. In addition, this thesis shows that n is lower and upper bounded by the number of channels, number of time slots, sampling rate, uploading and backscattering data rates.

1.5.3 Link Scheduling in Multi-Hop Backscatter IoT Wireless Networks

Lastly, this thesis studies data collection in a multi-hop IoT wireless network with passive or batteryless tags equipped with sensor(s). These tags forward data via tag-to-tag communications to a gateway. The aim is for the gateway to collect the maximum amount of data from tags over a given time frame. To do so, this thesis addresses a novel problem that requires a solution to jointly optimise the sensing time, the links to activate in each time slot as well as the duration of each time slot. The main challenges are ensuring all sensed data arrives at the gateway and scheduling T2T links with asymmetric transmission ranges.

This thesis outlines a Mixed Integer Non-Linear Program (MINLP) to determine the time trade-off between sensing and transmission; this is the first mathematical formulation for the said problem. The proposed MINLP also determines the transmitter-receiver pair(s) in a transmission set as well as the transmission duration. This thesis also proposes a novel heuristic approach that maximises the number of links in each transmission set. Its main goal is to reduce samples transmission time, and thus allowing tags to have more sensing time.

1.6 Publications

The outcomes of this thesis are as follows:

- **Y. Liu**, K-W Chin and C.L Yang, "Link Scheduling in Wireless Powered Communication Networks", *IEEE International Conference on Computing, Networking and Communication (ICNC)*, pp. 482-486, Hawaii, USA, February, 2020, doi: 10.1109/ICNC47757.2020.9049691. Submitted on

- **Y. Liu**, K-W Chin, and C. L Yang, "Uplinks Schedulers for RF-Energy Harvesting Networks with Imperfect CSI", *IEEE Transactions on Vehicular Technology*, vol. 69 no. 4, pp. 4233-4245, April, 2020, doi: 10.1109/TVT.2020.2970004. Submitted on October 6, 2019.

- **Y. Liu**, K-W Chin and C.L. Yang, "Maximizing Sampling Data Upload in Ambient Backscatter Assisted Wireless Powered Networks", *IEEE Internet of Things Journal*, 2021, doi: 10.1109/JIOT.2021.3061087. Submitted on March 26, 2020. (*Early Access*)

- **Y. Liu**, K-W Chin and C.L Yang, "Link Scheduling for Data Collection in Multi-Hop Backscatter IoT Wireless Networks", *IEEE Internet of Things Journal*, 2021. (*To Appear*)

1.7 Thesis Structure

- *Chapter 2.* This chapter provides a comprehensive survey of transmission scheduling works that consider NOMA, imperfect CSI and backscatter. Moreover, it discusses works that focus on user cooperation and multi-hop tag-to-tag communications. Lastly, this chapter highlights the novelties of this thesis.

- *Chapter 3.* This chapter proposes a NOMA link scheduler for a WPCN, which allows a HAP to learn the best transmission schedule without CSI knowledge.

- *Chapter 4.* This chapter investigates transmission scheduling for data collection in a cooperative AmBC assisted WPCN.

- *Chapter 5.* This chapter proposes a novel IoT system whereby passive tags equipped with sensors are tasked with data collection and forwarding. It investigates link scheduling and routing in a multi-hop backscatter T2T network.

- *Chapter 6.* This chapter summarises the main aims of the thesis and findings, and also outlines some future works.

Chapter 2

Literature Review

This chapter first discusses past works on channel access and transmit power allocation in WPCNs. It then discusses existing WPCNs works that consider NOMA, imperfect CSI, and backscatter. Special focus will be on backscatter-assisted WPCNs since they allow devices to transmit with zero energy cost. Lastly, Section 2.5 highlights the novelties of this thesis.

2.1 Wireless Powered Communications Networks (WPCNs)

Many works have considered point-to-point communications [48–56]. These works aim to maximise the throughput of a point-to-point channel given a deadline or to minimise the transmission completion time of a node, assuming random energy and data arrivals. The battery of an energy harvesting node can be either finite or infinite. The main problem is transmission scheduling, where a transmitter needs to determine when to transmit its data and also its transmit power. These paper addresses either offline [48–53] or online [54–56] transmission scheduling, depending on the energy harvesting process and channel state information that are available to a transmitter. Offline problems assume *non-causal* information, where nodes have

past, present and future channel conditions and their amount of harvested energy. On the other hand, online problems only assume *causal* information; specifically, only information from past and present is available.

The main limitation of the aforementioned works is that they do not consider collisions or interference between nodes. However, in WPCNs with multiple energy harvesting nodes, collisions may occur and thus nodes waste their precious harvested energy. Therefore, a channel access or MAC protocol is necessary to coordinate uplink information transmissions from different energy harvesting nodes. Some works have evaluated the use of standard MAC protocols in WPCNs considering dynamic energy and data arrival [57–59]. Specifically, Iannello et al. consider a wireless powered sensor network with multiple energy harvesting nodes transmitting data to a fusion centre [57] and [58]. They measure the system performance when using TDMA, framed Aloha, Dynamic framed Aloha in terms of the trade-off between delivery probability and time efficiency. In a different work [59], the authors propose an energy harvesting-aware reservation dynamic frame slotted Aloha protocol for a wireless powered Machine-to-Machine (M2M) network.

There are works that consider multi-user WPCNs with one HAP and multiple energy harvesting devices. This so called *harvest-then-transmit* protocol [39] requires the HAP to first charge energy harvesting devices for some time period for downlink energy transfer. Energy harvesting devices then use the harvested energy to carry out one or more tasks and transmit information to the HAP for uplink information transmission. For example, the work in [39, 60] considers single-antenna HAP assisted single-input and single-output (SISO) WPCNs. The authors aim to maximise the system throughput or weighted sum-rate by optimizing the time allocation of downlink energy transfer and uplink information transmission. Some other works investigate multi-antenna HAP assisted Multiple-Input and Multiple-Output (MIMO) WPCNs with beamforming, see [61–63]. In these works, the authors jointly optimise transmit power allocation at the HAP and time allocations between downlink and uplink phase to maximise the system sum-rate. Past works have also investigated

the resource allocation of various cooperative WPCNs such as wireless powered relay networks [64–68], cognitive radio networks [69–71] and secure communications networks [72].

Table 2.1 summarises related works in multi-user WPCNs in terms of their system, aim and problem. In general, past works aim to maximise the sum-rate at a HAP. In particular, for each energy harvesting device that utilises the harvest-then-transmit protocol, the time used for energy harvesting and data transmission has a significant impact on its transmission rate. To this end, many works aim to optimise the trade-off between energy harvesting time and data transmission time. Moreover, there are works that jointly optimise the transmit power and time for both downlink energy transfer and uplink information transmission. However, all these works consider TDMA, where HAP assigns an uplink data transmission slot to each energy harvesting device for data collection.

Table 2.1: Summary of transmission scheduling in multi-user WPCNs.

Paper	**System**	**Aim**	**Problem**
[39]	Multi-access SISO communication and infinite battery capacity and TDMA	Maximise sum throughput and maximise common throughput of devices	Schedule downlink energy transfer time and uplink data transmission time.
[60]	Multi-access SISO communications with stochastic geometry and both infinite and finite battery capacity	Maximise spatial throughput, i.e., the total throughput per unit network area	Jointly optimise downlink and uplink phases and the transmit power of energy harvesting devices.

[61]	Multi-access MIMO communications and infinite battery capacity	Maximise the minimum uplink throughput among all users	Optimise the downlink and uplink time allocation, the downlink energy beamforming, and the uplink transmit power allocation plus receive beamforming.
[62]	Multi-access MIMO communications and infinite battery capacity	Maximise the sum rate of all users	Optimise the time for downlink and uplink transmissions, the downlink energy transmit covariance matrices and the uplink information transmit covariance matrices of multiple antennas.
[63]	Multi-access MIMO communications with space-division multiple access	Maximise system sum throughput	Optimise downlink and uplink time, HAP downlink energy beamforming and uplink data receive beamforming.
[64]	Two user SISO relay communication and infinite battery capacity	Maximise weighted sum-rate of two users under a given total time constraint	Optimise the time for downlink energy transfer, uplink information transmission and information relaying, the transmit power of relaying and uplink transmissions.

[65]	SISO relay communication with both energy harvesting source and relays	Maximise average throughput for single relay and multi relay cases	Optimise downlink charging time, source uplink transmission time, relay uplink transmission time and relay selection.
[66]	SISO relay communications with multiple energy harvesting relays	Maximise end-to-end SNR	Optimise relay selection in terms of outage probability and throughput using both half-duplex and full-duplex time division relaying structures.
[67]	SISO energy harvesting relay communications with finite battery and finite data buffer	Maximise data delivered to the destination node by a deadline	Optimise time and transmit power for source transmission and relay forwarding considering power limitation and finite battery storage.
[68]	MIMO energy harvesting relay communications	Maximise system sum rate	Jointly optimise the relay processing matrix and the source precoder for both energy-flow assisted relaying and non energy-flow assisted relaying.

[69]	A cognitive radio network with mobile secondary users that opportunistically access the channel and harvest energy	Maximise spatial throughput of the secondary network	Optimise secondary users' transmit power and density under given outage-probability constraints.
[70]	A cognitive radio network with multiple primary channels, one secondary user opportunistically accesses one selected channel or harvests energy	Maximise throughput of the secondary user	Determine the optimal channel to access given the energy level and number of packets in data queue.
[71]	A cognitive radio network with multiple secondary users and multiple primary channels	Maximise average throughput of secondary users	Optimise channel access policy of secondary users without prior information of primary channels
[72]	Secure communication between a source-destination pair with an energy harvesting jammer	Maximise throughput of secure communication	Optimise jamming power and rate parameters of secure coding

2.2 NOMA-based WPCNs

This section presents works that consider NOMA-based WPCNs. Example works include [73–80]. These works assume a HAP has perfect CSI to/from energy harvesting devices. They aim to optimise transmission power, and charging and/or data transmission time based on given CSI to achieve one or more objectives. For example, in [73–75], the authors consider uplink data transmission in NOMA-WPCNs. The network has one base station and multiple energy harvesting devices. Devices harvest-then-transmit data to the base station using NOMA. References [73] and [74] consider two different decoding order strategies, namely fixed decoding order and time-sharing. The authors aim to optimise the time used for energy harvesting using different decoding orders under asymmetric and symmetric rates. They show that the solution of the formulated problems can be computed using either linear programming or convex optimization tools. Furthermore, the authors propose an efficient greedy algorithm for the time-sharing strategy. In [75], Chingoska et al. assume fixed decoding order at the base station. Specifically, the order is inverse to the distance of devices from the base station. The authors jointly optimise the energy harvesting time and base station transmit power to maximise the sum rate of the WPCN.

The work in [76] and [77] considers a separate energy source and access point. The authors propose Low Complexity Decoding (LCD) and Successive Interference Cancellation (SIC) Decoding schemes at the access point. In LCD, the AP uses a single-user decoder to detect signals without performing interference cancellation. They aim to optimise both energy harvesting time of devices and the transmit power of the energy source to maximise the sum throughput over a finite horizon. The work in [77] further considers maximizing the min-throughput of all users. The results show the importance of using successive interference cancellation in WPCNs with NOMA.

In [78], the authors consider a multiple-antenna HAP, which beamforms energy

to energy harvesting devices. The aim is to optimise the time allocation of energy transfer and uplink transmissions, the downlink energy beamforming and receiver beamforming to maximise the sum rate. The proposed optimization problem is non-convex. The authors propose a two-stage method to solve the said problem. In the first stage, they use successive convex approximation to find the optimal energy and receiver beamforming weights under fixed time allocation. In the second stage, they use a one-dimensional search to obtain the optimal time allocation between downlink and uplink transmissions.

The work in [79] and [80] considers energy and spectrum efficiency in NOMA-based WPCNs. Specifically, the authors of [79] consider half duplex and asynchronous transmissions. In half duplex transmission, devices harvest energy first and then start transmitting data to the AP simultaneously. In asynchronous transmission, devices start harvesting energy at the same time, but they begin transmitting data signals to the AP at different time instants. Therefore, some devices are able to harvest more energy while others are scheduled for uplink information transfer. The authors aim to optimise the time allocation of downlink and uplink to maximise system energy efficiency, which is defined as the ratio of the system throughput over the total energy consumed by devices. Moreover, the authors consider the buffer length of devices to avoid data transmission delays. They also address the impact of data overflow on energy-efficient time allocation. In [80], the authors aim to compare the spectral efficiency of NOMA-WPCN and TDMA-NOMA on circuit energy consumption of devices. They first derive the optimal time allocation to maximise system throughput for both TDMA-WPCN and NOMA-WPCN. After that, the authors prove that NOMA-WPCN requires a longer downlink charging time duration than TDMA-WPCN, which implies that NOMA-WPCN is more energy demanding. Moreover, they prove that NOMA-WPCN in general achieves a lower spectral efficiency than TDMA-WPCN.

In a different work, Lei et al. [81] consider a SIC-capable sink and multiple uplink time slots. In each uplink slot, a number of devices are scheduled to transmit

simultaneously. The authors consider decoding capacity, such that the sink can only decode a certain number of simultaneous transmissions which is less or equal to the decoding capacity. They aim to determine the devices to be scheduled in each uplink slot in order to maximise system throughput. To this end, they propose a linear program to schedule users into these time slots.

Table 2.2 presents a comparison of aforementioned related works in NOMA-WPCNs. In summary, only references [79] and [81] thus far assume multiple uplink time slots. The authors of [81] further consider SIC decoding capacity. However, link scheduling, non-linear RF energy harvesting or imperfect CSI has not been addressed in NOMA-WPCNs past works, which is the motivation of this thesis. The novelties of this thesis will be discussed in details in Section 2.5.

Table 2.2: Comparison of related works on NOMA-WPCNs.

Reference	[73]	[74]	[75]	[76]	[77]	[78]	[79]	[80]	[81]
Multiple slots	×	×	×	×	×	×	✓	×	✓
SIC decoding capacity	×	×	×	×	×	×	×	×	✓
Link scheduling	×	×	×	×	×	×	×	×	×
Non-linear RF conversion	×	×	×	×	×	×	×	×	×
Imperfect CSI	×	×	×	×	×	×	×	×	×

2.3 WPCNs with Imperfect CSI

In practice, perfect CSI is not available. To this end, some past works have investigated WPCNs with imperfect CSI. As examples, references [82–84] investigate a massive MIMO WPCN with channel estimation errors. Specifically, in reference [82], the authors consider energy harvesting devices that use a fraction of their harvested energy to send pilots, while the HAP estimates the uplink channels and obtains the downlink CSI by exploiting channel reciprocity. The aim is to maximise the minimum rate among all devices by jointly optimizing the time for channel estimation,

downlink energy transfer and uplink information transmission, the energy allocation weights in the downlink phase, as well as the fraction of energy used for channel estimation at each device. In a different work [83], the objective is to maximise system energy efficiency in terms of channel estimation errors. The authors propose a novel antenna selection scheme to find the optimal number of transmit antennas at the base station. Moreover, they jointly optimise energy beamforming of the HAP, its energy transfer and data transmission time to maximise energy efficiency. The work in [84] derives a robust resource allocation solution to address imperfect CSI. The authors also consider non-linear energy harvesting. In particular, they jointly optimise downlink time and energy beamforming for a multi-antenna power station as well as uplink data transmission time and power beamforming for each multi-antenna device. Two different design objectives are considered, namely maximization of the system sum throughput (max-sum) and maximization of the minimum individual throughput (max-min) at each device.

There are some works that consider dual-hop relay assisted WPCNs. For example, the work in [85] considers a number of single antenna energy harvesting relays that decode and forward data for a transmitter-receiver pair. Both transmitter and receiver have multiple antennas. The energy harvester at each relay, which has a finite battery, is assumed to be non-linear with a saturation threshold. The authors investigate outage probability, antenna and relay selection, assuming imperfect CSI at both transmitter and receiver. Reference [86] also studies relay selection for a source-destination pair. Moreover, the authors consider relays with spatially random locations. Two different scenarios are considered: 1) a single-antenna source with perfect CSI, and 2) a multiple-antenna source with transmit antenna selection and imperfect CSI. In both scenarios, the authors aim to select the best relay to forward information to the destination in order to improve system performance. In particular, they investigate outage probability and system throughput over Nakagami-m fading channels.

Some other past works consider Secrecy WPCNs with eavesdroppers. For ex-

ample, Wu et al. [87] consider an information source that harvests energy from a power source and sends its message to a destination. There is also an eavesdropper that intends to intercept information from the information source. The power source and the information source both have multiple antennas. The authors aim to maximise the secrecy rate assuming imperfect eavesdropper CSI at the information source. They propose a robust resource allocation to optimise the energy harvesting time, information time, transmit power from the power source and power beamforming from the information source. In a different work [88], the authors consider communication between a base station equipped with multiple antennas and a data user. In addition, there are a number of energy harvesting devices that function as eavesdroppers. The authors study antenna selection at the base station and power splitting ratio at eavesdroppers in order to optimise secrecy performance. The work in [89] considers a hybrid base station that not only powers an energy harvesting transmitter but also generates artificial noise to protect against eavesdroppers. Both the hybrid base station and information transmitter have multiple antennas. The authors consider both the perfect CSI and imperfect CSI cases. They aim to maximise secrecy rate, which is defined as the data rate at a information receiver minus the maximum data rate at eavesdroppers. The authors jointly optimise downlink energy beamforming, signal beamforming from the information transmitter, artificial noise transmit power and time allocation between power transfer and information transmission.

Table 2.3 summaries prior research on transmission scheduling in WPCNs with imperfect CSI. Past works have focused on optimizing the trade-off between downlink charging and uplink data transmissions, power beamforming and antenna selection of multi-antenna HAP to achieve various objectives. Note that, no prior work has considered NOMA-WPCNs with imperfect CSI or investigated uplink transmission schedule in WPCNs with imperfect CSI.

Table 2.3: Summary of transmission scheduling in WPCNs with imperfect CSI.

System	**Paper**	**Aim**	**Problem**
MIMO WPCNs	[82–84]	Maximise minimum rate, sum rate and energy efficiency	Optimise time allocation, downlink and uplink energy beamforming, antenna selection
Dual-hop relay WPCNs	[85, 86]	Investigate outage probability and system throughput	Optimise antenna and relay selection
Secrecy WPCNs	[87–89]	Maximise secrecy rate	Optimise time allocation, power beamforming and antenna selection

2.4 Backscatter assisted WPCNs

Figure 2.1 outlines the transmission scheduling issues in backscatter assisted WPCNs. Note that, there are two major common issues in different backscatter WPCNs systems. The first one is time allocation among different working modes for a backscatter device. For each device, the time used for energy harvesting and data transmission has a significant impact on its transmission rate. To this end, many works aim to optimise the tradeoff between energy harvesting time and data transmission time, i.e., both active and passive transmission, to maximise the transmission rate of a device. Moreover, when a device is backscattering, it reflects a portion of the incident signal by adjusting the reflection coefficient of its antenna, and the remaining signal can be used to power its circuit directly. Therefore, some works jointly optimise the reflection coefficient as well as the time allocated to energy harvesting and data

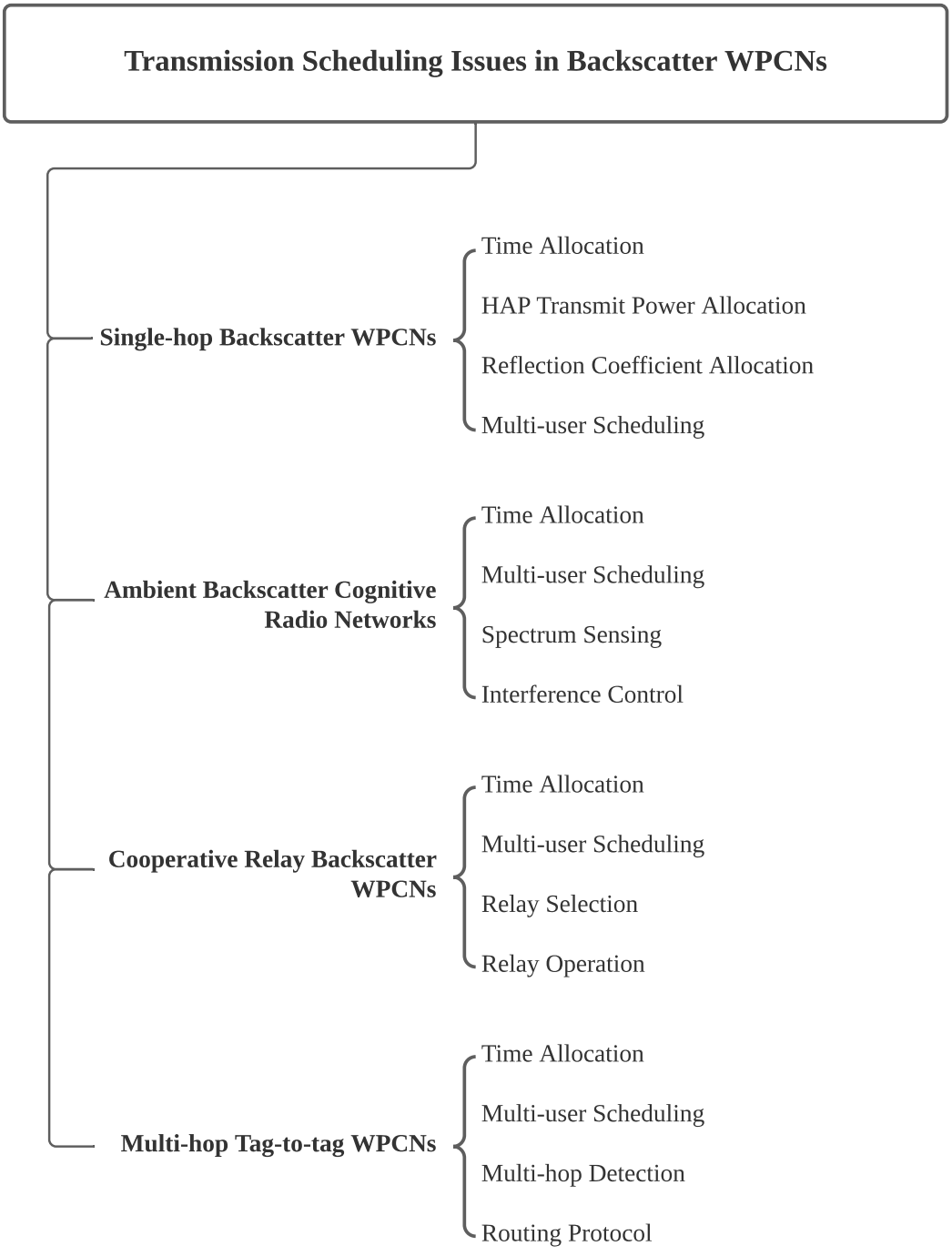

Figure 2.1: Outline of transmission scheduling issues in backscatter assisted WPCNs.

transmission. Another major issue is multi-user scheduling in backscatter WPCNs with multiple devices. Each device is able to harvest energy from an RF source and transmits data via either backscattering or active RF transmission. Past works consider uplink data transmission in TDMA or NOMA. Therefore, time allocation trade-off among multiple devices in uplink transmission has been addressed as well as time allocated to different operations for each device. The rest of this section will provide a detailed review in transmission scheduling issues in various types of backscatter WPCNs.

In bistatic backscatter assisted WPCNs, there is usually one RF source, one or multiple energy harvesting devices and one gateway. These devices can either be passive tags that only transmit data via backscattering or hybrid devices that transmit data in both active and backscatter modes. Devices harvest energy from the RF source, and also use the excitation signal from the power source to enable backscattering to the gateway. References [90–92] consider only one device. Specifically, reference [90] studies the duty cycle of an ambient backscatter tag, which can be in either sleep mode to harvest energy or in active mode to transmit data via backscattering. The authors jointly optimise the time period for the tag to be in sleep and active mode, and its backscatter reflection coefficient to maximise its transmission rate. The work in [91] considers a hybrid device that transmits in three phases: energy harvesting, ambient backscattering and active RF transmission. In addition, the authors consider two reflection coefficient types for backscattering: variable reflection coefficient and fixed reflection coefficient. In the variable reflection coefficient case, device's reflection coefficient changes with the given CSI. In the fixed reflection coefficient case, device's reflection coefficient is fixed to one. The authors aim to maximise the average achievable rate for both cases considering device's circuit power consumption constraints. To this end, they study the optimal time allocation for energy harvesting, ambient backscattering and active RF transmission. In a different work [92], the authors consider dynamics of ambient RF signals and they introduce spectrum sensing to detect ambient RF signal. In particular, when

the level of incident signal power is sensed to be higher than a predetermined value, the device starts energy harvesting or backscattering. The authors introduce two spectrum sensing techniques at a passive tag: single frequency detection and compressive sensing. The authors aim to optimise time allocation for spectrum sensing, energy harvesting and backscattering for a passive tag to maximise sum rate. The authors also optimise the tradeoff between power used for energy harvesting and backscattering when compressive sensing is used.

There are some works that consider multiple hybrid devices transmitting to one gateway [93–97]. For example, the authors of [93] study the optimal backscattering time among multiple hybrid devices by considering a two-phase transmission protocol. In the first phase, each device backscatters to the gateway in a TDMA manner, and harvests energy in the time allocated to other devices. In the second phase, devices actively transmit to the gateway using the energy harvested in the first phase. TDMA and NOMA are employed during the active data transmission phase of multiple devices. In the TDMA scheme, when a device is transmitting to the gateway, other devices harvest energy. In the NOMA scheme, all devices transmit data simultaneously. The authors aim to maximise system throughput by optimizing time allocation policies for backscattering in both TDMA and NOMA. In a different work [94], the authors further study the optimal transmit power from an RF source in a heterogeneous IoT network. The network contains active, passive and hybrid devices. To ensure energy efficiency, the authors assume that the RF source adjusts its transmission power based on channel conditions, energy harvesting efficiency and backscatter reflection coefficient of different devices. The authors jointly optimise the backscattering and active transmission time of devices, as well as the RF source's transmit power. Their objective is to maximise both the total throughput of all devices and the system energy efficiency.

A number of works have considered channel estimation errors. For example, reference [97] considers imperfect CSI for a multiple passive tags network. Specifically, the authors consider two scenarios, namely, CSI estimation errors follow the Gaus-

sian distribution and no exact distribution of CSI estimation errors. They define two types of outage based on throughput and harvested energy of tags, respectively. In particular, an outage occurs when the throughput of a tag does not meet a minimum requirement or the harvested energy of a tag is lower than the consumed energy due to CSI estimation error. The authors aim to optimise backscattering time and power reflection coefficient of each tag to maximise the minimum transmission rate. At the same time, they ensure a bound on outage probability.

Another set of works considers monostatic backscatter assisted WPCNs. There is a full-duplex HAP and multiple devices. In the downlink, the HAP broadcasts energy to all devices continuously, whereas each device switches between 'Harvest-then-transmit' (HTT) mode and backscatter mode to transmit or backscatter data to the HAP via TDMA in the uplink. Similar to bistatic backscatter system, time scheduling among different working modes, namely energy harvesting, backscattering and active transmission, also affects the overall system performance. Therefore, many works aim to optimise the time allocated to multiple devices as well as the tradeoff between time period used for different working modes for each device to achieve different objectives. Specifically, in [98], the authors first propose a backscatter assisted WPCN with multiple hybrid devices. They investigate the optimal time used for energy harvesting, backscattering and active transmission for each device to maximise the sum throughput of all devices.

Some works have considered backscattering in legacy communications systems. In [99], a HAP simultaneously transmits Orthogonal Frequency Division Multiplexing (OFDM) signals to a legacy user and receives backscatter signals from multiple backscatter devices. The authors investigate the optimal backscatter time allocation among devices, and the power reflection coefficient at devices for backscattering. They also consider the HAP's subcarrier power allocation, interference to legacy communications. The aim of [99] is to maximise the minimum throughput of devices and also ensure the the throughput of legacy users is above a given threshold.

The transmission range of AmBC is limited to a few feet as shown in [11].

Therefore, a HAP can only receive backscatter signal from its nearby devices. To overcome this problem, Kim et al. propose hybrid backscatter communications for WPCN to increase backscatter transmission range [100]. There are two types of RF sources: an ambient RF source, i.e., HAP, that covers both an outdoor and an indoor zone, and a dedicated RF source that only covers the indoor zone. Therefore, a device located in the indoor zone is able to harvest energy from both ambient and dedicated RF source, backscatter data to the HAP via incident signal from the dedicated RF source and actively transmit data when it has sufficient energy. The authors jointly optimise the energy harvesting time, backscatter time and active data transmission time to maximise throughput of a single device in the indoor zone. The authors extend their work in [101] by considering outdoor scenarios. There are two zones in outdoor scenarios: an outdoor Wi-Fi and macro zone. The outdoor Wi-Fi zone is similar to the indoor zone as indicated in [100], where the authors consider both long-range bistatic and short-range AmBC communications. However, in the macro zone, a device can only transmit data to another device using ambient RF signal from the HAP to realise short-range AmBC. Therefore, multi-hop AmBC transmission is used to deliver information to the HAP. In the last hop, a device actively transmits data to the HAP if it is in the macro zone or bistatic backscatters to the HAP if it is in the outdoor Wi-Fi zone. In order to maximise the overall system throughput, the authors optimise time allocated to different working modes for each device based on its location: outdoor Wi-Fi zone or Macro-zone. They also show that the proposed hybrid backscatter communications is able to achieve extended coverage with multi-hop data transmission.

The authors of [102] consider a wireless powered backscatter sensor network. There is a HAP that is charged by an external energy source. In addition, each backscatter sensor has a finite data queue with packets classified into normal and important. A new arrival packet at a sensor will either be dropped or stored based on its classification. The HAP makes a decision to sleep, collect data from a sensor via backscattering or harvest energy based on the data queue of all sensors, the

energy level of the HAP, as well as the channel condition between the external RF source and the HAP. The authors aim to determine the optimal decision of the HAP to minimise the weighted data queue length of all sensors, which at the same time minimises the average packet loss among all sensors.

The following works consider AmBC assisted RF-powered cognitive radio networks. The network consists of a primary transmitter, e.g., a base station, transmitting RF signals on a licensed channel. When the channel is busy, a number of secondary transmitters either transmit their data to a secondary gateway by using backscatter communications or harvest energy from the RF signals through RF energy harvesting techniques. When the channel is idle, secondary transmitters use their harvested energy to transmit data to the gateway via conventional radios. Reference [103] studies two configurations of an overlay and underlay network. In the overlay network, primary channel has idle time, while in the underlay network, primary channel is always busy. In order to achieve the maximum transmission rate of a single secondary transmitter, the authors optimise its time tradeoff between backscattering and energy harvesting when primary channel is busy and optimise active data transmission time when primary channel is idle in the overlay configuration. Moreover, in the underlay configuration, the authors jointly optimise backscattering time, energy harvesting time and active data transmission time, together with the transmit power of the secondary transmitter in order to avoid interference to the primary receiver.

In [104], the authors consider a secondary transmitter with spectrum sensing. Depending on the state of the primary channel, namely busy or idle, it switches between energy harvesting, backscattering or data transmission. The aim is to maximise energy efficiency of secondary communications, which is defined as the ratio of its average achievable throughput to its average energy consumption. The authors present closed-form expressions of the energy efficiency under different scenarios. Moreover, they formulate an optimization problem that maximises the energy efficiency of the considered network, and evaluate the optimal spectrum sensing

threshold, the optimal time for spectrum sensing, energy harvesting, backscattering and active data transmission. Their formulation also ensures the interference level at a primary user remains below a certain threshold. In addition, they ensure the secondary transmitter's energy expenditure is within its energy harvesting rate.

Some prior works consider multiple secondary transmitters in RF powered cognitive radio networks with AmBC [102]. Each transmitter has a harvest-then-transmit mode and a backscatter mode for energy harvesting and data transmission. The authors in [102] assume each secondary transmitter follows a TDMA manner to transmit data to a secondary receiver. They investigate the optimal time of different operation modes for each transmitter as well as the optimal transmission time sharing among different transmitters in order to maximise overall network throughput of the secondary system. On the contrary, reference [105] considers RF-powered AmBC underlay cognitive radio NOMA networks, where the secondary transmitters use the harvested energy to simultaneously transmit their information based on power-domain NOMA. Moreover, the authors consider interference to primary user, so that if the interference from secondary transmitters to primary users exceeds a predetermined threshold, secondary transmitters will choose the ABC mode to perform the data transmission. The authors formulate a convex optimization problem with the aim to maximise the throughput of the secondary system. They derive the optimal time resource allocation between the harvest-then-transmit mode and the AmBC mode for multiple secondary transmitters.

2.4.1 User collaboration

A set of works have considered user collaboration in AmBC assisted WPCNs, where some devices serve as relays to assist data transmissions. These relays can be passive devices [106–109], active devices [110] or hybrid devices [111, 112].

The work in [106–109] considers backscatter device-to-device (D2D) communications assisted by a multi-antenna power beacon. The power beacon beamforms

RF signals to power the backscatter transceiver pairs. They consider a passive relay network, where each device can switch its radio mode for active data transmission and passive data transmission based on its channel condition and its harvested energy. In addition, when a device is transmitting data actively, other passive devices can either harvest energy for their own use or relay information for active RF transmissions. These works jointly optimise the time for active and passive transmissions for each device, the beamforming from the multi-antenna HAP to each device as well as the reflection coefficient for passive relays, with the objective is to maximise the sum throughput for all devices. Specifically, Gong et al. propose to use a semi-definite program with an adaptive relay strategy to update the reflection coefficients of relays [106]. Moreover, they propose heuristic algorithms to maximise the overall relay performance by jointly optimizing the transmit beamforming, mode switching, and the passive reflection coefficients of relays. The authors then extend the passive relaying network to a two-hop power beacon assisted relay scheme in [107]. In [108], the authors propose a game theory approach, in which each relay as a player iteratively adjusts its reflection coefficient over multiple time slots to maximise its own utility. The utility of the relay is a function of the reward that the relay receives from backscattering data for other D2D transmitters. Recently, the authors of [109] propose to use the Deep Deterministic Policy Gradient (DDPG) algorithm to determine the optimal reflection coefficients of passive relays.

In contrast, reference [110] considers an active relay that forwards information for a passive device in decode and-forward mode. Specifically, the passive device first backscatters the incident signals from an RF source to both the receiver and the relay simultaneously, and then the relay decodes the received signals and forwards the decoded signals to the receiver. The authors consider two cases that whether the relay has to harvest energy from the RF source or not. The authors formulate system throughput maximization problems for both cases by finding the optimal time allocation schemes. Moreover, the authors investigate the time required to deliver a given amount of data.

The work in [111] considers using a single hybrid relay to assist dual-hop data transmissions between a source node and a destination node. The hybrid relay determines the relay protocol to coordinate between the active and passive relaying based on the CSI. To this end, the authors study two cases: the hybrid relay has or does not have CSI. They investigate relay mode selection protocols in both cases with the aim to maximise system throughput.

Recently, Yang et al. propose a novel IoT network, where hybrid devices do not rely on the RF source but other devices to transmit data via backscattering [112]. Specifically, when a device transmits data actively, a nearby device is able to backscatter data to another device using the incident signal. Also, when a device receives backscattered data from other device, it will forward these data to the HAP via active RF. This increases the throughput of devices with low energy. The authors assume that in each time slot, a device operates in either active transmission, backscatter transmission and backscatter reception mode. The authors determine the optimal operation mode for each device in each time slot to maximise the minimum throughput among all devices.

2.4.2 Multi-Hop Tag-to-Tag Communications

Recently, a few works have considered T2T communications. These works either consider hardware prototypes to enable T2T communications [113–115] or design routing protocols to select the optimal paths between two tags [116, 117].

The work in [113–115] focuses on hardware design of multi-hop T2T systems. They aim to improve the range or Bit Error Rate (BER) of T2T communications. For example, the work in [113] proposes a Backscattering T2T Network (BTTN). In this network, tags use passive envelope detection techniques to demodulate backscatter signals from neighboring tags. A major challenge is that the excitation signal and a backscattered signal superimpose with different phases at a receiving tag depending its location. This causes phase cancellation problem, which significantly

affects the range and robustness of a passive tag-to-tag link. To this end, the authors develop a novel multiphase backscatter modulation technique with a learning mechanism. Moreover, they demonstrate multi-hop operation for up to four hops.

Majid et al. develop a hardware backscatter T2T transceiver and a novel backscatter T2T MAC protocol [114]. The proposed T2T transceiver hardware avoids all energy hungry components in order to reduce energy consumption. The authors also show experimentally that backscatter reception is orders of magnitude more energy costly than transmission. Therefore, the proposed MAC protocol uses low-power listening approach. Each tag wakes up periodically every 26.5 ms to observe the channel before backscattering. They also implement a flooding mechanism to forward messages among tags.

In [115], Zhao et al. propose a novel multiple T2T backscatter system that works with commodity WiFi devices. Sensing tags modulate their sensing data into a single backscatter packet and work as relays for previous hops. The packet can be decoded with any commercial WiFi radios. The authors propose to change the backscattered frequency in each hop in order to relay the original WiFi packet among multiple tags. They also design a smart data field allocation mechanism to coordinate multi-hop transmissions.

Reference [116] and [117] consider routing in multi-hop T2T networks. Niu et al. [116] propose a routing protocol called the optimal link cost multipath routing (OLCMR). They propose that each tag maintains a lookup table that stores multiple candidate paths to each destination. This lookup table is established using a brute-force approach. If a tag suffers a link failure, it switches to another candidate path that has the minimum distance to the destination.

The authors of [117] propose a basic routing protocol from tags to the reader and design three distinct tag-to-tag routing protocols for tags with different hardware capabilities. The aim is to maximise network capacity, while reducing inter-tag interference. Specifically, the three different hardware scenarios are as follows: 1) standard tag design, 2) tags with power detectors that are able to measure the

received signal strength and 3) tags with power detectors and attenuators that can measure the received signal strength and attenuate the backscattered signal. In each scenario, the reader first identifies all the tags within its coverage area and determines the uplink routing paths for each tag. After that, the reader discovers the neighboring tag information and determines direct T2T transmission schedules. Moreover, the authors introduce a novel region partition scheme to enable large-scale multi-hop routing.

2.5 Summary

In summary, this thesis differs from past works in the following manners:

1. This thesis first considers a NOMA enable network to identify the *best* uplink schedule for use in a WPCN with a SIC-capable HAP. In all previous NOMA-WPCN works, their HAP has perfect CSI to/from energy harvesting devices. This information is used to determine the optimal transmit power of the HAP, transmission order or user groupings. In contrast, this thesis considers a HAP that has imperfect CSI. A number of works have considered imperfect CSI. They, however, consider a different system and do not consider deriving an uplink transmission schedule. In contrast to prior works, this thesis investigates a different problem: identify the *best* uplink schedule for use in a WPCN with a SIC-capable HAP. Identifying such a schedule is challenging due to the exponential number of schedules and also the fact that the HAP does not have CSI of energy harvesting devices. Consequently, existing solutions do not apply as they do not aim to solve the same problem or require CSI from energy harvesting devices.

2. This thesis then studies AmBC assisted WPCN. It addresses the energy trade-off between sampling and data transmissions, and study how it affects the number of samples collected by the HAP over T time slots. This also means

unlike prior works such as [43, 91, 92, 94, 101, 107, 108, 110, 111], devices *do not* have infinite amount of data. In fact, the amount of data they have is a function of their sampling frequency, which in turn is determined by their available energy. Second, unlike prior works that assume fixed relays, this problem involves selecting hybrid devices to function as relays. Third, except for [112], all prior works do not consider link scheduling. Although reference [112] considers link scheduling, they do not consider sample collection or aim to enable AmBC transmissions to facilitate devices with an active transmission to the HAP. Fourth, different to works such as [107, 108, 110, 111], for practical reasons, this thesis does not consider the asymptotic capacity of a link. Instead, it considers collecting packets or samples from a network of hybrid devices over *multiple* time slots.

3. Lastly, this thesis considers a network consisting solely of passive backscatter tags. Past works either consider hardware prototypes to enable T2T communications [113–115] or design routing protocols to select the optimal paths between two tags [116, 117]. However, this thesis aims to optimise the trade-off between data sensing and transmission within a given time frame. There are no past works that aim to optimise the number of samples collected by passive tags and also ensure these samples can be forwarded to a gateway within the said frame.

Chapter 3

Link Scheduling for NOMA-WPCNs with Imperfect CSI

This chapter outlines a challenging problem: scheduling uplink transmissions, whereby the HAP has *imperfect* CSI. The main research question is to determine the *best* transmission schedule, where one or more Energy Harvesting Devices (EHDs) are assigned into a time slot, that yields the highest average sum-rate at the HAP. Henceforth, this chapter contains the following contributions:

- It addresses a novel uplinks transmission scheduling problem in RF-energy harvesting networks. This problem is significant as future RF energy harvesting systems will require the HAP to collect data from EHDs quickly. Critically, this work considers a challenging but practical aspect: imperfect CSI.
- It presents two novel solutions. First, given a collection of transmission schedules, it outlines a discrete optimization solution that allows a HAP to pick the best transmission schedule. It also outlines a heuristic approach that allows a HAP to construct a schedule iteratively by greedily shifting EHDs from a slot to another slot in the hope of shortening the schedule length.

The remainder of the chapter is structured as follows. Section 3.1 outlines a toy

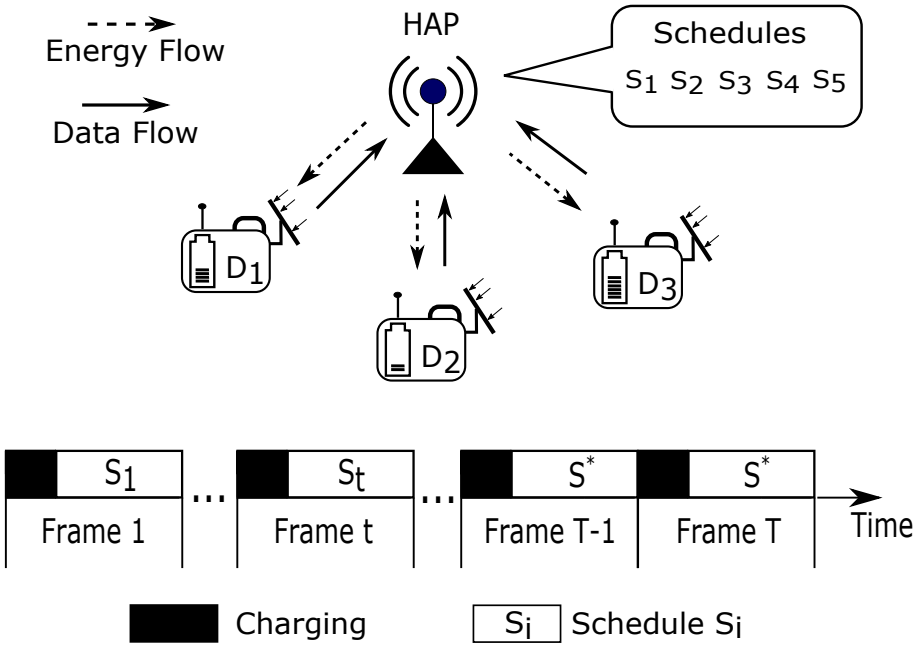

Figure 3.1: A WPCN with three EHDs D_1, D_2 and D_3, and five transmission schedules S_1, S_2, S_3, S_4 and S_5. In each frame t, all EHDs transmit data to the HAP using the transmission schedule provided by the HAP. The best transmission schedule is denoted as S^*.

model that illustrates the research problem and challenges. Sections 3.2 and 3.3 formalise the system and problem, respectively. Then Sections 3.4 and 3.5 introduce the proposed discrete optimization formulation and heuristic approach. After that, the evaluation methodology is presented in Section 3.6. Section 3.7 concludes this chapter.

3.1 A Toy Model

To illustrate the research problem, consider the WPCN shown in Figure 3.1. There is a half-duplex HAP and three EHDs; namely D_1, D_2 and D_3. This so called *harvest-then-transmit* protocol [39] requires the HAP to first charge EHDs for some time period. EHDs then use the harvested energy from the transmissions made by the HAP to carry out one or more tasks. The HAP then assigns an uplink data transmission slot to each EHD for data collection. The HAP is equipped with a Successive Interference Cancellation (SIC) radio [118]. This allows the HAP to de-

code multiple signals or transmissions assuming these signals meet a given set of Signal-to-Interference-plus-Noise Ratio (SINR) conditions; see Section 3.2 for details. Figure 3.1 also shows five transmission schedules. The HAP is responsible for prescribing *one* of these available transmission schedules in each time frame for collecting data from EHDs. As shown in Figure 3.1, different transmission schedules are used in earlier frames before the HAP converges onto the optimal or best transmission schedule S^*.

The said problem has a number of challenges. First, the number of transmission schedules increases with each additional EHD. Second, the HAP needs to select *one* of these transmission schedules without using CSI. If the HAP selects a schedule arbitrarily, it may find many SIC failures. Consequently, the chosen transmission schedule will have a very low sum-rate.

3.2 Preliminaries

3.2.1 Network Model

There is one HAP and K EHDs that are denoted as D_k, where $k \in \{1, \ldots, K\}$. The HAP transmits with power P. Each EHD has a rechargeable battery with maximum capacity $\mathcal{B}$. Time is divided into T frames. Each frame $t \in \{1, \ldots, T\}$ has duration τ. Each frame consists of a charging and a transmit phase, which has duration τ_D and τ_U, respectively. The transmit phase is further divided into upload slots, which will be discussed later. For each frame t, let g_k^t denote the channel gain from the HAP to an EHD D_k. Assume the channel has block fading, where g_k^t varies independently across frames but remains constant in each frame. Also note that the HAP has imperfect channel gain information or CSI. The path loss $\mathcal{L}_k$ from the HAP to EHD D_k is governed by the Log-distance path loss model. That is,

$$\mathcal{L}_k = \frac{d_0^\alpha 10^{(-\mathcal{L}_0 - \mathcal{X}^t)/10}}{d_k^\alpha} \tag{3.1}$$

where $\mathcal{L}_0$ is the path loss at reference distance d_0; i.e., $\mathcal{L}_0 = (4\pi d_0/\lambda)^2$, where λ is the wavelength. Moreover, d_k is the Euclidean distance between the HAP and EHD D_k, α is the path loss exponent and $\mathcal{X}^t$ is a normal Gaussian distributed variable with zero mean and standard deviation σ (in dB).

3.2.2 Energy Harvesting Model

The system considers a practical non-linear energy harvesting model [119]. Let $\phi(\cdot)$ be the Logistic/Sigmoid function that takes as input the received power at the antenna of an EHD and returns the output power from the RF harvester. For an EHD D_k at frame t, its incident power is,

$$P_k^t = P g_k^t = P \mathcal{A}_0 \mathcal{A}_k \mathcal{L}_k |h_k^t|^2 \tag{3.2}$$

where $\mathcal{A}_0$ and $\mathcal{A}_k$ are the antenna gains of the HAP and the EHD D_k, respectively, h_k is the channel coefficient that is given by the complex normal random variable $h_k \sim \mathcal{CN}(0,\, 1)$. The harvested energy of D_k in frame t is therefore,

$$E_k^t = \text{MIN}\{\tau_D \phi(P_k^t), \mathcal{B}\}. \tag{3.3}$$

In (3.3), the function $\phi(P_k^t)$ is defined as follows

$$\phi(P_k^t) = \frac{\psi(P_k^t) - \zeta_3 Z}{1 - Z}, \quad Z \triangleq \frac{1}{1 + \exp(\zeta_1 \zeta_2)},$$
$$\psi(P_k^t) = \frac{\zeta_3}{1 + \exp(-\zeta_1 (P_k^t - \zeta_2))}.$$

The term $\psi(P_k^t)$ is the standard logistic function that takes the incident power P_k^t at EHD D_k as input. The constant Z ensures a zero-input/zero-output response. The constant ζ_1, ζ_2 and ζ_3 are related to the resistance, capacitance, and diode turn-on voltage of a RF harvester circuit. Their values are obtained from least square fitting of measurement data of a given hardware [119]. Lastly, in this network, each

EHD is able to use E_k^t amount of energy for data transmissions in each frame t. In practice, a node may retain some constant amount of harvested energy to power its components. Also, as shown by the authors of [120], the residual energy at a node reduces the amount of harvested energy. Note that these system aspects only scale the results, and do not affect the proposed solutions nor conclusions.

3.2.3 Transmission Model

The HAP is responsible for informing EHDs of their uplink data transmission schedule. This allows the HAP to collect data from each EHD. Let S_i denote the i-th transmission schedule that contains one or more EHDs assigned to each time slot. Record the collection of transmission schedules in the set Φ, where $i \in \{1, 2, \ldots, |\Phi|\}$. As a concrete example, assume there are three EHDs: D_1, D_2 and D_3. Further, consider only those transmission schedules whereby all EHDs transmit *once* in a frame; they are $S_1 = \{\{D_1, D_2, D_3\}\}$, $S_2 = \{\{D_1, D_2\}, \{D_3\}\}$, $S_3 = \{\{D_1, D_3\}, \{D_2\}\}$, $S_4 = \{\{D_1\}, \{D_2, D_3\}\}$ and $S_5 = \{\{D_1\}, \{D_2\}, \{D_3\}\}$. Thus $\Phi = \{S_1, S_2, S_3, S_4, S_5\}$. Note that the order of time slots does not matter as the channel gain is fixed in each frame. Hence, the schedule $S_1 = \{\{D_1, D_2, D_3\}\}$ and $S_1 = \{\{D_3, D_2, D_1\}\}$ have the same sum-rate. In each uplink slot, the set of transmitting EHDs belongs to a *transmission set*. As an example, schedule S_1 has three simultaneous transmissions in one uplink slot. Denote the length of each transmission schedule as $|S_i|$; e.g., $|S_5| = 3$ slots.

Figure 3.2 shows an example where in each frame, the HAP adopts a given transmission schedule. For example, in frame $t = 1$, it uses transmission schedule S_1, whereas in frame $t = 2$ and $t = 3$, it uses transmission schedule S_2 and S_5, respectively. Finally, in frame $t = T$, the HAP learns the best schedule S_2. The width of each block denotes the duration of transmission, which corresponds to the number of time slots in a transmission schedule.

Referring to each slot using ω and use $\mathcal{C}(S_i, \omega)$ to denote the transmission set

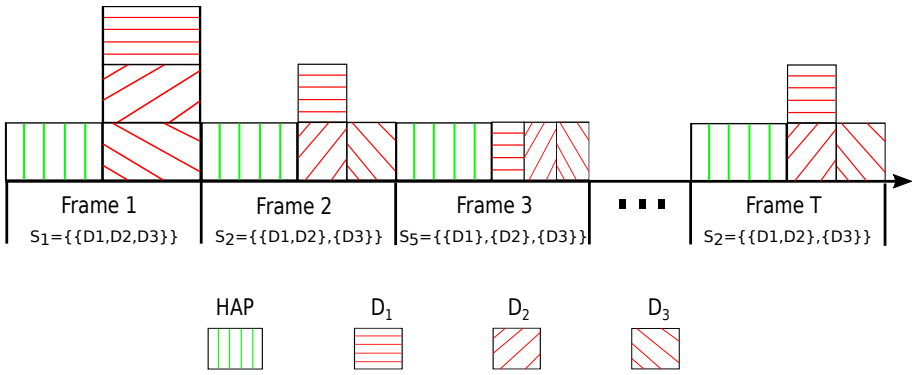

Figure 3.2: A different transmission schedule is used in each frame; the block with green lines represents downlink energy transfer and blocks with red lines represent uplink data transfer from three EHDs.

of schedule S_i in slot ω. The received power at the HAP from EHD D_k can be calculated as follows: $\gamma_k^t = \frac{E_k^t}{\tau_U/|S_i|} g_k^t$, where the term $\frac{\tau_U}{|S_i|}$ corresponds to the duration of each upload slot when using schedule S_i.

Note, it is straightforward to consider circuit power consumption during data transmissions. This can be modelled as in [121], where the total power or energy consumed during data transmission is a function of the transmit power divided by inefficiency of the RF chain plus a constant non-ideal circuit power. Note that incorporating the said inefficiency and non-ideal circuit power have the effect of scaling the results; they are thus ignored for ease of exposition.

Assume the HAP supports SIC [118, 122, 123]. To ensure SIC is successful, the received power of signals must be different from each other and to ensure each transmission satisfy their SINR threshold. The SIC process is explained as follows. Let the transmission set $\mathcal{C}(S_i, \omega)$ contain M transmitting EHDs with index $k = 1, \ldots, M$, and received power at the HAP that is ordered as follows: $\gamma_1^t \leq \gamma_2^t \leq \ldots \leq \gamma_M^t$. Decoding starts in the following order: l_M, $l_{(M-1)}, \ldots, l_1$, where l_k denotes the transmission from EHD D_k to the HAP. Let Γ_k^t denote the SINR for transmission l_k.

The HAP successfully decodes transmission l_M from EHD M if the following

inequality holds,

$$\Gamma_M^t = \frac{\gamma_M^t}{\sigma_0^2 + \sum_{i=1}^{i=M-1} \gamma_i^t} \geq \beta, \tag{3.4}$$

where σ_0^2 is the ambient noise power and β is the SINR threshold for a required data rate. Note that, the works in Chapter 3 does not consider setting the value of β. In fact, β is just a parameter value in Chapter 3. In practice, each radio such as IEEE 802.11 have different β values. The HAP then subtracts the decoded transmission or signal from EHD M, and proceeds to the next transmission with the highest received power. In this example, transmission $l_{(M-1)}$ is decoded successfully if the following inequality is satisfied,

$$\Gamma_{(M-1)}^t = \frac{\gamma_{(M-1)}^t}{\sigma_0^2 + \sum_{i=1}^{i=M-2} \gamma_i^t} \geq \beta. \tag{3.5}$$

Observe that the transmission from EHD M has been subtracted from the denominator of the previous inequality as part of the SIC process. If all $M-1$ transmissions are decoded successfully, it arrives at the last inequality,

$$\Gamma_1^t = \frac{\gamma_1^t}{\sigma_0^2} \geq \beta. \tag{3.6}$$

Define the maximum decoding capacity of SIC as κ, where SIC decoding is successful in a slot ω only if the number of simultaneous transmissions satisfies,

$$|\mathcal{C}(S_i, \omega)| \leq \kappa \tag{3.7}$$

Lastly, let $\mathcal{K}(S_i, \omega) \subseteq \mathcal{C}(S_i, \omega)$ contain all successful transmissions in uplink slot ω.

3.3 The Problem

The problem is to determine an uplink transmission schedule that maximises the expected throughput at the HAP. Let $F^t(S_i)$ be the system throughput if the HAP uses transmission schedule S_i in frame t. The system throughput is the sum of the throughput of all upload slots $\omega = 1, \ldots, |S_i|$. For each upload slot, it is the sum of throughput of all successful transmissions $l_k \in \mathcal{K}(S_i, \omega)$. Formally, $F^t(S_i)$ is defined as,

$$F^t(S_i) = \sum_{\omega=1}^{|S_i|} \sum_{l_k \in \mathcal{K}(S_i,\omega)} \mathcal{R}_k^t \frac{\tau_U}{|S_i|} \tag{3.8}$$

where the data rate $\mathcal{R}_k^t$ of transmission l_k is defined as,

$$\mathcal{R}_k^t = B \log_2(1 + \Gamma_k^t) \tag{3.9}$$

where B is the channel bandwidth.

The problem is then to find the 'best' schedule $S \in \Phi$, denoted as S^*, that yields the maximum expected throughput $F(S)$. Formally,

$$S^* = \arg\max_{S \in \Phi} \mathbb{E}[F(S)] \tag{3.10}$$

where the expectation is taken over random channel gains to/from EHDs over multiple time slots.

The problem has many challenges. The first is the size of Φ. Recall that each upload slot can only have κ EHDs as per the maximum decoding capacity. Let $\varphi = \frac{K}{\kappa}$ be an integer, which represents the length of schedule, i.e., the number of upload slots of a schedule. Then there are $\frac{K!}{(\kappa!)^\varphi}$ different schedules of length φ. For example, if there are 10 EHDs and each slot contains $\kappa = 2$ EHDs, then there are $\frac{10!}{(2!)^5} = 113400$ schedules. In addition, different values of κ need to be considered, which further increases the number of schedules. Section 3.5 addresses above challenge via a

heuristic protocol. The second challenge is imperfect channel gain knowledge. This means the HAP is unable to determine the transmission order of EHDs because it does not know the amount of energy harvested by each EHD. Consequently, if the HAP arbitrarily selects two devices to transmit together, the respective transmission of each device may not meet the required SINR threshold. Consequently, the HAP will experience SIC failure. Lastly, the HAP needs to identify the optimal schedule in Φ. One solution is to simply obtain the sample mean of each schedule in Φ; i.e., it computes $\mathbb{E}[F(S)] = \frac{1}{L}\sum_{t=1}^{L} F^t(s)$, where L is some large number of frames. As L approaches infinity, by the law of large numbers, it obtains the expected performance of schedule s. The HAP then selects the schedule with the highest expected value. This *brute-force* method, however, is inefficient.

Although adapting the transmission power or/and data rate of EHDs are not considered, they can be incorporated as follows. Assume there are two EHDs, denoted as D_1^r and D_2^r, where r denotes a data rate, and two data rates $r \in \{1, 2\}$. Example schedules in this case include $S_1 = \{\{D_1^1\}, \{D_2^1\}\}$, $S_2 = \{\{D_1^2\}, \{D_2^1\}\}$, $S_3 = \{\{D_1^1\}, \{D_2^2\}\}$, $S_4 = \{\{D_1^2\}, \{D_2^2\}\}$, $S_5 = \{\{D_1^1, D_2^1\}\}$ and so forth. In particular, in transmission schedule S_1, both EHDs transmit with data rate $r = 1$ in two separate slots. As for transmission schedule S_5, both EHDs transmit in the same slot using data rate $r = 1$. In a similar manner, adding various transmit power levels results in additional transmission schedules whereby each EHD has a data rate and also a transmit power when it is assigned a slot. From the aforementioned example, it shows that the search space increased significantly when considering data rates and transmit power. It is required to list all combinations of EHDs in each slot, their transmit power levels and data rates. Moreover, as the HAP is unaware of the energy at EHDs, some transmission schedules may not be feasible.

To conclude this section, the following presents an analytical comparison of the theoretical throughput of TDMA and SIC schedules for K EHDs. Given the following proposition:

Proposition 3.1. *Assuming SIC is always successful, the throughput of a SIC sched-*

ule is always higher than a TDMA schedule as EHDs $K \to \infty$.

Proof. Let $\hat{F}(S)$ be the throughput of SIC schedule calculated using (3.8). As SIC is always successful, i.e., $\beta \to 0$, and the received power from EHDs at the HAP is ordered as $\hat{\gamma}_1 \leq \hat{\gamma}_2 \leq \ldots \leq \hat{\gamma}_K$, the throughput is formulated as the sum of the total received data from all K EHDs. Thus,

$$\hat{F}(S) = \tau_U \sum_{k=1}^{K} \log_2(1 + \frac{\hat{\gamma}_k}{\sigma^2 + \sum_{i=1}^{i=k-1} \hat{\gamma}_i}) = \tau_U \sum_{k=1}^{K} \log_2(\frac{\sigma^2 + \sum_{i=1}^{i=k-1} \hat{\gamma}_i + \hat{\gamma}_k}{\sigma^2 + \sum_{i=1}^{i=k-1} \hat{\gamma}_i}). \tag{3.11}$$

Using the property that sum of logarithms with the same base is the logarithm of a product, it has

$$\hat{F}(S) = \tau_U \log_2 \Big(\prod_{k=1}^{K} (\frac{\sigma^2 + \sum_{i=1}^{i=k} \hat{\gamma}_i}{\sigma^2 + \sum_{i=1}^{i=k-1} \hat{\gamma}_i}) \Big) = \tau_U \log_2(1 + \frac{\sum_{k=1}^{K} \hat{\gamma}_k}{\sigma^2}). \tag{3.12}$$

On the other hand, for a TDMA schedule, the received power $\breve{\gamma}_k$ is K times that of a SIC schedule. This is because, as shown in Section 3.2.3, the duration of the upload slot for SIC schedule is K times of a TDMA schedule. Thus, it has

$$\breve{\gamma}_k = K\hat{\gamma}_k, \quad \forall k = 1, \ldots, K, \tag{3.13}$$

and the throughput of TDMA, denoted as $\breve{F}(T)$, is

$$\breve{F}(T) = \frac{\tau_U}{K} \sum_{k=1}^{K} \log_2(1 + \frac{\breve{\gamma}_k}{\sigma^2}) = \frac{\tau_U}{K} \log_2 \Big(\prod_{k=1}^{K} (1 + \frac{K\hat{\gamma}_k}{\sigma^2}) \Big). \tag{3.14}$$

Thus, according to (3.12) and (3.14), it has $\hat{F}(S) \geq \breve{F}(T)$ if the following inequality holds,

$$(1 + \frac{\sum_{k=1}^{K} \hat{\gamma}_k}{\sigma^2})^K \geq \prod_{k=1}^{K} (1 + \frac{K\hat{\gamma}_k}{\sigma^2}), \tag{3.15}$$

which can also be represented as

$$\frac{\prod_{k=1}^{K}(1+\frac{K\hat{\gamma}_k}{\sigma^2})}{(1+\frac{\sum_{k=1}^{K}\hat{\gamma}_k}{\sigma^2})^K} \leq 1 \tag{3.16}$$

Specifically, when the number of EHD K approaches infinity, and by applying L'Hospital's rule, it has

$$\lim_{K\to\infty} \frac{\prod_{k=1}^{K}(1+\frac{K\hat{\gamma}_k}{\sigma^2})}{(1+\frac{\sum_{k=1}^{K}\hat{\gamma}_k}{\sigma^2})^K} = \frac{\frac{\partial}{\partial K}\prod_{k=1}^{K}(1+\frac{K\hat{\gamma}_k}{\sigma^2})}{(1+\frac{\sum_{k=1}^{K}\hat{\gamma}_k}{\sigma^2})^K \ln(1+\frac{\sum_{k=1}^{K}\hat{\gamma}_k}{\sigma^2}).} \tag{3.17}$$

Note that, the denominator of (3.17) is derived by using the property that $\frac{\partial}{\partial x}a^x = \ln(a)a^x$, where $a \in \mathbb{R}$. Here, both $\hat{\gamma}_k$ and $\sum_{k=1}^{K}\hat{\gamma}_k$ are constants. Hence, by applying L'Hospital's rule K times, it has

$$\lim_{K\to\infty} \frac{\prod_{k=1}^{K}(1+\frac{K\hat{\gamma}_k}{\sigma^2})}{(1+\frac{\sum_{k=1}^{K}\hat{\gamma}_k}{\sigma^2})^K} = \frac{a}{(1+\frac{\sum_{k=1}^{K}\hat{\gamma}_k}{\sigma^2})^K\Big(\ln(1+\frac{\sum_{k=1}^{K}\hat{\gamma}_k}{\sigma^2})\Big)^K}, \tag{3.18}$$

where it uses a to represents the numerator of (3.18) as it is a real number, i.e., $a \in \mathbb{R}$. Note that the denominator of (3.18) is $\to \infty$. Hence, it has

$$\lim_{K\to\infty} \frac{\prod_{k=1}^{K}(1+\frac{K\hat{\gamma}_k}{\sigma^2})}{(1+\frac{\sum_{k=1}^{K}\hat{\gamma}_k}{\sigma^2})^K} = 0. \tag{3.19}$$

This proves that inequality (3.16) is always true for $K \to \infty$, and thus, $\hat{F}(S) > \breve{F}(T)$. □

In Proposition 3.1, we focus on the average sum-rate given an uplink transmission schedule with K time slots. Although SIC is assumed to be always successful, it is worth noting that SIC allows multiple devices transmitting simultaneously in a single time slot. Thus the number of slots decreases compare to TDMA. As a result, the duration of each slot becomes larger, which mathematically results in a lower transmit power by devices. In this respect, we show that having multiple transmissions as enabled by SIC remains superior to simply scheduling one device

per slot, e.g. TDMA. However, note that in high interference scenarios, SIC does not meet the required SINR threshold. TDMA would typically be the optimal uplink schedule that leads to the maximum sum-rate.

3.4 A Discrete Optimization Approach

This section proposes a solution based on the discrete stochastic optimization approach outlined in [124]. The *basic* idea is to view the set of transmission schedules in Φ as the states of a Markov chain. If a transmission schedule or state has a high reward, then this state will be visited more frequently than others, this state then has a high occupancy probability. As it will show later, the algorithm starts in a random state. Initially, there is uniform probability of transitioning to any states. It then evaluates the average sum-rate of a given state and compare that against another randomly selected state. Then the algorithm selects the state with the higher reward. After that, it updates the occupancy probability of states to reflect how often a state or transmission schedule has been visited. Upon convergence, the state with the highest occupancy probability is the optimal transmission schedule.

3.4.1 Preliminaries

The approach operates over N episodes. Recall that the approach needs to evaluate the reward, i.e., average sum-rate, of a given state and compare that against another randomly selected state in each episode. To do so, each episode $n \in \{1, \ldots, N\}$ consists of two superframes; each of which is further divided into T frames. A frame $t \in \{1, \ldots, T\}$ consists of a charging and a transmit phase. Each frame will be used to obtain the sample average reward of a transmission schedule. To represent the occupancy probability of the transmission schedules in Φ in episode n, define the one dimensional probability vector $\boldsymbol{\mathcal{P}}[n] \in [0,1]^{|\Phi|}$. Also, let $\mathcal{P}[n,j]$ be the occupancy probability of transmission schedule $j \in \Phi$. For example, given $\Phi = \{S_1, \ldots, S_M\}$, it then has $\boldsymbol{\mathcal{P}}[n] = [\mathcal{P}[n,1], \ldots, \mathcal{P}[n,M]]^T$. Note, for any episode n, the following

condition holds: $\sum_{m\in\Phi} \mathcal{P}[n,m] = 1$.

The following presents the notation used to identify a transmission schedule. Define S^n as the transmission schedule selected in episode n, and a two dimensional matrix $\theta = \{\boldsymbol{e}_1, \boldsymbol{e}_2, \ldots, \boldsymbol{e}_M\}$, where $\boldsymbol{e}_m \in \{0,1\}^{|\Phi|}$ is a column vector with its m-th element set to one and all other elements are zero. For example, if it has $M = 3$ transmission schedules in Φ, then it has $\theta = \{[1,0,0],[0,1,0],[0,0,1]\}$; note that for each vector or column, the entry with a value of one identifies the transmission schedule in question. Let $\boldsymbol{\mathcal{S}}[n] \in \theta$ denote the selected transmission schedule in episode n. As an example, assume it has selected the first transmission schedule in Φ, namely $\mathcal{S}[n] = [1,0,0]$ or $S^n = S_1$. If instead it has $\mathcal{S}[n] = [0,1,0]$, then this means the selected transmission schedule in episode n is $S^n = S_2$. In each episode, the occupancy probability of transmission schedules is updated as follows,

$$\boldsymbol{\mathcal{P}}[n+1] = \boldsymbol{\mathcal{P}}[n] + \mu[n+1](\boldsymbol{\mathcal{S}}[n+1] - \boldsymbol{\mathcal{P}}[n]) \tag{3.20}$$

where the *step size* is $\mu[n] = 1/n$, meaning it decreases with increasing number of episodes. To gain some intuition of (3.20), consider the following example. Let there be ten episodes and transmission schedules S_1 and S_2. Assume S_1 has been used eight out of ten times. Then its occupancy probability will be 0.8 at episode $n = 10$. In other words, (3.20) computes the running average of the number of times in which a schedule is selected over n episodes.

To make specific the reward of each transmission schedule, let $Q[n, S^n]$ be the reward of the selected transmission schedule S^n in episode n. Note that the reward is the average system throughput over T frames based on Equ. (3.8). Formally,

$$Q[n, S^n] = \frac{1}{T}\sum_{t=1}^{T} F^t(S^n) \tag{3.21}$$

3.4.2 Step by Step Details

This subsection explains the proposed discrete optimization approach in detail; see Algorithm 3.1. Algorithm 3.1 is executed by the HAP. At the beginning of each scheduling time slot, the HAP runs Algorithm 3.1 to update the occupancy probability of all transmission schedules. Algorithm 3.1 converges to the best uplink schedule at the end of the scheduling period. The algorithm starts by selecting an initial transmission schedule S^1 uniformly from Φ, see line 1. Here, the function $\mathcal{U}(\Phi)$ is a function that returns a transmission schedule S_i from the set Φ in a uniform manner. Also, the initially selected schedule has an occupancy probability of one. The occupancy probability of other transmission schedules is set to zero; see line 2. The algorithm runs for N episodes. In each episode n, see line 3 to line 19, it calculates the average reward of the given schedule S^n, see line 4 to line 7. After that, it uniformly selects another transmission schedule $\hat{S}_n$, see line 8, and calculate its average reward over T frames, see line 9 to line 12. Then starting from line 13 to line 17, the algorithm compares the average reward of the given schedule S^n against the randomly selected schedule $\hat{S}^n$, and selects the transmission schedule with the higher reward. Lastly the occupancy probability $\boldsymbol{\mathcal{P}}[n]$ is updated in line 18. As mentioned earlier, the optimal transmission schedule achieves the highest occupancy probability. This is exactly line 20, which returns the schedule S^* that has the maximum occupancy probability in $\boldsymbol{\mathcal{P}}[N+1]$.

Proposition 3.2. *The run-time complexity of discrete optimization approach is* $\mathcal{O}(KTN + \frac{K!}{(\kappa!)^{\frac{K}{\kappa}}}N)$.

Proof. From Algorithm 3.1, it shows that in each episode, it calculates $F^t(S^n)$ for each frame $t \in \{1, \ldots, T\}$ and the reward using Equ. (3.21). Recall that, $F^t(S^n)$ is derived from the the throughput of all K EHDs, see Equ. (3.8). Therefore, these step has a run-time complexity of $\mathcal{O}(KT)$. The algorithm then randomly selects another schedule $\hat{S}^n$ and calculates $F^t(\hat{S}^n)$, which also has a run time complexity of $\mathcal{O}(KT)$. Next, it compares the reward between the two schedules, which has run-

time of $\mathcal{O}(1)$. However, it requires $\mathcal{O}(M)$ time to update the occupancy probability of schedule $\hat{S}^{n+1}$, where $M = \frac{K!}{(\kappa!)^{\frac{K}{\kappa}}}$. Thus, the total run time complexity for each episode is $\mathcal{O}(KT + M)$ and there are N episodes. Hence, the run-time complexity of Algorithm 3.1 is $\mathcal{O}(KTN + \frac{K!}{(\kappa!)^{\frac{K}{\kappa}}}N)$, as desired. □

Also note that the communication overhead is $\mathcal{O}(KT)$ because the HAP needs to communicate to all K devices in each episode, i.e., T frames, to schedule their uplink data transmissions. The communication overhead is less than $1/N$ compared to the run-time, where N is the number of episodes.

Algorithm 3.1: Pseudocode of discrete optimization.

$S^1 = i = \mathcal{U}(\Phi)$
$\mathcal{P}[1, i] = 1$, $\mathcal{P}[1, m] = 0$ for all $m = 1, \ldots, M \setminus i$.
for $n = 1, \ldots, N$ **do**
  for $t = 1, \ldots, T$ **do**
    Use S^n and calculate $F^t(S^n)$
  end
  Obtain reward $Q[n, S^n]$ as per Equ. (3.21)
  $\hat{S}^n = \mathcal{U}(\Phi \setminus S^n)$
  for $t = 1, \ldots, T$ **do**
    Use $\hat{S}^n$ and calculate $F^t(\hat{S}^n)$
  end
  Obtain reward $Q[n, \hat{S}^n]$ as per Equ. (3.21)
  if $Q[n, S^n] > Q[n, \hat{S}^n]$ **then**
    set $S^{n+1} = S^n$
  else
    set $S^{n+1} = \hat{S}^n$
  end
  $\boldsymbol{\mathcal{P}}[n+1] = \boldsymbol{\mathcal{P}}[n] + \mu[n+1](\boldsymbol{\mathcal{S}}[n+1] - \boldsymbol{\mathcal{P}}[n])$
end
Return $S^* = \arg\max_{s \in \Phi} \mathcal{P}[N+1, s]$

Next, the next result shows that Algorithm 3.1 converges to the optimal solution, where it will eventually spend more time in the state or transmission schedule with the maximum average system throughput. The previous claim uses the following result from [124]:

Proposition 3.3. *Let S^*, S and $\tilde{S}$ be transmission schedules, where $S^* \neq S$ and*

$S^* \neq \tilde{S}$, Algorithm 3.1 converges to the optimal transmission schedule S^* subject to,

$$P\{Q[n, S^*] > Q[n, S]\} > P\{Q(n, S) > Q[n, S^*]\} \tag{3.22}$$

$$P\{Q[n, S^*] > Q[n, \tilde{S}]\} > P\{Q[n, S] > Q[n, \tilde{S}]\}. \tag{3.23}$$

Inequality (3.22) represents the fact that for any episode n, the optimal transmission schedule S^* has a higher probability than transmission schedule S because $Q[n, S^*]$ has a higher value than $Q[n, S]$. Similarly, inequality (3.23) represents the probability that the optimal transmission schedule is preferred over any other transmission schedule $\tilde{S} \in \Phi$. The next proposition proves Algorithm-3.1 meets inequalities (3.22) and (3.23), and thus it is optimal.

Proposition 3.4. *Algorithm-3.1 finds the optimal transmission schedule S^*.*

Proof. The quantity $Q[n, S]$ can be approximated as a Gaussian distribution $\mathcal{N}(\mu, \sigma^2)$ according to the Central Limit Theorem; this is reasonable as it is a sum of independent data rate from each EHD. The variance σ^2 is in the finite range $[0, M \times R_{max}]$, where R_{max} is the maximum data rate supported by an EHD. Note that the transmit power of EHDs is bounded by their battery capacity $\mathcal{B}$. Hence, MR_{max} is also bounded. Denote the mean and variance of $Q[n, \omega]$ by μ_ω and σ^2_ω, respectively. Consider three schedules S^*, S and $\tilde{S}$. Assume μ_{S^*} is larger than μ_S and $\mu_{\tilde{S}}$. Referring to (3.22), as $Q[n, S^*] > Q[n, S]$, it has $\mu_{S^*} > \mu_S$. Rewriting (3.22), we have

$$P\{(Q[n, S^*] - Q[n, S] > 0\}) > P\{(Q[n, S) - Q[n, S^*]) > 0\}.$$

The previous inequality can be rewritten as,

$$P\{\big(\mathcal{N}(\mu_{S^*}, \sigma^2_{S^*}) - \mathcal{N}(\mu_S, \sigma^2_S)\big) > 0\} > P\{\big(\mathcal{N}(\mu_S, \sigma^2_S) - \mathcal{N}(\mu_{S^*}, \sigma^2_{S^*}\big) > 0\}. \tag{3.24}$$

Equivalently, it has

$$P\{\mathcal{N}(\mu_{S^*} - \mu_S, \sigma_{S^*}^2 + \sigma_S^2) > 0\} > P\{\big(\mathcal{N}(\mu_S - \mu_{S^*}, \sigma_S^2 + \sigma_{S^*}^2\big) > 0\}. \quad (3.25)$$

As the variance is the same, it thus has $\mu_{S^*} - \mu_S > \mu_S - \mu_{S^*}$. This proves Algorithm-3.1 satisfies (3.22). The steps above also show that Algorithm-3.1 satisfies (3.23), and noting that transmission schedules have the same variance. □

3.5 A Heuristic Approach

This section presents an approach that does not require the HAP to have all possible transmission schedules.

3.5.1 Overview

An overview of the approach is depicted in Figure 3.3. Initially, the HAP applies a TDMA schedule whereby each slot contains one EHD; i.e., there is no SIC. After that, the HAP selects an upload slot and attempts to move each EHD in the selected slot into a new slot. In particular, the HAP always select the slot that contains the fewest number of EHDs. The main idea is to maximise the number of EHDs in each slot, and thereby, reduce the overall schedule length. However, a challenging issue is that EHDs in the same time slot may not meet the SINR threshold requirement. Hence, it is important that EHD(s) that are moved into a slot have a suitable received power difference with existing EHD(s) in the slot. Therefore, when moving a EHD into another slot, the HAP first calculates the power difference between the EHD to existing EHDs in all other slots. It then moves the EHD into the slot that has the maximum received power difference; see details in later section. After relocating an EHD, the HAP compares the reward, i.e., the throughput, of the revised schedule. If the new schedule leads to a higher reward, the new schedule is adopted. Otherwise,

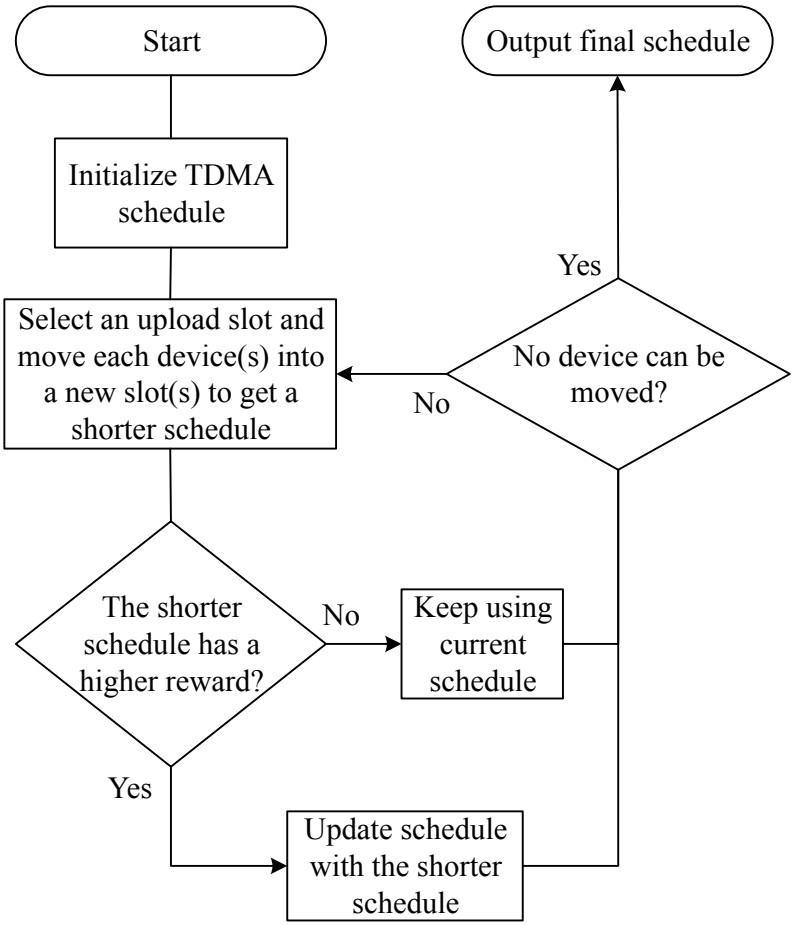

Figure 3.3: Flowchart of the heuristic approach.

the HAP reverts back to the old schedule and proceeds to the next iteration. The HAP then identifies the next EHD to be moved and the above process repeats. The algorithm/scheduler ends when it can no longer move a device(s) from any slots.

3.5.2 Preliminaries

Similar to the discrete optimization approach proposed in Section 3.4, the heuristic approach also operates over $n = 1, \ldots, N$ episodes. Each episode consists of two superframes, which are divided into T frames; each frame consists of a charging and a transmit phase. Using S^n and $\hat{S}^n$ to denote the transmission schedule in the first and the second superframes of episode n, respectively. Recall that there are k EHDs. Define $g^n[k, m]$ as the received power difference at the HAP between device D_k and device D_m in episode n, where $k, m \in \{1, \ldots, K\}$. It is calculated as follows. Let

$\hat{\gamma}(k,n)$ be the average received power from EHD D_k to the HAP over T frames in one superframe of episode n,

$$\hat{\gamma}(k,n) = \frac{1}{T}\sum_{t=1}^{T}\gamma_k^t \tag{3.26}$$

Let $\overline{\gamma}(k)$ be the average received power from EHD D_k to the HAP over the first to the n-th episodes, which is,

$$\overline{\gamma}(k) = \frac{1}{n}\sum_{\nu=1}^{\nu=n}\hat{\gamma}(k,\nu) \tag{3.27}$$

Then, the average received power difference $g^n[k,m]$ is calculated as,

$$g^n[k,m] = |\overline{\gamma}(m) - \overline{\gamma}(k)| \tag{3.28}$$

Recall that $\mathcal{C}(S^n,\omega)$ represents the transmission set in upload slot ω of schedule S^n, where $\omega = 1,\ldots,|S^n|$. Let $G(m,\omega)$ be the minimum gap between device D_m and all devices in the upload slot ω. In other words,

$$G(m,\omega) = \text{MIN}\{g^n[k,m] \mid k \in \mathcal{C}(S^n,\omega)\} \tag{3.29}$$

Note that, $G(m,\omega) = 0$ if slot ω reaches the maximum decoding capacity κ, i.e., $|\mathcal{C}(S^n,\omega)| = \kappa$. Let $\hat{\omega}$ be the index of upload slot that contains the minimum number of devices. In other words,

$$\hat{\omega} = \underset{\omega=1,\ldots,|S^n|}{\arg\min}\{|\mathcal{C}(S^n,\omega)|\} \tag{3.30}$$

As represented in Section 3.5.1, the aim is to move device(s) in slot $\hat{\omega}$ to another slot. Specifically, a device D_m will be moved to slot $\omega^*(m)$ which has the maximum

minimum power gap. That is,

$$\omega^*(m) = \underset{\omega \in \{1,\dots,|S^n|\} \setminus \{\hat{\omega}\}}{\arg\max} \{G(m,\omega)\}, \quad \forall m \in \mathcal{C}(S^n, \hat{\omega}) \tag{3.31}$$

The motivation for the previous expression is to ensure transmissions have the highest possible SINR. This ensures the HAP be able to decode each transmission, and thus subtract it from the interference of subsequent transmissions.

3.5.3 Step by Step Details

This subsection presents the proposed heuristic protocol in Algorithm 3.2. Initially, the protocol uses TDMA schedule as S^1.

The algorithm then runs for N episodes. In each episode n, given schedule S^n, the algorithm first obtains its average reward $Q[n, S^n]$ over T frames, as shown from line 3 to line 6; it then calculates the average received power $\overline{\gamma}(k)$ for each EHD k over n episodes, see line 7. Here, note that schedule S^n changes in different episodes, thus, the received power from EHD k also changes according to the schedule length, i.e., the received power is in proportion to the number of upload slot of a schedule. Therefore, in order to calculate the average received power from EHD k, it is needed to normalise $\hat{\gamma}(k,n)$ in Equ. (3.27) to a unit upload slot. After that, the algorithm finds an upload slot $\hat{\omega}$ with the minimum number of devices; see line 8. Then for each device in slot $\hat{\omega}$, the algorithm determines a destination slot for the device; i.e., $\omega^*(m)$ in line 11. It then moves each device $m \in \mathcal{C}(S^n, \hat{\omega})$ to $\omega^*(m)$ and obtains a new schedule $\hat{S}^n$; see line 12. Given the new schedule, the algorithm calculates the average reward over T frames, see line 14 to line 17; compare the average reward of schedule $\hat{S}^n$ against that of the original schedule S^n and update the schedule with the one has higher reward, see line 18 to line 21. In subsequent episodes, the algorithm iteratively moves the device(s) in $\mathcal{C}(S^n, \hat{\omega})$ to $\omega^*(m)$ and generates a new schedule $\hat{S}^n$ in each episode. The algorithm terminates when the current schedule reaches the minimum length, i.e., $|S^{n+1}| = \lceil \frac{K}{\kappa} \rceil$ from line 23 to line 24. This means

that no device can be moved because all other slots are at the maximum decoding capacity.

Algorithm 3.2: Pseudocode of the heuristic solution.

$S^1 = \{\{1\}, \{2\}, \cdots, \{K\}\}$
for $n = 1, \ldots, N$ **do**
  for $t = 1, \ldots, T$ **do**
    Use S^n to calculate $F^t(S^n)$ and γ_k^t
  end
  Obtain reward $Q[n, S^n]$ as per Equ. (3.21)
  Calculate $\overline{\gamma}(k)$ as per Equ. (3.26) and Equ. (3.27)
  Find $\hat{\omega}$ as per Equ. (3.30)
  for $m \in \mathcal{C}(S^n, \hat{\omega})$ **do**
    Calculate $G(m, \omega)$ as per Equ. (3.29) and $G(m, \omega) = 0$ if $|\mathcal{C}(S^0, \hat{\omega})| = \kappa$
    Obtain $\omega^*(m)$ as per Equ. (3.31)
    Move device D_m to slot $\omega^*(m)$ to generate a new schedule $\hat{S}^n$
  end
  for $t = 1, \ldots, T$ **do**
    Use $\hat{S}^n$ to calculate $F^t(\hat{S}^n)$
  end
  Obtain reward $Q[n, \hat{S}^n]$ as per Equ. (3.21)
  if $Q[n, \hat{S}^n] > Q[n, S^n]$ **then**
    set $S^{n+1} = \hat{S}^n$
  else
    set $S^{n+1} = S^n$
  end
  if $|S^{n+1}| = \lceil \frac{K}{\kappa} \rceil$ **then**
    Break
  end
end
Return $S^* = S^{n+1}$

Proposition 3.5. *The run time complexity of the heuristic solution is* $\mathcal{O}((T + \kappa)KN + N^2)$.

Proof. In each episode, the heuristic solution first calculate the received power γ_k^t for all K devices and obtain $F^t(S^n)$ over T frames. This step has a run time complexity of $\mathcal{O}(KT)$. Next, it calculate reward $Q[n, S^n]$ by summing all $F^t(S^n)$ for $t = 1, \ldots, T$, which has a run time complexity of $\mathcal{O}(T)$. It then calculate $\overline{\gamma}(k)$ by averaging from the first episode to the current episode n, which run time complexity

Table 3.1: Simulation Parameters

Parameter	**Value(s)**
Proportion of charging duration and data transfer duration in a frame	1:1
The HAP's transmit power P [125]	30 dBm (1 Watt)
Antenna gain for HAP and EHDs	3 dBi and 2 dBi as per the Waspmote datasheet[2]
Slow fading variance σ [126]	3 dB
Path loss $\mathcal{L}_0$ at reference distance 1 m [126]	30 dB
Path loss exponent α [126]	2.5
Parameters for non-linear energy harvesting model ζ_1, ζ_2 and ζ_3 [119]	150, 0.014 and 24mW
Noise variance σ_0^2 [127]	-80 dBm
Bandwidth B [127]	1 MHz

[2] http://www.libelium.com

is $\mathcal{O}(n)$ and total of $\mathcal{O}(\frac{N(N+1)}{2}) = \mathcal{O}(N^2)$ over all episodes. After this, the algorithm takes $\mathcal{O}(|S^n|)$ time to find $\hat{\omega}$, and $\mathcal{O}(|\mathcal{C}(S^n, \hat{\omega})||S^n|)$ time to calculate $\omega^*(m)$ and moving. Note that $|\mathcal{C}(S^n, \hat{\omega})| \leq \kappa$ and $|S^n| \leq K$. Thus, these steps, i.e., line 8-12, have a total run time complexity of $\mathcal{O}(\kappa K)$. The algorithm then takes $\mathcal{O}(KT)$ to run and calculate the reward of new schedule. Therefore, the total run time of heuristic solution over N episodes is $\mathcal{O}((KT + \kappa K)N + N^2) = \mathcal{O}((T + \kappa)KN + N^2)$. □

3.6 Evaluation

The following parameters are used for the non-linear energy harvesting model [119]: $\zeta_1 = 150$, $\zeta_2 = 0.014$ and $\zeta_3 = 24$. The sensing field is a circle with a radius of 10 meters. It places the HAP at the centre of circle and randomly deploy EHDs with an uniform probability. There are three sets of experiments that are used to demonstrate the convergence of discrete optimizer, and then evaluate the proposed approaches in small and large scale random networks. Other simulation parameters are shown in Table 3.1 or in the corresponding subsections. In particular, the values of noise variance and bandwidth are derived from LTE CAT-M standard.

3.6.1 Convergence of discrete optimizer

This section studies the convergence of the proposed discrete optimization algorithm to the best schedule. The number of frames in each super-frame of the discrete optimization approach is set to 20. The network places three EHDs D_1, D_2 and D_3 at 6.4, 3.1 and 4.7 meters away to the HAP, respectively. In this case, there are five possible transmission schedules: $S_1 = [(D_1, D_2, D_3)]$, $S_2 = [(D_1), (D_2, D_3)]$, $S_3 = [(D_2), (D_1, D_3)]$, $S_4 = [(D_3), (D_1, D_2)]$ and $S_5 = [(D_1), (D_2), (D_3)]$. Recording the occupancy probability of these schedules for the following SINR threshold β values: 0, 2, 4 dB.

Figure 3.4 shows the occupancy probability of all schedules fluctuates significantly in the first 200 episodes. This is because the initially selected schedule has an occupancy probability of one but it may not have a high reward. Consequently, the HAP continues to select other schedules. In addition, the step size $1/n$ is large initially. Therefore, in each episode, the schedule with a large reward will have a large occupancy probability. With increasing number of episodes, the step size reduces, which allows the algorithm to converge to the schedule with the best reward.

It shows from Figures 3.4a and 3.4c that there exists a best schedule for each SINR threshold. In Figure 3.4a and Figure 3.4b, when $\beta = 0$ dB and 2 dB, schedule [(D1, D2, D3)] has the highest occupancy probability. However, when $\beta = 4$ dB, see Figure 3.4c, the occupancy probability of schedule [(D1, D2, D3)] decreased significantly. In contrast, schedule [(D3), (D1, D2)] becomes the best schedule. This is expected because when the SINR threshold β is small, more transmitting devices can co-exist together in the same time slot, which results in a higher throughput. Conversely, a large β value results in more SIC failures.

The next study concerns the average throughput of all five schedules for different SINR threshold values. A brute-force method is used to calculate the average throughput by running each schedule for 1000 frames as per Equ. (3.21). From Figure 3.5a, it shows that the performance of these schedules is consistent with the

occupancy probability shown in Figure 3.4. Specifically, when $\beta = 0$ dB, schedule [(D1, D2, D3)] achieves an average throughput of 8.3 Mbps. It also has the highest occupancy probability of around 0.97 as shown in Figure 3.4a. This is expected as the difference in received power can be low in order for SIC to be successful. Then with an increasing SINR threshold from 0 dB to 2 dB, the throughput of schedule [(D1, D2, D3)] experiences a significant decrease from 8.3 to 6.8 Mbps, which also

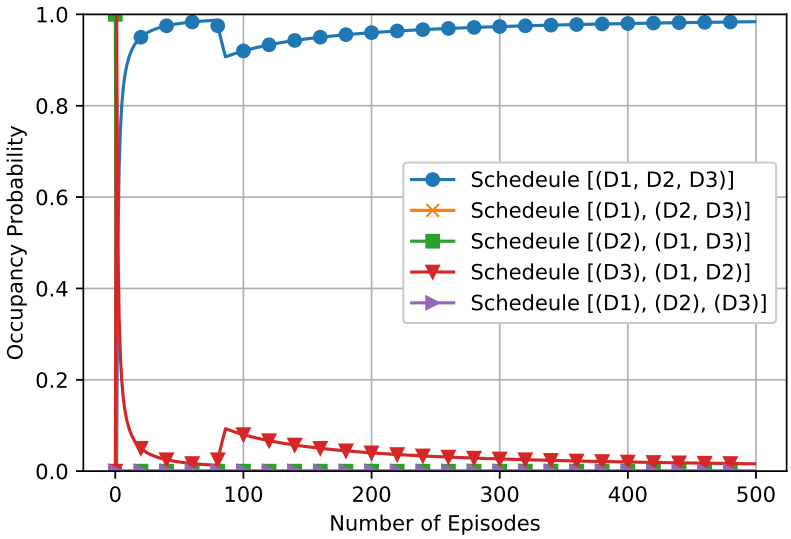

(a)

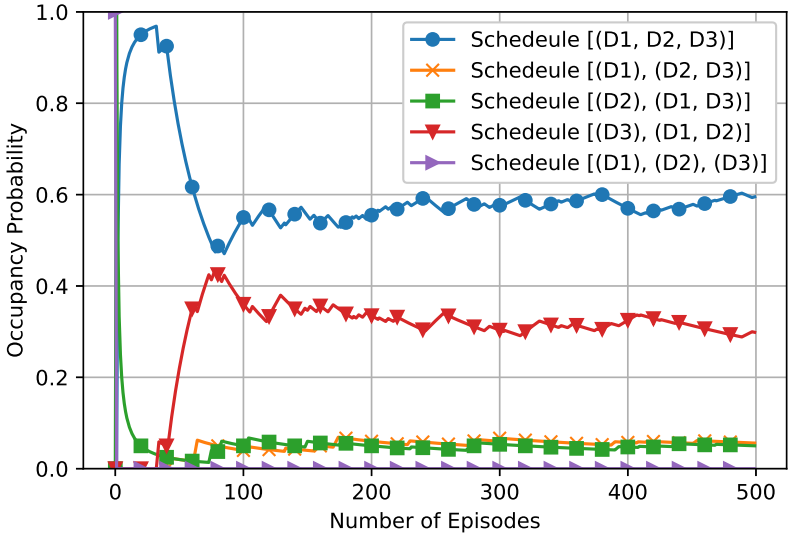

(b)

Figure 3.4: Occupancy probability for three EHDs with five schedules under different SINR thresholds: (a) $\beta = 0$ dB, (b) $\beta = 2$ dB, (c) $\beta = 4$ dB.

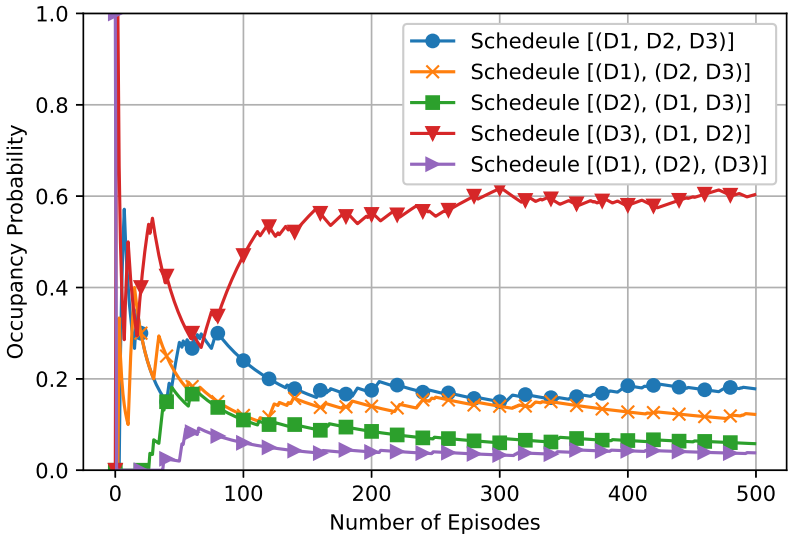

(c)

Figure 3.4: Occupancy probability for three EHDs with five schedules under different SINR thresholds: (a) $\beta = 0$ dB, (b) $\beta = 2$ dB, (c) $\beta = 4$ dB. (cont.)

causes its occupancy probability to drop from nearly 1.0, see Figure 3.4a, to 0.6, see Figure 3.4b. Finally, when β exceeds 3 dB, schedule [(D3), (D1, D2)] achieves an average throughput of 5.6 Mbps, which outperforms schedule [(D1, D2, D3)]. This means schedule [(D3), (D1, D2)] has the highest occupancy probability of around 0.6.

This last experiment first obtains the best schedule using the proposed solution. It then compares the throughput of the best schedule with the TDMA schedule and Slotted Aloha. Briefly, TDMA schedule refers to the schedule that only allows one device to transmit in a given upload slot. The Slotted Aloha schedule has a given slot number, where EHDs randomly select a slot to transmit. These experiments study different SINR threshold β values and number of EHDs K. The average system throughput is calculated over 500 frames as per Equ. (3.21).

Figures 3.5b and 3.5c compare the best schedule computed by the approach against the TDMA schedule and Slotted Aloha schedule over different SINR threshold β values and number of EHDs K. As explained earlier, there is a corresponding best schedule for a given β value. Therefore, the best schedule shown in Figure 3.5b

contains two schedules, i.e., [(D1, D2, D3)] and [(D3), (D1, D2)] under different β values.

Figure 3.5b shows the impact on the average throughput for different SINR thresholds. It considers the topology with three EHDs. Notice that, with the increase of SINR threshold, both of the best schedule and Slotted Aloha schedule

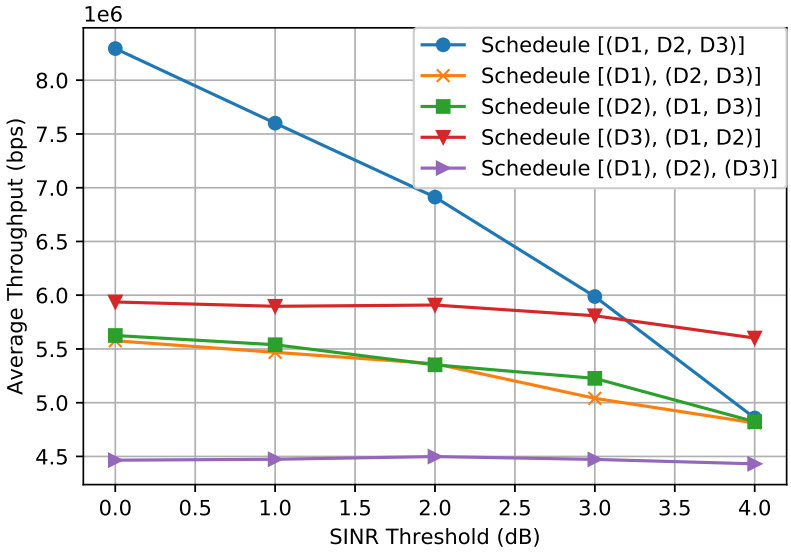

(a)

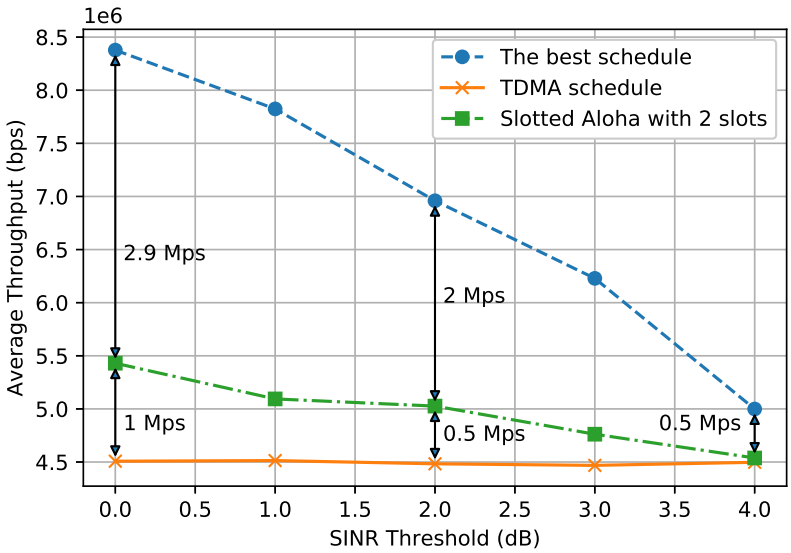

(b)

Figure 3.5: (a) Average system throughput for $K = 3$ EHDs with five schedules under different SINR thresholds; (b) A comparison of average throughput when there are $K = 3$ EHDs under different SINR thresholds; (c) Average system throughput with $\beta = 2$ dB versus number of EHDs.

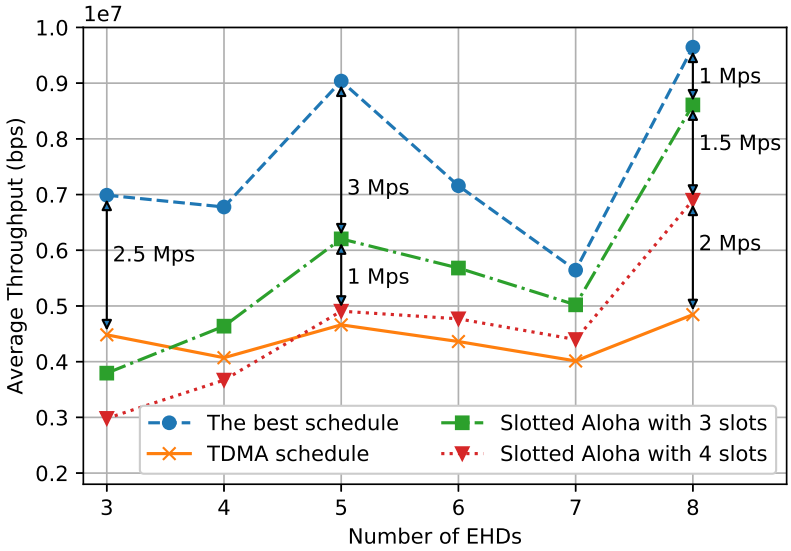

(c)

Figure 3.5: (a) Average system throughput for $K = 3$ EHDs with five schedules under different SINR thresholds; (b) A comparison of average throughput when there are $K = 3$ EHDs under different SINR thresholds; (c) Average system throughput with $\beta = 2$ dB versus number of EHDs.(cont.)

experience throughput degradation. As explained earlier, a large β value means there needs to be a high received power difference in order to ensure a successful SIC. As a result, there is a higher chance of SIC failures. In addition, when $\beta = 0$ dB, the throughput obtained by the best schedule is 1.5 times of the throughput by Slotted Aloha, and nearly twice the throughput of TDMA. When $\beta = 2$ dB, the best schedule outperforms Slotted Aloha by 2 Mps. The performance of Slotted Aloha is the same as TDMA when $\beta = 4$ dB. the schedule outperforms them by 0.5 Mbps. Note that in high interference scenarios or the required SINR threshold is a very large value. An orthogonal multiple access approach TDMA would typically be the optimal uplink schedule that leads to the maximum sum-rate.

Figure 3.5c compares the average throughput of different schedules over different number of EHDs. The SINR threshold β is set to 2 dB. First, note that since β is small, the probability of SIC failure is low. Therefore, the Slotted Aloha schedule with three slots outperforms the case with four slots. This is because there are more EHDs in each time slot. Moreover, when $K = 3$, TDMA outperforms both Slotted

Aloha with three and four slots. The reason is because Slotted Aloha randomly select EHDs into different slots, which may lead to idle slot(s). Consequently, the resulting schedule has a low throughput. Figure 3.5c also shows that the best schedule from the solution achieves the highest throughput, which outperforms Slotted Aloha by 50% when there are five EHDs.

3.6.2 Small scale random networks

This section contains an evaluation of the heuristic approach, discrete optimization, Frame Slotted Aloha and TDMA in small scale networks with five devices. Specifically, the heuristic approach is run three times with 1, 50, and 200 frames, denoted as HA-1, HA-50 and HA-200, respectively. Frame Slotted Aloha has two or three slots, which is denoted as FSA-2 and FSA-3, respectively. In addition, this section shows the throughput when the HAP has perfect CSI, denoted as pSIC; that is, the HAP constructs a schedule using perfect CSI where each slot contains the maximum number of transmissions that it decode successfully using SIC. In the first experiment, the average throughput is computed over 100 random network realizations. The second experiment studies the convergence time of discrete optimization and heuristic approach using 1, 50, and 200 frames. In particular, the discrete optimization is assumed to converge if one schedule has the highest occupancy probability over 100 subsequent episodes. Similarly, the heuristic approach converges if the learned best schedule does not change over 100 subsequent episodes. The results are averaged based on 500 topologies realizations.

From Figure 3.6, it shows that the perfect SIC achieves the highest throughput. This is reasonable because the perfect SIC scheduling is based on exact CSI information, thus it enables SIC to be successful in each upload slot. In addition, it shows that with the increase of SINR threshold, the throughput of perfect SIC first increases reaching the maximum when $\beta = 2$ dB, and then reduces. This is because when SINR threshold is very small, i.e., less than 2 dB, there is a high

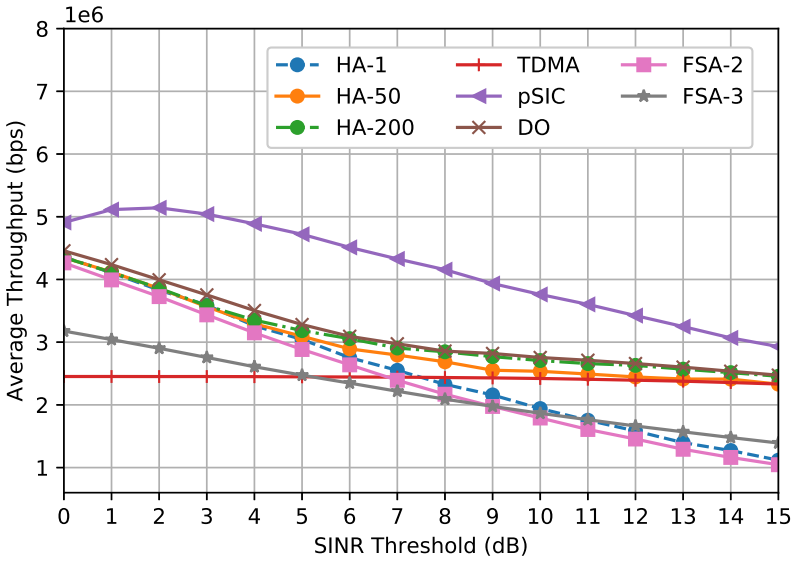

Figure 3.6: Average throughput of heuristic approach with 1 (HA-1), 50 (HA-50) and 200 frames (HA-200), discrete optimization, Frame Slotted Aloha with two (FSA-2) and three slots (FSA-3), perfect SIC and TDMA under different SINR thresholds in random networks with five devices.

probability that SIC will success between any devices. However, such simultaneously transmission does not guarantee a high throughput because the difference in received power does lead to a SINR that exceeds the required threshold. Moreover, the throughput of HA-50, HA-200, discrete optimization and perfect SIC reduce and approach TDMA with the increasing of SINR threshold. This is because there are more SIC failures and eventually no simultaneously transmission occurs. From Figure 3.6, it shows that HA-200 outperforms HA-1 and HA-50, especially when SINR threshold is greater than 5 dB. This is because the estimated received power for each device is more accurate with more frame realizations. Thus, HAP has a higher chance of learning a better transmission schedule. Another observation is that discrete optimization outperforms heuristic approach by about 10^5 bps when SINR threshold is less than 6 dB. This is because discrete optimization learns the best schedule by measuring the reward of all possible schedules. However, with increasing SINR thresholds, the throughput of discrete optimization is the same as HA-200 and approaches TDMA due to SIC failures.

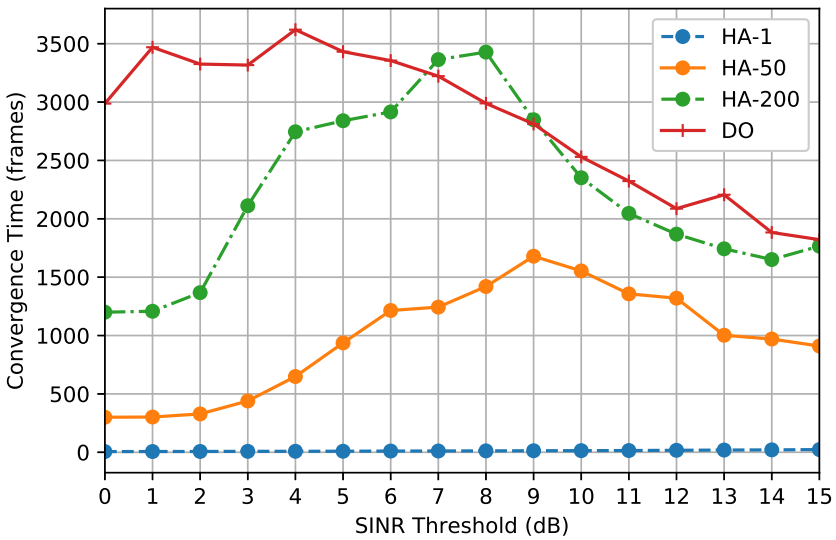

Figure 3.7: Convergence time in frames of discrete optimization, heuristic approach with 1 (HA-1), 50 (HA-50) and 200 frames (HA-200) in five device random networks.

Lastly, Figure 3.6 shows that the throughput of FSA-3 is lower than FSA-2 when SINR threshold is less than 9 dB. This is because when there are three fixed slots, the probability that a slot has not been assigned any device to transmit is higher than that with two slots. Thus, FSA-3 wastes more transmit opportunities than FSA-2 and results lower throughput. However, when SINR threshold is greater than 9 dB, FSA-3 has a higher throughput than FSA-2. This is because the probability of SIC failure increases and FSA-2 has more simultaneously transmissions than FSA-3 in each upload slot. Thus, FSA-2 is easier to result in a low throughput. Also note that, HA-1 has a similar throughput as FSA-2. This is because HA-1 arbitrarily generates a schedule based on an estimated over one frame. Thus, it has a similar performance as the random approach, e.g., Frame Slotted Aloha.

Figure 3.7 shows the convergence time of discrete optimization and heuristic approach with 1, 50, and 200 frames under small scale networks. It shows that the discrete optimization converges after more than 3000 frames when SINR threshold is between 0 and 7 dB. This is because when the SINR threshold is small, any combination of simultaneously transmissions has a high chance of success. Thus, schedules with many simultaneous transmissions may have a similar reward. There-

fore, discrete optimization requires a longer time to find the best schedule. However, it shows that the convergence time reduces gradually with higher SINR thresholds. This is because SIC failures occur, which enlarge the difference in received reward between schedules. This allows discrete optimization to find the best schedule quickly. On the other hand, the convergence time of HA-50 and HA-200 first increases and then reduces with increasing SINR thresholds. This is because when SINR threshold is small, heuristic approach is able to successfully move any device to any slot. Thus, it quickly reaches the maximum decoding capacity. In contrast, when the SINR threshold is large, i.e., larger than 12 dB, it likely retains the TDMA schedule because any simultaneously transmitting leads to SIC failure.

Note that when the SINR threshold is between 7 and 9 dB, the convergence time of HA-200 is higher than that of DO in terms of frames. This is because HA-200 has 200 frames in each superframe. However, DO only has 20 frames in each superframe. Recall that both DO and HA calculate the average throughput of two schedules in both super-frames. After that it selects the schedule with a higher throughput. When the SINR threshold is 8 dB, HA-200 converges to a schedule after 9 episodes, whilst DO converges to a schedule after 75 episodes. However the convergence time of HA-200 is 3600 frames, which is still larger than the required convergence time of DO, which is 3000 frames.

Another observation from Figure 3.7 is that the convergence time of HA-1 is much lower than that of HA-50 and HA-200. The reason is because the heuristic approach arbitrarily moves devices to transmit simultaneously due to the lack of accurate estimation of the average received power. Thus, the approach converges fast as it quickly reaches the maximum decoding capacity. However, recall that in Figure 3.6, the average throughput of HA-1 is significantly lower with maximum gap of more than 10^6 bps than that of HA-50 and HA-200, especially when SINR threshold is larger than 6 dB.

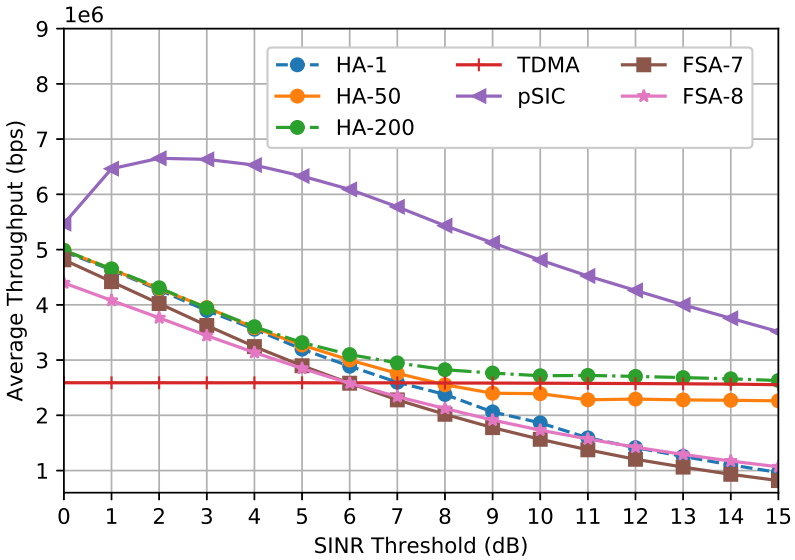

Figure 3.8: Average throughput of the heuristic approach with 1 (HA-1), 50 (HA-50) and 200 frames (HA-200), Frame Slotted Aloha with seven (FSA-7) and eight slots (FSA-8), perfect SIC and TDMA under various SINR thresholds in 20 devices networks.

3.6.3 Large scale random networks

This set of experiments compares the heuristic approach, perfect SIC, and Frame Slotted Aloha with TDMA in large scale networks with 20 EHDs. Similar to the small scale simulations, this section also evaluates the heuristic approach with 1, 50, and 200 frames. Note that, given the maximum decoding capacity of three, the minimum schedule length is six slots. Therefore, Frame Slotted Aloha uses seven and eight slots, which are denoted by FSA-7 and FSA-8, respectively. The average throughput is obtained over 500 random network realizations. After that, this section investigates the average throughput under different number of EHDs when the SINR threshold is fixed to 4 dB. Both results are averaged based on 100 networks realizations.

Figure 3.8 shows the average throughput is the highest if the HAP has perfect SIC, see the curve for pSIC. Also note that, the throughput of pSIC first increases and then reduces with increasing SINR threshold. This is consistent with the results for small scale networks as shown in Section 3.6.2. On the other hand, notice that

HA-50 has a lower throughput than TDMA when the SINR threshold is greater than 8 dB. This is because the estimates of devices received power when using HA-50 is inaccurate, and thus, SIC failures occur and lead to a lower throughput. In contrast, the throughput of HA-200 is always higher than TDMA. This is because HA-200 has more accurate estimation than HA-50. Moreover, the throughput of HA-1, FSA-7 and FSA-8 reduces with increasing SINR thresholds. These results are consistent with those in the small scale networks; see Section 3.6.2.

3.7 Conclusion

An important problem in future IoT systems is to collect data from RF-energy harvesting devices. To this end, this chapter outlines an uplinks scheduling problem from these devices. Specifically, it outlines a novel problem whereby a HAP has to select the best transmission schedule without CSI knowledge. This problem is significant because it allows a HAP to collect data without first collecting CSI. To solve the said problem, this chapter contains a discrete optimization approach to find the best one among all possible schedules. However, the number of schedules increases exponentially with the number of devices. Thus, it proposes a heuristic approach that allows the HAP to learn the best schedule. The simulation results show that both proposed solutions are able to find a "good" schedule even though the HAP has imperfect CSI. Moreover, the results show that the heuristic approach is able to compute a solution for large-scale networks and has a near optimal solution as compared to the discrete optimization approach in small networks.

The proposed link scheduling does not consider energy trade-off between data sampling and transmissions, or study how it affects the number of samples collected by the HAP over T time slots. These limitations are addressed in Chapter 4.

Chapter 4

Link Scheduling for Ambient Backscatter assisted WPCN

This chapter aims to maximize the number of uploaded samples by devices in wireless powered Internet of Things (IoTs) networks. To do so, it takes advantage of ambient backscatter communications (AmBC) to help sensor devices conserve energy, and thus leaving them with more energy to collect samples. Specifically, this chapter contains the following contributions:

- It considers hybrid devices with the following operation modes: (a) sampling, (b) data upload to the HAP via their conventional radio, (c) transmit samples via AmBC to a neighbour, or (d) receive data via AmBC from a neighbour. Note that, feature (c) and (d) mean any device can become a relay if doing so helps increase the number of samples that arrive at the HAP in future time slots.

- It contains a novel Mixed Integer Linear Program (MILP) for determining the operation mode of each device in each time slot. Its objective is to maximise the amount of samples collected over a given time horizon. It also presents a heuristic approach that allows the HAP to efficiently schedule the operation

mode of each device in large scale IoT networks. It uses two weights that correspond to a device's preference as to whether it should transmit via its conventional radio or AmBC.

- Lastly, it contains a mathematical analysis that compares the total uploaded data in cases with and without AmBC. The analysis shows that equipping devices with AmBC does lead to more samples at the HAP. The analysis shows rigorously that even when all devices have sufficient energy, there exists a real value n, which is the number of devices gathering backscattered data from neighbours, whereby a AmBC-assisted system uploads more samples than one without AmBC. In addition, this chapter shows that n is lower and upper bounded by the number of channels, number of time slots, sampling rate, uploading and backscattering data rates.

The rest chapter is structured as follows, Section 4.1 shows a toy example to illustrate the research problem. Section 4.2 presents the system model and notation. The MILP is presented in Section 4.3 followed by the proposed heuristic in Section 4.4. Section 4.5 discusses the simulation methodology and results. Section 4.6 concludes this chapter .

4.1 Toy Model

This section shows a novel AmBC assisted wireless powered IoT network; see Figure 4.1. In this network, devices have the ability to transmit data via their conventional radio or use AmBC; such hybrid devices have been studied in [43, 91, 92, 94, 101]. A Hybrid Access Point (HAP) first supplies energy to charge these devices. Using their harvested RF energy, they then collect one or more samples and transmit these samples to the HAP. A unique feature of the said IoT network is that devices have the option of transmitting their sample(s) directly to the HAP using their conventional radio, which incurs non-negligible energy cost, or take advantage of AmBC

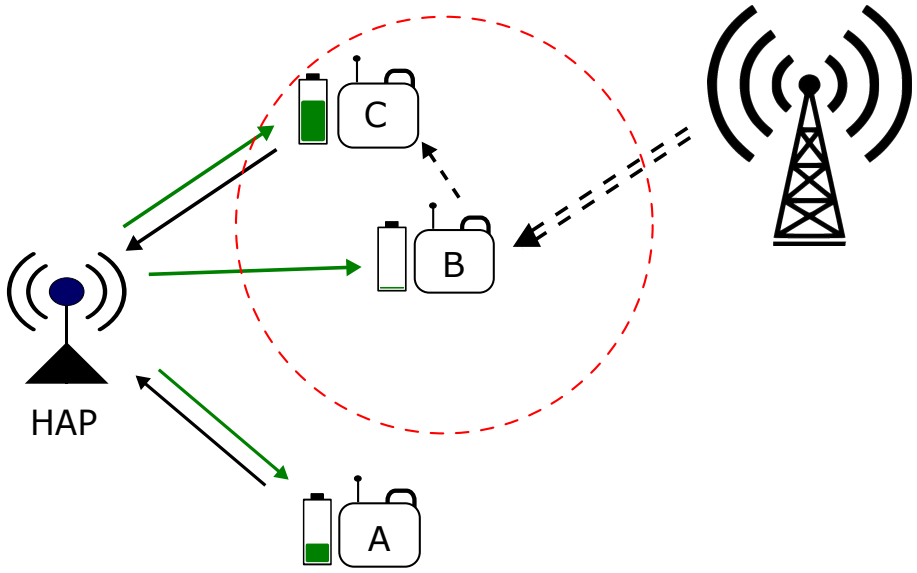

Figure 4.1: An example of an AmBC assisted wireless powered IoT network. The green and black arrows represent the RF energy transfer and the data upload. The dashed red circle indicates the AmBC's transmission range. The double dashed arrow represents ambient RF signals from an existing energy source and the single dashed arrow represents data transmission via AmBC.

to relay data to another device. For example, as shown in Figure 4.1, assume device B has insufficient energy to power its conventional radio. It thus backscatters its samples to device C with negligible energy cost. Device C then collects and packages all samples before sending them to the HAP using its conventional radio.

Given the aforementioned network, this chapter studies a *novel* problem: maximise the number of samples uploaded by AmBC capable devices over multiple slots. A key consideration is the fundamental trade-off between the energy used for sampling, and data transmissions over a conventional radio or AmBC.

4.2 System Model

Let $\mathcal{I}$ be the set of devices with index i, where $i \in \mathcal{I} = \{1, \ldots, I\}$. The system considers a Harvest-Sample-Transmit (HST) model. Figure 4.2 shows an example of the HST model; the HAP h first charges all devices in $\mathcal{I}$ via RF for λ seconds followed by a Sample-Transmit period. Using the harvested energy, each device samples and transmits its sampled data to the HAP during the Sample-Transmit period. Observe

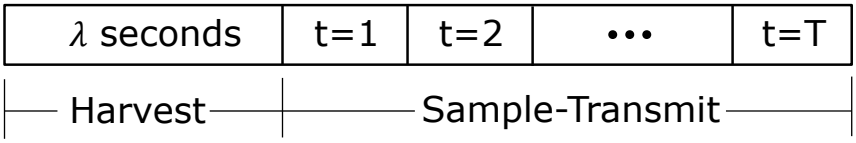

Figure 4.2: An example of the HST model.

that the Sample-Transmit period is divided into T time slots. Each time slot has duration τ (in seconds) and is indexed by t, where $t \in \mathcal{T} = \{1, \ldots, T\}$. In each time slot t, the HAP determines sampling and transmission operations, i.e., *uploading*, *backscatter transmission* or *backscatter reception* of all devices. Binary variables s_i^t, u_i^t, b_i^t and r_i^t are used to indicate whether device i is in the following modes: sampling, uploading, backscatter transmission (B-tx) or backscatter reception (B-rx). The corresponding binary indicator is set to one if a device is in a given mode, and zero otherwise. Further details regarding constraints related to the above binary indicators will be detailed in Sections 4.2.2 and 4.2.3.

4.2.1 RF Energy Harvesting Model

By using g_i to indicate the channel coefficient between the HAP and device $i \in \mathcal{I}$ and it is given by,

$$g_i = \kappa d_{hi}^{-\alpha}, \tag{4.1}$$

where d_{hi} is the distance from HAP to device i, and κ and α are the path loss and environment components, respectively. Hence, using Equ. (4.1), the incident RF power at device i is

$$p_i = P\kappa d_{hi}^{-\alpha}, \tag{4.2}$$

where P is the HAP's transmit power. The harvested energy at device i is thus,

$$E_i = \eta\lambda p_i, \tag{4.3}$$

where η is the energy conversion efficiency.

4.2.2 Transmission Model

Devices within communication range of one another transmits/receives at a given data rate. Devices have two transmission modes: (i) active RF transmissions via their conventional radio, or (ii) backscattering. Devices are located within the transmission range of the HAP, and communicate via active RF transmissions using one of F channels. In addition, devices can use AmBC to transmit their data by exploiting signals from external RF sources such as those from a television and cellular tower; see [11] for further information. Devices have a uniform backscattering range of γ meters. Let $\mathcal{B}(i)$ be the neighbours of device i that is within its backscattering communication range. Formally,

$$\mathcal{B}(i) = \{j \mid j \in \mathcal{I}, d_{ij} \leq \gamma\}. \tag{4.4}$$

Let the binary variable l_{ij}^t indicate whether device i is backscattering to device j in time slot t. Note that, devices can only backscatter to or receive backscattered data from one device at a time. Thus, it has

$$\sum_{j \in \mathcal{B}(i)} (l_{ij}^t + l_{ji}^t) \leq 1, \quad \forall i \in \mathcal{I}, \forall t \in \mathcal{T}. \tag{4.5}$$

In addition, a device i experiences interference if any of its neighbours within γ is backscattering data. In other words, at most one device $j \in \mathcal{B}(i)$ can backscatter at a time. Formally,

$$\sum_{j \in \mathcal{B}(i)} \sum_{k \in \mathcal{B}(j)} l_{jk}^t \leq 1, \quad \forall i \in \mathcal{I}, \forall t \in \mathcal{T}. \tag{4.6}$$

Note, Equ.(4.6) does not comprehensively consider all situations. For example, suppose devices j, l, m and k are neighbours of device i. Device j is backscattering

data to l, and at the same time m is backscattering data to k. However, d_{jk} and d_{ml} are both larger than γ. In this case, both links can be scheduled in the same time slot. Hence, the interference constraint is improved and modified in Chapter 5, e.g., Equ.(5.11).

In each time slot t, a device can be in *one* of three transmission modes: *uploading*, *B-tx* or *B-rx*. The corresponding binary indicators u_i^t, b_i^t and r_i^t are constrained by,

$$u_i^t + b_i^t + r_i^t \leq 1, \quad \forall i \in \mathcal{I}, \forall t \in \mathcal{T}. \tag{4.7}$$

The indicator variable b_i^t and r_i^t are set as follows,

$$b_i^t = \begin{cases} 1, & \text{if } \sum_{j \in \mathcal{B}(i)} l_{ij}^t = 1, \\ 0, & \text{Otherwise.} \end{cases}, \tag{4.8}$$

and

$$r_i^t = \begin{cases} 1, & \text{if } \sum_{j \in \mathcal{B}(i)} l_{ji}^t = 1, \\ 0, & \text{Otherwise.} \end{cases}. \tag{4.9}$$

Using (4.8), and (4.9), inequality (4.7) and (4.5) can be written as

$$u_i^t + \sum_{j \in \mathcal{B}(i)} (l_{ij}^t + l_{ji}^t) \leq 1, \quad \forall i \in \mathcal{I}, \forall t \in \mathcal{T}. \tag{4.10}$$

4.2.3 Sampling and Storage

In this section, it is assumed that devices are able to sample and transmit via active RF or AmBC simultaneously in one time slot. Samples collected by a device in a time slot can only be transmitted in the next time slot. All devices have a uniform data generation rate of R_s bps when they are in the sampling mode. Also, R_u and R_b (bps) denote the data transmission rate when device is in the *uploading* and *backscattering* mode, respectively. It is assumed that devices can only upload when

it has at least τR_u sampled data, and can only backscatter when the sampled data is at least τR_b. This is reasonable because devices need sufficient data before they can form a packet for transmission. The data buffer D_i^t of device i at the beginning of time slot $\hat{t}$ is

$$D_i^{\hat{t}} = \tau \sum_{t=1}^{t=\hat{t}-1} (R_s s_i^t - R_u u_i^t) + R_b \tau \sum_{t=1}^{t=\hat{t}-1} \sum_{j \in \mathcal{B}(i)} (l_{ji}^t - l_{ij}^t). \tag{4.11}$$

It assumes devices have a sufficiently large data buffer and D_i^t is unbounded because any data that has not been transmitted will be discarded at the end of the HST period. The total data receive by the HAP over T time slots is

$$\hat{D} = R_u \tau \sum_{t=1}^{t=T} \sum_{i \in \mathcal{I}} u_i^t. \tag{4.12}$$

Let ρ_s and ρ_u be the respective energy consumption rate when devices are in the *sampling* and *uploading* mode. Devices are assumed to have the same energy consumption rate of ρ_b when in the *B-tx* and *B-rx* mode. Thus, the battery level B_i^t of device i at the beginning of time slot $\hat{t}$ is

$$B_i^{\hat{t}} = E_i - \tau \sum_{t=1}^{t=\hat{t}-1} (\rho_s s_i^t + \rho_u u_i^t) - \rho_b \tau \sum_{t=1}^{t=\hat{t}-1} \sum_{j \in \mathcal{B}(i)} (l_{ji}^t + l_{ij}^t), \tag{4.13}$$

which is calculated as the difference between the total harvested energy and total energy consumed by different operation modes from time slot $t = 1$ to $t = \hat{t} - 1$. Note, when device i uses up all of the harvested energy, i.e., we have $B_i^{\hat{t}} = 0$ or a very small value, it will remain in 'sleep' mode with no further operations. On the other hand, similar to the data buffer, any energy that has not been used will be discarded at the end of the HST period.

4.3 Problem Statement and Formulations

The MILP to follow determines the operation mode of devices at each time slot. Recall that the backscatter link status l_{ij}^t corresponds to the operation mode b_i^t and r_i^t. Thus, using (4.12), the MILP has the following objective function

$$\max_{\{s_i^t, u_i^t, l_{ij}^t\}} R_u \tau \sum_{t=1}^{t=T} \sum_{i \in \mathcal{I}} u_i^t. \tag{4.14}$$

Its constraints are related to the operation mode of devices, interference, energy and data conservation. Firstly, in terms of operation mode, it has (4.10). Secondly, for upload channels it has

$$\sum_{i \in \mathcal{I}} u_i^t \leq F, \quad \forall t \in \mathcal{T}. \tag{4.15}$$

The third constraint is related to backscatter interference, as shown in Section 3.2.3, which is represented by (4.6).

Fourthly, to ensure the data buffer of devices is always non-negative, using (4.11), it has

$$\tau \sum_{t=1}^{t=\hat{t}-1} (R_s s_i^t - R_u u_i^t) + R_b \tau \sum_{t=1}^{t=\hat{t}-1} \sum_{j \in \mathcal{B}(i)} (l_{ji}^t - l_{ij}^t) \geq 0, \quad \forall i \in \mathcal{I}, \forall \hat{t} \in \mathcal{T}. \tag{4.16}$$

Fifth, it needs to ensure devices only use energy they have harvested. Using (4.2), (4.3) and (4.13), it has

$$\lambda \eta P \kappa d_{hi}^{-\alpha} - \tau \sum_{t=1}^{t=T} (\rho_s s_i^t + \rho_u u_i^t) - \rho_b \tau \sum_{t=1}^{t=T} \sum_{j \in \mathcal{B}(i)} (l_{ji}^t + l_{ij}^t) \geq 0, \forall i \in \mathcal{I}. \tag{4.17}$$

Note that, $\lambda \eta P \kappa d_{hi}^{-\alpha}$ is a constant under a given topology. Finally, the proposed

MILP is defined as

$$\max_{\{s_i^t, u_i^t, l_{ij}^t\}} R_u \tau \sum_{t=1}^{t=T} \sum_{i \in \mathcal{I}} u_i^t \qquad \textbf{(4.P1)}$$

$$\text{s.t.} \quad (4.6), (4.10), (4.15), (4.16), (4.17).$$

Note that, (**4.P1**) has $TI(I+2)$ binary variables and $3TI+I+T$ constraints. Each device has four transmission modes in each time slot: uploading, B-tx, B-rx and idle; each mode has two sample status, i.e., either to sample or not to sample. Thus, there are $(8I)^T$ possible combinations of operation modes for all devices in T time slots. Hence, the problem becomes intractable with increasing network size. The proposed MILP (**4.P1**) can be solved using any commercial solvers; e.g., Gurobi [128].

To conclude this section, please note the following points. First, the topology is known to the HAP, meaning the HAP is aware of the nodes that will be interfered by a backscattering transmission. In practice, a network operator may instruct each device to backscatter a HELLO message in turn. Devices then record whether they have received the HELLO message from a device. This information is then used to build the set $\mathcal{B}(i)$ of device i. Also, the HELLO messages can be used to ascertain the average channel gain. This information is then used to calculate the amount of energy harvested by each device, which in turn is used by the MILP solution to determine the mode of each device for each time slot. The HAP then programs each device with their mode over T time slots accordingly. Note that this schedule remains fixed and only needs to be revised when there is a change to the network.

The next section shows an example of AmBC assisted data transmissions doubling the number of samples uploaded to the HAP. After that, it proves rigorously the benefits of using AmBC in an IoT network.

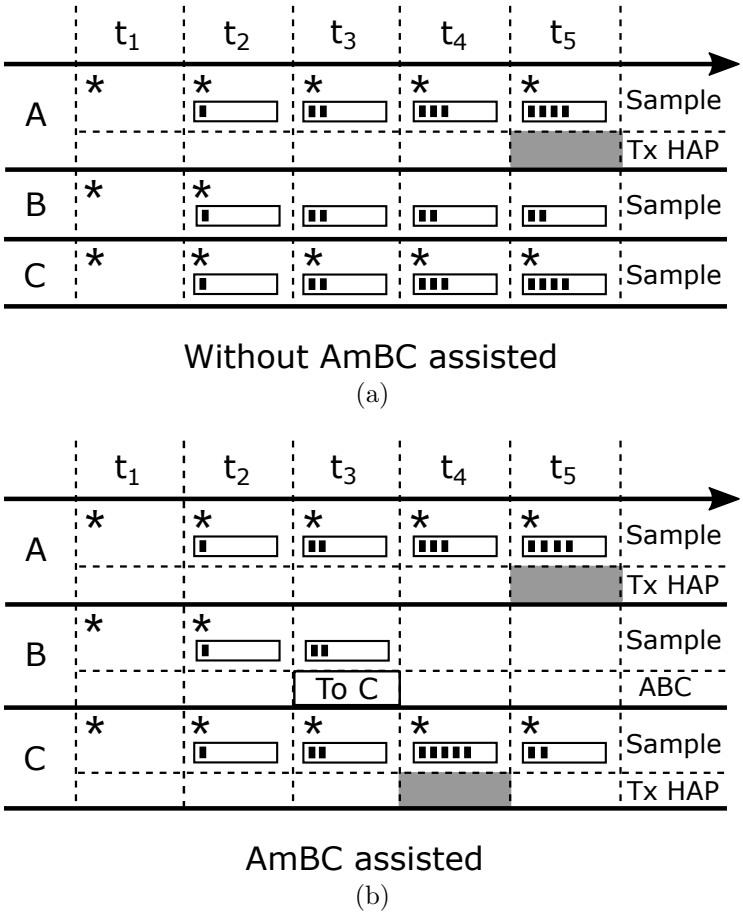

Figure 4.3: Data transmissions (a) without and (b) with AmBC assisted. The symbol $\star$ denotes a device in sampling mode, which results in a new sample in the next time slot. Filled blocks indicate the number of samples. The blank and grey blocks indicate AmBC and conventional radio transmissions, respectively.

4.3.1 An Example

Consider the topology depicted in Figure 4.1. Assume $T = 5$, $R_s = 1$, $R_b = 2$ and $R_u = 4$. Moreover, assume after charging, device A and C have sufficient energy while device B can only sample for the first two time slots but has insufficient energy to transmit directly to the HAP. In case of no AmBC, referring to the data transmission schedule in Figure 4.3a, only device A or C is able to transmit its samples to the HAP. This results in a total upload of four samples. The remaining samples are wasted. On the other hand, in the case of AmBC, see Figure 4.3b, device B is able to backscatter its two samples to device C. Then device C has five samples at time t_4, including its own, and thus it can transmit four ($R_u = 4$)

samples to the HAP. Lastly, device A transmits its four samples to the HAP. Hence, HAP receives a total of eight samples, which doubles the case without AmBC.

4.3.2 Analysis

This section contains a mathematical proof that shows the total uploaded data for a WPCN with and without backscatter capability; viz. Lemma 4.1 and 4.2. It assumes all devices have sufficient energy for sampling and data transmissions.

Lemma 4.1. *Given $R_s \ll R_b \ll R_u$ and $F < I$, the maximum total data uploaded to the HAP over T time slots, denoted as $\hat{D}(T)$, without backscatter is*

$$\hat{D}(T) = \begin{cases} 0, & \text{if } T \leq \frac{R_u}{R_s}, \\ (T - \frac{R_u}{R_s})F\tau R_u, & \text{if } \frac{R_u}{R_s} < T \leq \phi'_u, \\ N'_u \times I\tau R_u + \hat{D}'(T'), & \text{if } T > \phi'_u, \end{cases} \tag{4.18}$$

where

$$N'_u = \lfloor \frac{T - \phi'_o}{\phi'_u - \phi'_o} \rfloor, \tag{4.19}$$

and

$$\hat{D}'(T') = \begin{cases} 0, & \text{if } T' \leq \frac{R_u}{R_s}, \\ (T' - \frac{R_u}{R_s})F\tau R_u, & \text{if } \frac{R_u}{R_s} < T' < \phi'_u, \end{cases} \tag{4.20}$$

and

$$T' = T - N'_u \times (\phi'_u - \phi'_o), \tag{4.21}$$

$$\phi'_u = \frac{R_u}{R_s} + \frac{I}{F}, \tag{4.22}$$

$$\phi'_o = \min\{\frac{R_u}{R_s}, \frac{I}{F}\}. \tag{4.23}$$

Proof. It starts with a few key definitions. In order to acquire data for transmission, a device needs to sample for t'_s time slots, where

$$t'_s = \frac{R_u}{R_s}. \tag{4.24}$$

The frequency of upload (in slots) to the HAP is

$$t'_u = \frac{I}{F}. \tag{4.25}$$

Define an upload cycle (U-cycle) as the number of time slots taken by devices to sample and upload once. Each U-cycle has length $\phi'_u = t'_s + t'_u$. Recall that devices must first sample for t'_s time slots to acquire sufficient data to upload to the HAP. There are two cases to consider: i) $t'_u \leq t'_s$, meaning a device's data upload completes before it has the next sample ready. Thus, there is an *overlap period* between two U-cycles; see Figure 4.4a. This overlap period has length ϕ'_o, where $\phi'_o = t'_u$ when $t'_u \leq t'_s$, ii) $t'_s < t'_u$, meaning each device samples for t'_s time slots and it is ready to upload again. Referring to Figure 4.4b, it shows that a device has a sample ready before it has finished uploading the previous sample. Therefore, it has the following relation

$$\phi'_o = \begin{cases} t'_u, & \text{if } t'_u \leq t'_s, \\ t'_s, & \text{Otherwise.} \end{cases} \tag{4.26}$$

The total uploaded data $\hat{D}(T)$ over T time slots is proportional to the number of U-cycles over T time slots since all devices upload once every U-cycle. Note that, there is no *overlap period* in the last U-cycle. Specifically, $\hat{D}(T)$ is dependent on the following cases:

1. $T \leq t'_s$, meaning devices have not sampled sufficient data to upload. Therefore, the total uploaded data is zero.

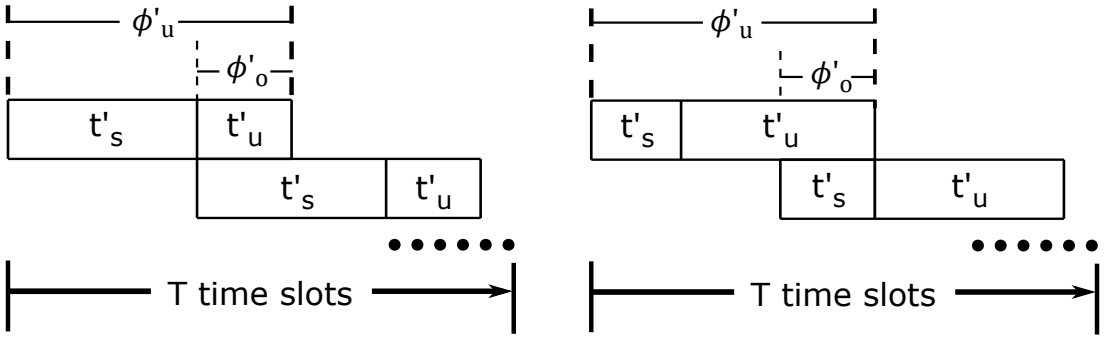

Figure 4.4: The overlap between two U-cycles for devices under two cases: (a) $t'_u \leq t'_s$, and (b) $t'_s < t'_u$.

2. $t'_s < T \leq t'_s + t'_u$, meaning all devices have sufficient data to upload, but not all of them are able to upload once over time T. Therefore, the total uploaded data is $(T - t'_s)F\tau R_u$.

3. $T > t'_s + t'_u$, meaning all devices will be able to upload their data at least once. Thus, the total uploaded data is calculated based on the number of U-cycles over T time slots. Let N'_u denote the number of *complete* U-cycles, which is defined as

$$N'_u = \lfloor \frac{T - \phi'_o}{\phi'_u - \phi'_o} \rfloor. \tag{4.27}$$

Let $T' = T - N'_u \times (\phi'_u - \phi'_o)$ denote the number of remaining time slots. Consider $T' = 0$, meaning it has exactly N'_u U-cycles. Thus, the total uploaded data is $N'_u I\tau R_u$. Next, consider $T' > 0$, meaning there is an incomplete U-cycle. It thus needs to account for the data uploaded over these T' time slots. Let this amount be $\hat{D}'(T')$. This means over time T, the total uploaded data is $N'_u I\tau R_u + \hat{D}'(T')$. If $T' \leq t'_s$, then devices have insufficient data to upload during T'. Thus, $\hat{D}'(T') = 0$. Otherwise, when $t'_s < T' < \phi'_u$, all devices have sufficient data, but not all of them are able to upload, meaning $\hat{D}'(T') = (T' - t'_s)F\tau R_u$.

It thus has the total uploaded data over T time slots as represented by Equ. (4.18)

as desired.

□

Lemma 4.2. *When $R_s \ll R_b \ll R_u$ and $F < I$, the maximum total uploaded data $\tilde{D}(T)$ to the HAP over T time slots with backscatter is as follows*

$$\tilde{D}(T) = \begin{cases} 0, & \text{if } T \leq \hat{T}, \\ (T - \hat{T})F\tau R_u, & \text{if } \hat{T} < T \leq \phi_u, \\ N_u \times n\tau R_u + \tilde{D}'(\tilde{T}), & \text{if } T > \phi_u, \end{cases} \tag{4.28}$$

where

$$N_u = \lfloor \frac{T - \hat{\phi}_o}{\phi_u - \hat{\phi}_o} \rfloor, \tag{4.29}$$

and

$$\tilde{D}'(\tilde{T}) = \begin{cases} 0, & \text{if } \tilde{T} \leq \hat{T}, \\ (\tilde{T} - \hat{T})F\tau R_u, & \text{if } \hat{T} < \tilde{T} < \phi_u, \end{cases} \tag{4.30}$$

and

$$\tilde{T} = T - N_u \times (\phi_u - \hat{\phi}_o), \tag{4.31}$$

$$\phi_u = \hat{T} + \frac{n}{F}, \tag{4.32}$$

$$\hat{\phi}_o = \frac{n}{F}, \tag{4.33}$$

$$\hat{T} = \frac{nR_u(\phi_b - \phi_o) + \phi_o(I - n)R_b}{nR_s(\phi_b - \phi_o) + (I - n)R_b}, \tag{4.34}$$

$$\phi_b = \frac{R_b}{R_s} + \frac{I}{n} - 1, \tag{4.35}$$

$$\phi_o = \min\{\frac{R_b}{R_s}, \frac{I}{n} - 1\}. \tag{4.36}$$

Proof. It starts by dividing I devices into n clusters. Each cluster has a *sink*; all other devices in the cluster backscatter their data to the sink. This means each

cluster has a minimum of two devices, and there is at least one backscattering or non-sink device; this means $I \geq 2n$. The sink also samples data when it is receiving backscattering data from non-sink devices. Let t_s be the required number of time slots a non-sink device uses to sample data until it is able to start backscattering its data. It has

$$t_s = \frac{R_b}{R_s}. \tag{4.37}$$

Let t_b denote the total number of time slots taken by the sink of each cluster to receive backscatter data from its non-sink devices. As there is only one backscatter transmission at time, it has

$$t_b = \frac{I}{n} - 1. \tag{4.38}$$

It has $t_b \geq 1$ because each cluster has at least one backscatter device.

Let a Backscatter Cycle (B-cycle) denote the number of time slots taken by a non-sink device to sample and backscatter to the sink. It has length $\phi_b = t_s + t_b$. Similar to the case in Lemma-4.1, there is also an overlap period between B-cycles. Let ϕ_o denote the overlap length, which is

$$\phi_o = \begin{cases} t_b, & \text{if } t_b \leq t_s, \\ t_s, & \text{Otherwise.} \end{cases} \tag{4.39}$$

Let $\hat{T}$ denote the number of time slots a sink is sampling data. Note that, a sink also receives backscattering data from other devices during $\hat{T}$. Also define $B(\hat{T})$ to be the total backscatter data received by a sink over time $\hat{T}$. It thus has

$$\hat{T}\tau R_s + B(\hat{T}) = \tau R_u. \tag{4.40}$$

To quantify $B(\hat{T})$, define N_B as the number of B-cycles over $\hat{T}$ time slots. Note

that, there is no overlap period in the last B-cycle. Thus, it has

$$B(\hat{T}) = N_B \left(\frac{I}{n} - 1\right) \tau R_b = \frac{\hat{T} - \phi_o}{\phi_b - \phi_o} \left(\frac{I}{n} - 1\right) \tau R_b, \tag{4.41}$$

where it assumes $N_B = \frac{\hat{T}-\phi_o}{\phi_b-\phi_o}$ is an integer value. Substituting Equ. (4.41) into Equ. (4.40), it has

$$\hat{T} = \frac{nR_u(\phi_b - \phi_o) + \phi_o(I-n)R_b}{nR_s(\phi_b - \phi_o) + (I-n)R_b}. \tag{4.42}$$

Let the length of an Upload-cycle (U-cycle) be $\phi_u = \hat{T} + t_u$. Here, the term t_u is the required number of time slots for all sinks to upload their data to the HAP. It has

$$t_u = \frac{n}{F}. \tag{4.43}$$

In an U-cycle, all sinks upload to the HAP once. Note that there is also overlap between two U-cycles; its length is $\hat{\phi}_u$. Figure 4.5 shows an example of the time slots occupied for sampling, backscattering and uploading for a non-sink device and a sink over T time slots. In this example, there are two B-cycles ($N_B = 2$) in one U-cycle. During time $\hat{T}$, it can be seen that a non-sink device backscatters its sampled data to the sink twice, and the sink sampling data for upload.

In each slot, a sink cannot receive and transmit backscatter data simultaneously. Thus, in the overlap period between two U-cycles, a sink can only sample and upload simultaneously. To this end, it only considers the case where $t_u \leq t_s < \hat{T}$. This is because, if $t_u > t_s$, then a non-sink device cannot backscatter its data to the sink as the sink is still uploading. Therefore, $\hat{\phi}_o$ is defined as,

$$\hat{\phi}_o = t_u. \tag{4.44}$$

The total uploaded data $\tilde{D}$ by all n sinks over T time slots can then be calculated

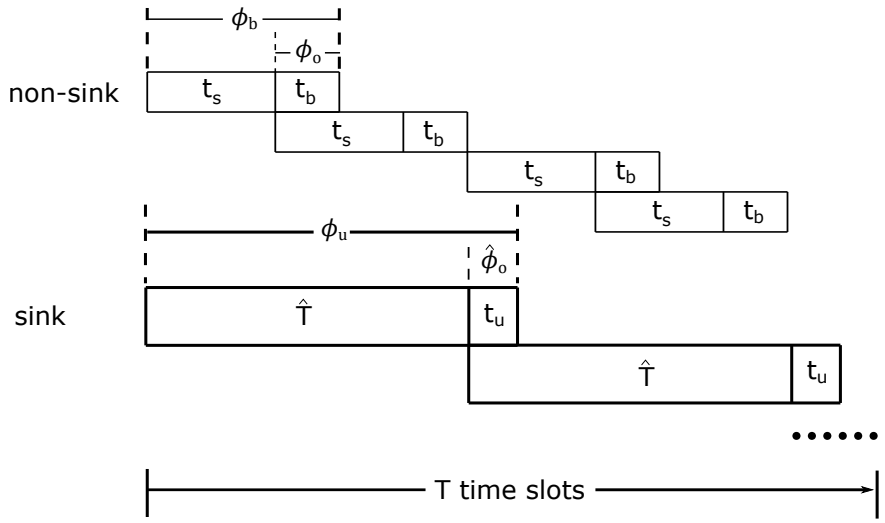

Figure 4.5: Time slots occupied for sampling, backscattering and uploading for a non-sink device and a sink over T time slots when $N_B = 2$.

based on the number of U-cycles over T time slots. Specifically, its value is set as follows:

1. $T \leq \hat{T}$, meaning sinks have not received or sampled sufficient data to upload. Therefore, the total uploaded data is zero.

2. $\hat{T} < T \leq \hat{T} + t_u$, meaning all sinks have sufficient data to upload, but not all of them are able to upload once over time T. Therefore, the total uploaded data is $(T - \hat{T})F\tau R_u$.

3. $T > \hat{T} + t_u$, meaning all sinks will be able to upload their data at least once. Note that there is no overlap period in the last U-cycle. The number of *completed* U-cycles over T time slots is

$$N_u = \lfloor \frac{T - \hat{\phi}_o}{\phi_u - \hat{\phi}_o} \rfloor. \tag{4.45}$$

Let $\tilde{T} = T - N_u \times (\phi_u - \hat{\phi}_o)$ denote the number of remaining time slots. Consider $\tilde{T} = 0$, meaning it has exactly N_u U-cycles. Thus, the total uploaded data is $N_u \times n\tau R_u$. Next, consider $\tilde{T} > 0$, meaning there is some time slots after the last completed U-cycle. Let $\tilde{D}'(\tilde{T})$ be the amount of data uploaded over these $\tilde{T}$ time slots. Therefore, the total uploaded data over T time slots is

represented as $N_u \times n\tau R_u + \tilde{D}'(\tilde{T})$. If $\tilde{T} \leq \hat{T}$, then sinks have not sampled or received sufficient data to upload during $\tilde{T}$. Thus $\tilde{D}'(\tilde{T}) = 0$. Otherwise, when $\hat{T} < \tilde{T} < \phi_u$, sinks have sufficient data to upload but not all sinks can upload. Thus, $\tilde{D}'(\tilde{T}) = (\tilde{T} - \hat{T})F\tau R_u$.

It thus has the total uploaded data over T time slots as claimed, see Equ. (4.28). □

Lastly, it has the following proposition:

Proposition 4.1. *When $R_s \ll R_b \ll R_u$ and $F \leq n < I$, and the number of clusters n set as per (4.53) and (4.62), the total uploaded data with backscatter is at least that of the case without backscatter.*

Proof. First, note two important inequalities that follow Lemma 4.1 and Lemma 4.2. Using Equ. (4.40) and assuming that there is at least one backscatter transmission, it has

$$\tau R_u - \hat{T}\tau R_s = B(\hat{T}) > 0, \tag{4.46}$$

where it has $B(\hat{T}) > 0$ according to Equ. (4.41). Thus, it has the first inequality

$$\tau R_u > \hat{T}\tau R_s, \quad \text{and} \quad \frac{R_u}{R_s} > \hat{T}. \tag{4.47}$$

For the second inequality, given

$$\phi'_u = \frac{R_u}{R_s} + \frac{I}{F}, \quad \text{and} \quad \phi_u = \hat{T} + \frac{n}{F}, \tag{4.48}$$

and using (4.47) with $I \geq 2n$ from Lemma 4.2, it has

$$\phi'_u > \phi_u. \tag{4.49}$$

The next exposition compares the total uploaded data over T time slots with and without backscatter. According to Equ. (4.18) in Lemma 4.1 and Equ. (4.28)

in Lemma 4.2, different T values lead to different expressions for both $\hat{D}(T)$ and $\tilde{D}(T)$. Specifically, it has the following cases of T:

1. $T \leq \hat{T}$: it has $\hat{D}(T) = 0$ because $T \leq \hat{T} < \frac{R_u}{R_s}$, see the first case of (4.18); and $\tilde{D}(T) = 0$, see the first case of (4.28), therefore, $\hat{D}(T) = \tilde{D}(T)$.

2. $\hat{T} < T \leq \frac{R_u}{R_s}$: similarly, it has $\hat{D}(T) = 0$ because $T \leq \frac{R_u}{R_s}$, and $\tilde{D}(T) = (T - \hat{T})F\tau R_u > 0$, see the second case of (4.28). Thus, it has $\hat{D}(T) < \tilde{D}(T)$.

3. $\frac{R_u}{R_s} < T \leq \phi_u$: it has $\hat{D}(T) = (T - \frac{R_u}{R_s})F\tau R_u$ and $\tilde{D}(T) = (T - \hat{T})F\tau R_u$, see the second case of both (4.18) and (4.28). Thus, based on (4.47), where $\frac{R_u}{R_s} > \hat{T}$, it has $\hat{D}(T) < \tilde{D}(T)$.

4. $\phi_u < T \leq \phi'_u$: it also has $\hat{D}(T) = (T - \frac{R_u}{R_s})F\tau R_u$. However, according to the third case of (4.28), the total uploaded data of the network with backscatter is

$$\begin{aligned}\tilde{D}(T) &= N_u \times n\tau R_u + \tilde{D}'(\tilde{T}) \\ &= \lfloor \frac{T - \hat{\phi}_o}{\phi_u - \hat{\phi}_o} \rfloor \times n\tau R_u + \tilde{D}'(\tilde{T}) \\ &= \lfloor \frac{T - \frac{n}{F}}{\hat{T}} \rfloor \times n\tau R_u + \tilde{D}'(\tilde{T}) \\ &\geq \frac{T - \frac{n}{F}}{\hat{T}} \times n\tau R_u, \end{aligned} \tag{4.50}$$

where it removes the *floor function* to simplify the analysis. Thus, it has

$$\begin{aligned}&\hat{D}(T) - \tilde{D}(T) \\ &\leq (T - \frac{R_u}{R_s})F\tau R_u - \frac{T - \frac{n}{F}}{\hat{T}} \times n\tau R_u \\ &= \frac{\tau R_u F}{\hat{T}} \left((T - \frac{R_u}{R_s}) \times \hat{T} - (T - \frac{n}{F}) \times \frac{n}{F} \right) \\ &= \frac{\tau R_u F}{\hat{T}} \left((\frac{n}{F})^2 - T\frac{n}{F} + (T - \frac{R_u}{R_s})\hat{T} \right). \end{aligned} \tag{4.51}$$

In (4.51), the coefficient $\frac{\tau R_u F}{\hat{T}}$ is greater than zero. Therefore, it has $\hat{D}(T) \leq$

$\tilde{D}(T)$ if the polynomial $(\frac{n}{F})^2 - T\frac{n}{F} + (T - \frac{R_u}{R_s})\hat{T}$ is less and equal to zero, which can be represented using (4.52). Therefore, $\hat{D}(T) \leq \tilde{D}(T)$ if n in the range satisfies (4.53).

$$\left(n - \frac{FT + \sqrt{T^2F^2 - 4 \times F^2\hat{T}(T - \frac{R_u}{R_s})}}{2}\right) \times \left(n - \frac{FT - \sqrt{T^2F^2 - 4 \times F^2\hat{T}(T - \frac{R_u}{R_s})}}{2}\right) \leq 0. \tag{4.52}$$

$$\frac{FT - \sqrt{T^2F^2 - 4 \times F^2\hat{T}(T - \frac{R_u}{R_s})}}{2} \leq n \leq \frac{FT + \sqrt{T^2F^2 - 4 \times F^2\hat{T}(T - \frac{R_u}{R_s})}}{2}. \tag{4.53}$$

5. $\phi'_u < T$: according to the third case of (4.18) it has

$$\hat{D}(T) = N'_u \times I\tau R_u + \hat{D}'(T') = \lfloor \frac{T - \phi'_o}{\phi'_u - \phi'_o} \rfloor \times I\tau R_u + \hat{D}'(T'). \tag{4.54}$$

According to the third case of (4.28), it has

$$\tilde{D}(T) = N_u \times n\tau R_u + \tilde{D}'(\tilde{T}) = \lfloor \frac{T - \frac{n}{F}}{\hat{T}} \rfloor \times n\tau R_u + \tilde{D}'(\tilde{T}). \tag{4.55}$$

When T is large, it has $\lfloor \frac{T-\phi'_o}{\phi'_u-\phi'_o} \rfloor \approx \frac{T-\phi'_o}{\phi'_u-\phi'_o}$ and $\lfloor \frac{T-\frac{n}{F}}{\hat{T}} \rfloor \approx \frac{T-\frac{n}{F}}{\hat{T}}$. Thus, as per (4.21) and (4.31), it has

$$T' = T - \frac{T - \phi'_o}{\phi'_u - \phi'_o} \times (\phi'_u - \phi'_o) = \phi'_o, \tag{4.56}$$

$$\tilde{T} = T - \frac{T - \hat{\phi}_o}{\phi_u - \hat{\phi}_o} \times (\phi_u - \hat{\phi}_o) = \hat{\phi}_o = \frac{n}{F}. \tag{4.57}$$

Hence, it shows that $T' = \phi'_o \leq \frac{R_u}{R_s}$ and $\tilde{T} = \frac{n}{F} \leq \hat{T}$. Therefore, according to Equ. (4.18) and Equ. (4.28), it has $\hat{D}'(T') = 0$ and $\tilde{D}'(\tilde{T}) = 0$. Then it has

$$\hat{D}(T) - \tilde{D}(T) = \frac{T - \phi'_o}{\phi'_u - \phi'_o} \times I\tau R_u - \frac{T - \frac{n}{F}}{\hat{T}} \times n\tau R_u, \tag{4.58}$$

where $\phi'_o = \min\{\frac{R_u}{R_s}, \frac{I}{F}\}$ according to Equ. (4.23). Note that, the value of $\hat{D}(T) - \tilde{D}(T)$ is based on the value of $\frac{R_u}{R_s}$ and $\frac{I}{F}$. Therefore, the first consideration is $\frac{R_u}{R_s} \leq \frac{I}{F}$, where $\phi'_o = \frac{R_u}{R_s}$, Equ. (4.58) can then be revised to

$$(T - \frac{R_u}{R_s})F\tau R_u - \frac{T - \frac{n}{F}}{\hat{T}} \times n\tau R_u, \tag{4.59}$$

which is the same as Equ. (4.51). The next consideration is $\frac{R_u}{R_s} > \frac{I}{F}$, where $\phi'_o = \frac{I}{F}$, Equ. (4.58) then can be rewritten as

$$\begin{aligned} &\hat{D}(T) - \tilde{D}(T) \\ &= \frac{T - \frac{I}{F}}{\frac{R_u}{R_s}} \times I\tau R_u - \frac{T - \frac{n}{F}}{\hat{T}} \times n\tau R_u \\ &= \frac{\tau R_u}{F\hat{T}} \left(n^2 - FTn + \frac{R_s I\hat{T}(FT - I)}{R_u} \right). \end{aligned} \tag{4.60}$$

In Equ. (4.60), the coefficient $\frac{\tau R_u}{F\hat{T}}$ is greater than zero. Therefore, it has $\hat{D}(T) \leq \tilde{D}(T)$ if the polynomial $n^2 - FTn + \frac{R_s I\hat{T}(FT-I)}{R_u}$ is less or equal to zero, which can be presented using inequality (4.61). Thus, based on Inequality (4.61), note that, $\hat{D}(T) \leq \tilde{D}(T)$ if n in the range shown in inequality (4.62).

$$\left(n - \frac{FT + \sqrt{T^2F^2 - 4 \times (FT - I)I\hat{T}\frac{R_s}{R_u}}}{2} \right) \left(n - \frac{FT - \sqrt{T^2F^2 - 4 \times (FT - I)I\hat{T}\frac{R_s}{R_u}}}{2} \right) \leq 0. \tag{4.61}$$

$$\frac{FT - \sqrt{T^2F^2 - 4 \times (FT - I)I\hat{T}\frac{R_s}{R_u}}}{2} \leq n \leq \frac{FT + \sqrt{T^2F^2 - 4 \times (FT - I)I\hat{T}\frac{R_s}{R_u}}}{2}. \tag{4.62}$$

Note that, inequalities (4.52) and (4.61) are both quadratic inequalities. Thus, to calculate the roots of both (4.52) and (4.61), the expression under the square root needs to be non-negative. For (4.52), it has

$$\begin{aligned} & T^2F^2 - 4 \times F^2\hat{T}(T - \frac{R_u}{R_s}) \\ &= T^2F^2 - 4 \times F^2\hat{T}T + 4 \times F^2\hat{T}\frac{R_u}{R_s} \\ &> T^2F^2 - 4 \times F^2\hat{T}T + 4 \times F^2\hat{T}\hat{T} \quad \text{(using (4.47))} \\ &= (TF - 2F\hat{T})^2 \geq 0. \end{aligned} \tag{4.63}$$

Next, for (4.61), it has

$$\begin{aligned} & T^2F^2 - 4 \times (FT - I)I\hat{T}\frac{R_s}{R_u} \\ &> T^2F^2 - 4 \times (FT - I)I\frac{R_u}{R_s}\frac{R_s}{R_u} \quad \text{(using (4.47))} \\ &= T^2F^2 - 4 \times (FT - I)I \\ &= (TF - 2I)^2 \geq 0. \end{aligned} \tag{4.64}$$

□

Next section proposes an efficient heuristic algorithm to iteratively decide the operation mode of devices in each time slot.

4.4 Double Weighted Protocol (DWP)

The proposed heuristic algorithm called Double Weighted Protocol (DWP) determines the operation mode of each device in each time slot; namely, sampling ($\mathcal{S}$), uploading ($\mathcal{U}$), backscatter transmission (B-tx) or backscatter reception (B-rx). It requires two weights: (i) *backscatter weight*, which represents the ability of a device to be selected as a backscatter transmitter, and (ii) *upload weight*, which on the other hand, indicates the ability of a device to be selected as an uploading transmitter. Both of the above weights are calculated based on the battery level and data buffer level of devices.

DWP runs in a slot-by-slot manner. In the first time slot, the data buffer of all devices is empty. Thus, all devices enter the $\mathcal{S}$ mode. Then, from the second time slot, DWP calculates the weights of all devices and determines their operation mode. Specifically, DWP first selects uploading devices based on their *upload* weight. Then, it determines device pairs that will be in either the B-tx and B-rx mode base on the *backscatter* weight. For devices not in B-tx or B-rx or upload mode, DWP greedily selects these remaining devices to sample their environment. Finally, DWP updates both the *backscatter* and *upload* weights for each device and repeats the above process for subsequent time slots.

Definitions of the *backscatter* and *upload* weight for each device i are given as follows. Specifically, the *backscatter* weight $\hat{w}_i^t$ of device i is defined as

$$\hat{w}_i^t = \frac{D_i^t}{B_i^t}, \quad \forall i \in \mathcal{I}, \forall t \in \mathcal{T}, \tag{4.65}$$

where D_i^t and B_i^t indicate the energy and data buffer level of device i in time slot t respectively. Note that, a higher weight $\hat{w}_i^t$ corresponds to the fact that device i has a large amount of sampled data and low energy level. On the other hand, the

upload weight $\bar{w}_i^t$ is defined as,

$$\bar{w}_i^t = D_i^t B_i^t, \quad \forall i \in \mathcal{I}, \forall t \in \mathcal{T}. \tag{4.66}$$

This means if device i has a large $\bar{w}_i^t$ value, then it has a large amount of sampled data as well as energy.

In each time slot, DWP first selects devices to upload. Specifically, let $\mathcal{I}^- = \mathcal{I}$ be a set of devices that have not been assigned any operation mode. Moreover, in order to ensure devices do not waste upload opportunities, DWP only allows those devices with sufficient amount of data to upload. Thus, let a set $\mathcal{A}$ that contains such devices where

$$\mathcal{A} = \{i \,|D_i^t \geq R_u \tau \wedge B_i^t \geq \rho_u \tau\}. \tag{4.67}$$

Here, R_u and ρ_u represent the data rate and energy consumption rate for uploading, respectively. DWP then chooses device k with the maximum *upload* weight that belongs to both $\mathcal{I}^-$ and $\mathcal{A}$ to upload. That is,

$$k = \underset{i \in \mathcal{I}^- \cap \mathcal{A}}{\arg\max} \{\bar{w}_i^t\}. \tag{4.68}$$

DWP then sets $u_k^t = 1$, and removes k from $\mathcal{I}^-$. Recall that there are a total of F upload channels. Thus, DWP iteratively chooses F different upload devices k.

The next step of DWP is to determine the backscatter transmitter/receiver pairs. Let $\mathcal{D}_{tx}$ and $\mathcal{D}_{rx}$ be sets that contain candidate devices that respectively can enter the B-tx and B-rx mode. Initially, it has $\mathcal{D}_{tx} = \mathcal{D}_{rx} = \mathcal{I}^-$. Similarly, in order to select uploading devices, it only allows devices that store sufficient amount of data, denoted as a set $\mathcal{H}$, to backscatter in order to avoid energy waste. Thus, it has

$$\mathcal{H} = \{i \mid D_i^t \geq R_b \tau \wedge B_i^t \geq \rho_b \tau\}. \tag{4.69}$$

The HAP then selects a node i^* from $\mathcal{D}_{tx}$ that has the maximum *backscatter* weight $\hat{w}_i^t$ to be in B-tx mode. Formally,

$$i^* = \underset{i \in \mathcal{D}_{tx} \cap \mathcal{H}}{\arg\max} \{\hat{w}_i^t\}. \tag{4.70}$$

Next, the HAP selects a node j^* from $\mathcal{D}_{rx}$ to be in the B-rx mode, which must satisfy the following two conditions:

1. $j^* \in \mathcal{B}(i^*)$, i.e., device j^* is in the backscatter range of device i^*; see Equ.(4.4).
2. device j^* has higher residual energy than all other devices in $\mathcal{B}(i^*) \cap \mathcal{D}_{rx}$.

Thus, it has

$$j^* = \underset{i \in \mathcal{B}(i^*) \cap \mathcal{D}_{rx}}{\arg\max} \{B_i^t\}. \tag{4.71}$$

and set $b_{i^*}^t = 1$, $r_{j^*}^t = 1$. At this point, DWP successfully found one pair of backscatter transmitter and receiver. It then removes $\mathcal{B}(i^*)$ from $\mathcal{D}_{rx}$ and $\mathcal{B}(j^*)$ from $\mathcal{D}_{tx}$ to prevent interference; see also the constraint (4.6). After this, DWP selects another pair of i^* and j^* until any of the two sets $\mathcal{D}_{rx}$ and $\mathcal{D}_{tx}$ is empty. Note that, if there is no available receiver in $\mathcal{B}(i^*)$, i.e., $\mathcal{B}(i^*) \cap \mathcal{D}_{rx} = \emptyset$, device i^* is removed from $\mathcal{D}_{tx}$. At this stage, the HAP has determined the backscatter transmission pairs in the current slot.

Lastly, all devices with sufficient energy for sampling, i.e., $B_i^t \geq \rho_s \tau$, enter the sampling mode. Note that, a device may sample and transmit/receive simultaneously. The HAP then updates D_i^t and B_i^t of all devices and calculates their new weights to determine their operation mode in the subsequent slot, until all devices exhaust their energy or t reaches T.

Algorithm 4.1 shows the steps of DWP. The inputs to DWP are the harvested energy $\{E_i\}$ of each device and the total number of time slots T. In the first time slot, all devices sample. DWP then determines the operation mode of all devices from the second time slot; see line 2 to line 31. In each time slot t, DWP first calculates

Algorithm 4.1: Pseudocode of DWP.

Input: $\{E_i\}$, T
Output: $\{s_i^t\}$, $\{u_i^t\}$, $\{l_{ij}^t\}$

$s_i^1 = 1$, $u_i^1, l_{ij}^1 = 0$ for all $i, j \in \mathcal{I}$
for $t = 2, \ldots, T$ **do**
  for *all* $i \in \mathcal{I}$ **do**
    Calculate D_i^t and B_i^t as per Equ. (4.11) and Equ. (4.13)
    Calculate $\hat{w}_i^t$ and $\bar{w}_i^t$ as per Equ. (4.65) and Equ. (4.66)
  end
  *** find upload devices ***
  Set $\mathcal{I}^- = \mathcal{I}$
  while $\mathcal{I}^- \neq \emptyset$ *and* $\sum_{i \in \mathcal{I}} u_i^t \leq F$ **do**
    Calculate k as per Equ. (4.68)
    Set $u_k^t = 1$, update $\mathcal{I}^-$ by removing k
  end
  *** find backscatter transmission pairs ***
  Set $\mathcal{D}_{tx}, \mathcal{D}_{rx} = \mathcal{I}^-$
  while $\mathcal{D}_{tx} \neq \emptyset$ *and* $\mathcal{D}_{rx} \neq \emptyset$ **do**
    Calculate i^* as per Equ. (4.70)
    if $\mathcal{B}(i^*) \cap \mathcal{D}_{rx} = \emptyset$ **then**
      $\mathcal{D}_{tx} = \mathcal{D}_{tx} - \{i^*\}$ and continue
    else
      Calculate j^* as per Equ. (4.71)
    end
    Set $b_{i^*}^t, r_{j^*}^t, l_{i^*j^*}^t = 1$
    $\mathcal{D}_{tx} = \mathcal{D}_{tx} - \mathcal{B}(j^*)$, $\mathcal{D}_{rx} = \mathcal{D}_{rx} - \mathcal{B}(i^*)$
  end
  *** find sampling devices ***
  for *all* $i \in \mathcal{I}$ **do**
    if $B_i^t \geq \rho_s \tau$ **then**
      $s_i^t = 1$
    end
  end
end

both the *backscatter* and *upload* weights for each device; see line 3 to line 6. It then selects devices to upload from line 7 to line 12. Note that, DWP selects F uploading devices for all uploading channels in one time slot. After that, from all the remaining devices in $\mathcal{I}^-$, DWP determines the backscatter transmitter/receiver pairs, denoted as i^* and j^*. This step is given from line 13 to line 24. Lastly, DWP selects devices to sample as shown from line 24 to line 30. The algorithm terminates when $t = T$ or all devices exhaust their energy, and it then outputs the operation mode, i.e., $\{s_i^t\}$, $\{u_i^t\}$ and $\{l_{ij}^t\}$, for each device in each time slot.

Proposition 4.2. *DWP's run time complexity is* $\mathcal{O}(TI^2 + TIF)$.

Proof. The DWP iteratively runs $T - 1$ time slots. In each time slot, it first takes $\mathcal{O}(I)$ to calculate the data, energy and the two weights of each device. Next, it determines the maximum *upload* weight in $\mathcal{I}^- \cap \mathcal{A}$, where $\mathcal{I}^-, \mathcal{A} \in \mathcal{I}$. Thus, the maximum run time complexity is $\mathcal{O}(IF)$ to select F upload devices. After this, the DWP determines the backscatter transmitter and receivers from $\mathcal{D}_{tx}$ and $\mathcal{D}_{rx}$ where $\mathcal{D}_{tx}, \mathcal{D}_{rx} \in \mathcal{I}$. Thus, for each selected i^*, it must traverse all other devices to determine j^*. In the worst case, the size of set $\mathcal{D}_{tx}$ reduces by one and $\mathcal{D}_{rx}$ remain same after each iteration, i.e., there is no possible backscatter links. The run time complexity in this case is $\mathcal{O}(I^2)$. Therefore, the total run time in each iteration is $\mathcal{O}(I^2 + IF)$. Hence, the run time complexity of DWP is $\mathcal{O}(TI^2 + TIF)$. □

Note that the communication overhead of DWP is $\mathcal{O}(I)$ because it initially requires the harvested energy of all I devices. Then the algorithm computes two weights and determines the operation mode of each device.

4.5 Evaluation

The evaluation is conducted using Python 3.6 running on a laptop with an Intel Core i7 eight cores CPU @ 2.2GHz, and use the Gurobi [128] Toolbox to solve the formulated MILP (**4.P1**); as reported in [129], Gurobi uses the branch and cut

framework to compute a solution. The evaluation shows a comparison between the total uploaded data from solving (**4.P1**) and DWP for the case with and without AmBC. To disable backscattering in the MILP formulation, it added the following constraint to (**4.P1**),

$$l_{ij}^{t} = 0, \quad \forall i, j \in \mathcal{I}, \forall t \in \mathcal{T}. \tag{4.72}$$

As for DWP, the backscatter transmission pairs selection steps are disabled; see line 13 to line 24 in Algorithm 4.1.

To benchmark against the proposed approaches, an evaluation is conducted using Random Protocol (RP), where the HAP randomly selects devices to upload, backscatter and sample when they have sufficient data/energy.

In the simulation, the network randomly deploys devices in a squared sensing field of 20 $m \times 20$ m. There are five sets of experiments in the evaluation, including varying number of devices, backscatter transmission range, HAP transmit power, number of upload channels and number of time slots. The results are an average of 100 random topologies. Table 4.1 shows other system parameter values used in the simulation studies. Note that, the achievable data rate for AmBC is limited by a specific transceiver design. For example, the authors of [11] design an AmBC prototype that performs binary on-off keying modulation at the transmitter. At the receiver end, the proposed design uses an envelope detector and RC (resistive/capacitive) circuit for averaging and thresholding to decode low rate information. The achievable AmBC data rate for this designed transceiver is 1 kbps over distance of 2.5 feets outdoor and over 1.5 feets indoor. In the simulation, the RF source for AmBC is from a WiFi router based on [130]. Other parameters such as the number of channels and the uploading data rate are based on the IEEE 802.15.4 standard.

The first evaluation studies increasing number of devices from five to 50 with an interval of five. From Figure 4.6, it shows that the total uploaded data increases with the number of devices. This is because more devices means more sampled

Table 4.1: System Parameters

Parameter	**Symbol**	**Value (Unit)**
Path loss component [131]	κ	1
Environment component [131]	α	2
Energy Conversion Efficiency [131]	η	0.4
Charging time duration	λ	100 (s)
Sampling energy cost [132]	ρ_s	2 (mW)
Uploading energy cost [132]	ρ_u	20 (mW)
Backscatter energy cost [41]	ρ_b	$\sim$ 0 (mW)
Sampling data generation rate [133]	R_s	20 (kbps)
Upload data rate [134]	R_u	250 (kbps)
Backscatter data rate [130]	R_b	100 (kbps)

data is generated and transmitted to the HAP. Also note that, the uploaded data of MILP and DWP with backscatter is 48% and 45% higher than the case without backscattering, respectively. These results confirm the advantage of backscatttering as devices are able to dedicate more energy to generating samples due to the energy savings attributed to backscattering communication. On the other hand, the uploaded data of RP with backscatter is less than other approaches. Compare to MILP and DWP, RP with AmBC only slightly improves the total uploaded data in a wireless powered IoT network. This is because the HAP randomly selects devices to sample, upload or backscatter. Thus, the devices that have a large amount of sampled data may not be chosen to upload their data. Moreover, a device may exhaust its energy after sampling, meaning they are unable to upload their sample data. Both result in a low amount of uploaded data. Lastly, it shows that DWP with backscatter achieves 76.3% of the total uploaded data as compared with the optimal MILP.

The actual run-time of MILP and DWP is around 0.5s and 0.02s when the number of devices is 5. When there are 10 devices, the actual run-time for MILP and DWP is around 2s and 0.04s, respectively. However, when the number of devices is 50, MILP requires about 50s to compute a solution whilst DWP requires 0.16s run-time. This indicates that MILP becomes intractable with increasing network size, which is the motivation of developing an efficient heuristic algorithm.

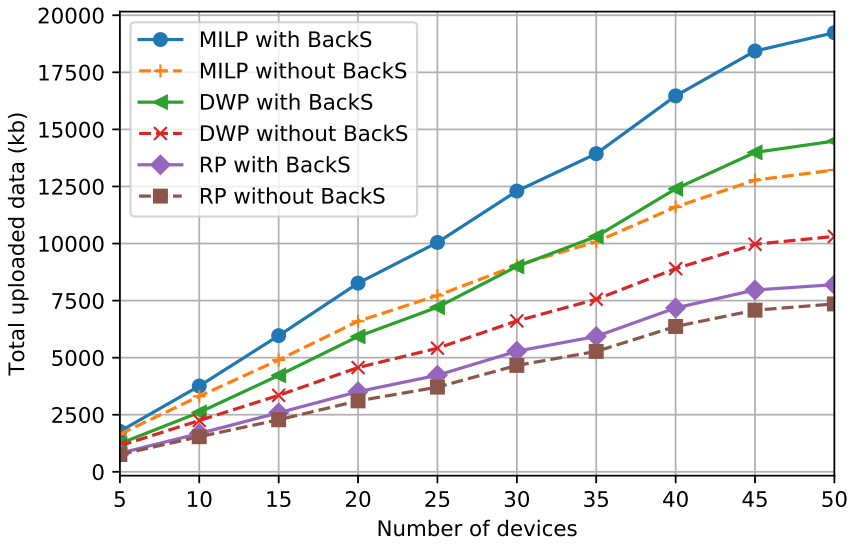

Figure 4.6: The total uploaded data versus number of devices.

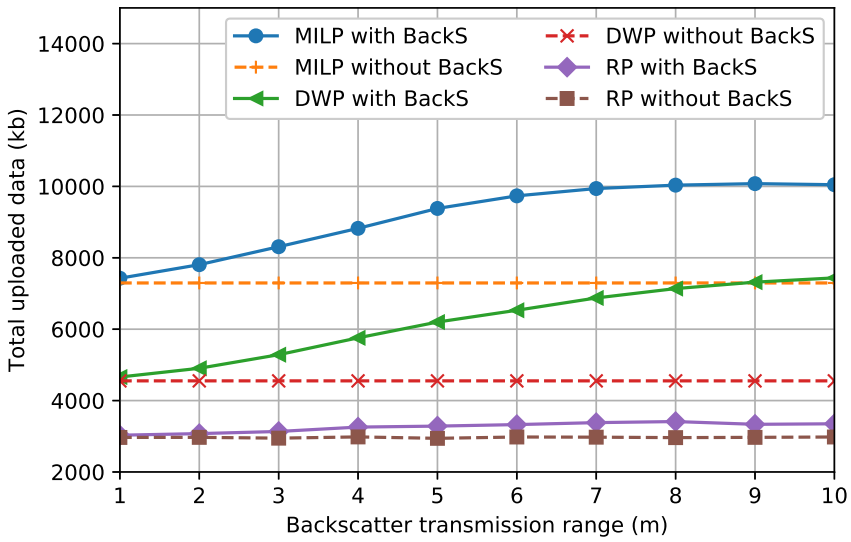

Figure 4.7: The total uploaded data versus backscatter transmission range.

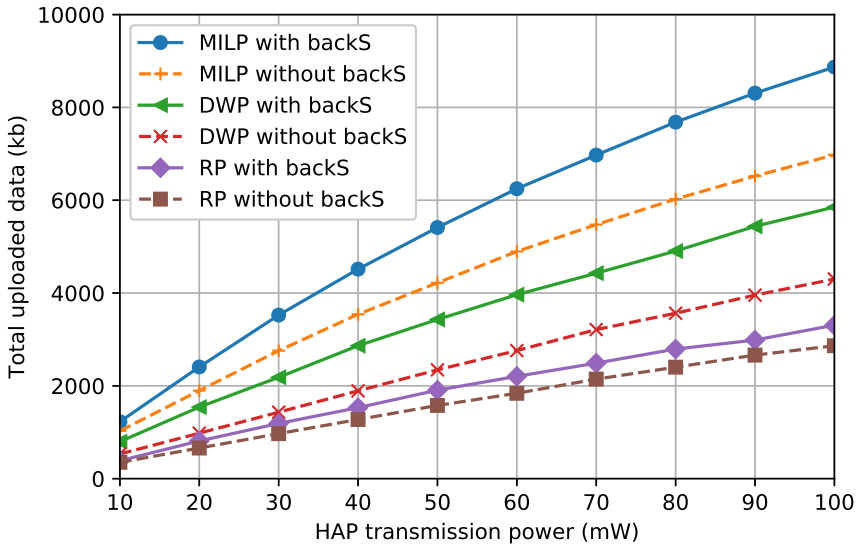

Figure 4.8: The total uploaded data versus HAP transmission power.

In the second set of experiments, the network increases the backscatter transmission range from one to ten meters with an interval of one meter. Referring to Figure 4.7, the uploaded data increased initially and then remains a constant with an increasing backscatter transmission range γ. This is because there are only a few backscattering opportunities when γ is small. Thus, most devices sample and upload their data directly to the HAP. On the other hand, with an increasing backscatter transmission range, devices are able to exploit backscatter communications. Consequently, the HAP receives more uploaded data. As shown in Figure 4.7, the uploaded data of DWP with backscatter increased by 66% when the backscatter range increased from one to eight meters. Lastly, when γ is large, i.e., $\gamma \geq 8\ m$, all devices are able to backscatter to each other. Thus, backscatter opportunities remain a constant regardless of the value of γ, and the uploaded data does not change when it further increases the backscatter transmission range.

Figure 4.8 shows the impact of the HAP's transmit power, ranging from 10 mW to 100 mW with an interval of 10 mW. It shows that the uploaded data increases dramatically for higher transmit power. The reason is because devices are able to harvest more energy, leading to more samples being collected and uploaded to the

HAP.

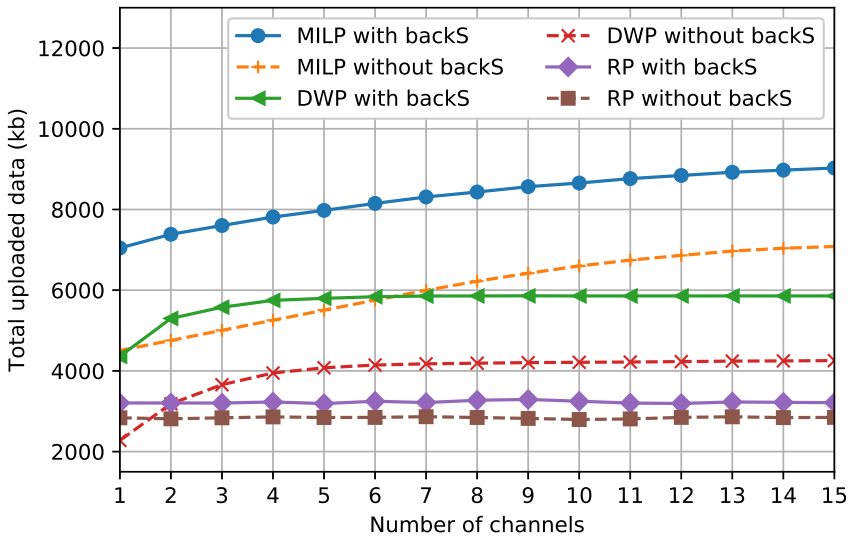

Figure 4.9: The total uploaded data versus number of channels.

Figure 4.9 shows how the total uploaded data varies when the number of channels ranges from one to 15. The total uploaded data of MILP with and without backscatter increased by 2000 kb and 2500 kb over the tested range. Similarly, the total uploaded data by DWP with and without backscatter increased by 1600 kb and 2000 kb, respectively. This is because devices have fewer chances to upload their sampled data to the HAP when the number of channels is small. However, with more channels, there is a higher upload capacity, meaning the amount of uploaded data also increases. In particular, when the number of channels is large, i.e., greater than five, devices are able to upload their data as soon as they have data. However, the total uploaded amount is bounded by their available energy. Hence, the total uploaded data only increased marginally when it increases the number of channels from ten to 15. Another observation is that the total uploaded data of RP remains unchanged when it varies the number of channels from one to 15 channels. This is because RP randomly selects devices to sample. Therefore, devices may not have sufficient data to upload and the channel is idle most of the time. Figure 4.10 demonstrates the average channel occupancy given different number of channels.

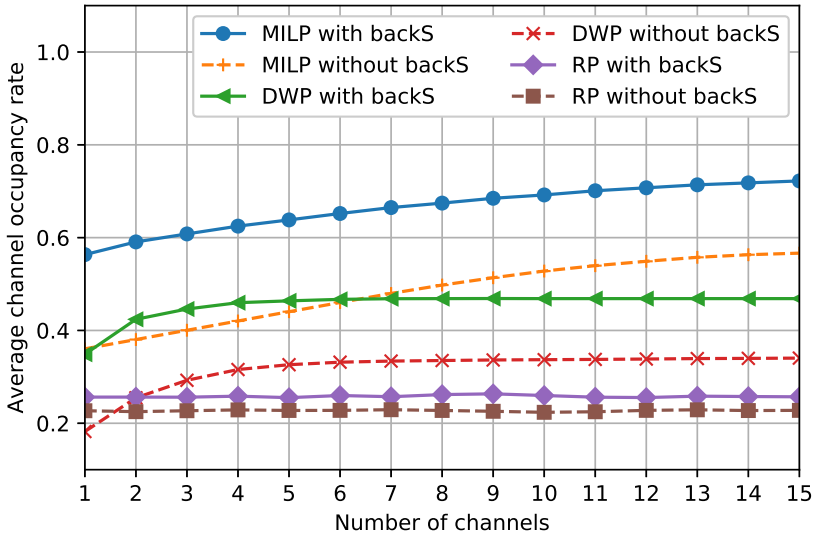

Figure 4.10: Average channel occupancy versus number of channels.

The channel occupancy shows the same increasing trend as the total uploaded data in Figure 4.9. This is reasonable as the channel occupancy is proportional to the number of devices that are uploading their data. Similarly, the total uploaded data $\hat{D}$ is a function of u_i^t according to Equ. (4.12). Moreover, it is interesting that RP outperforms DWP without AmBC when there is one or two channels. This is because devices have to wait to upload their data. Therefore, in the waiting time, devices spend a majority of their energy for sampling, meaning they do not leave sufficient energy to upload data. As for RP, given that it randomly selects devices to be placed in sample mode, a device may be left idle in a time slot. This means its energy is conserved for future use, which results in a higher amount of uploaded data than DWP without AmBC case.

The last evaluation concerns the number of upload time slots. Referring to Figure 4.11, the total uploaded data by MILP and DWP with/without backscattering first increase when there are five to 65 slots. This is because devices have a constant sample rate, meaning devices have more data to upload if they are more time slots. However, also notice that, the total uploaded data by devices remains a constant when the number of time slots is large. For instance, the total uploaded data of

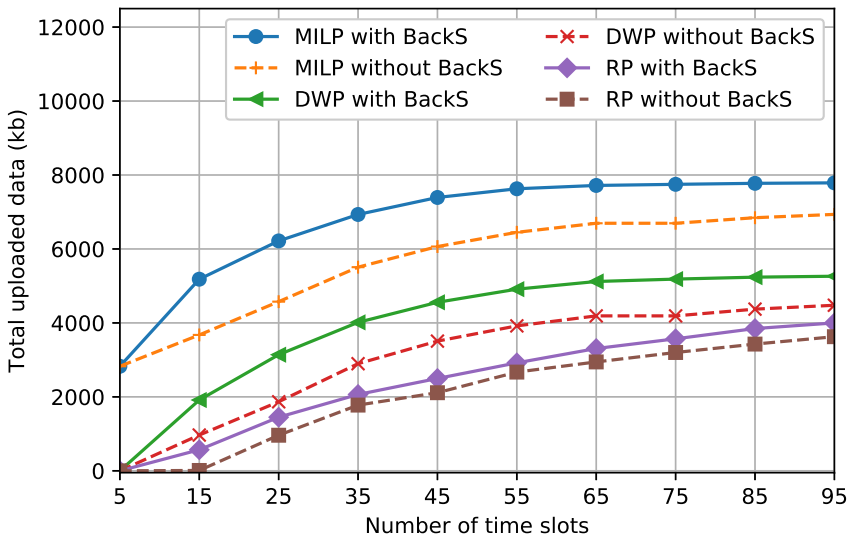

Figure 4.11: The total uploaded data versus number of time slots.

MILP with backscatter remains at 7800 kb when the number of time slots increased from 65 to 95. This is because devices have a limited amount of harvested energy. Thus, the total uploaded data does not further increase when all devices exhaust their energy. In addition, it shows that DWP with backscattering achieves 65% total uploaded data of the optimal MILP, and is 25% higher than DWP without backscattering when there are 65 time slots.

4.6 Conclusion

This chapter has outlined approaches that take advantage of AmBC to improve data collection in IoT networks. It formulates and solves the said problem as an MILP, and also present a heuristic approach to determine the operation mode of each device in each time slot over a given time horizon. Analytical and simulation results show that AmBC is able to improve the total samples uploaded to a HAP. Compared to the case without AmBC, the total data samples uploaded increased by 45% and 48% for MILP and the proposed heuristic protocol, respectively, when devices are AmBC capable.

One limitation of the work in this chapter is it only considers two-hop uplink data transmissions in IoT networks. In addition, the EHDs are hybrid devices that still can generate their own carrier signals to transmit data. To date, no works have considered data collection in a *multi-hop* IoT network with passive or batteryless tags equipped with sensor(s). In this respect, this thesis will address data sampling, link scheduling and routing in the said environment in Chapter 5.

Chapter 5

Link Scheduling for Multi-hop Backscatter IoT Wireless Networks

This chapter investigates data collection in a *multi-hop* Internet of Things (IoT) wireless network with passive or batteryless tags equipped with sensor(s). These tags forward data via tag-to-tag communications to a gateway. The aim is for the gateway to collect the maximum amount of data from tags over a given time frame. This work makes the following contributions:

- This chapter addresses a novel problem that requires a solution to jointly optimise the sensing time, the links to activate in each time slot as well as the duration of each time slot. The main challenges are ensuring all sensed data arrives at the gateway and scheduling T2T links with asymmetric transmission ranges.

- This chapter outlines a Mixed Integer Non-Linear Program (MINLP) to determine the time trade-off between sensing and transmission; this is the first mathematical formulation for the said problem. The proposed MINLP also determines the transmitter-receiver pair(s) in a transmission set as well as the transmission duration. This chapter also proposes a novel heuristic approach

that maximises the number of links in each transmission set. Its main goal is reduce samples transmission time, and thus allowing tags to have more sensing time.

The rest chapter is structured as follows. Section 5.1 shows a toy model to illustrate the research problem and challenge. Section 5.2 presents the system model and notation. Section 5.3 presents the said MINLP followed by the proposed heuristic in Section 5.4. Section 5.5 discusses the simulation methodology and results in. Section 5.6 concludes this chapter.

5.1 Toy Model

This section introduces a novel IoT network comprising of passive sensor tags; see Figure 5.1. A Hybrid Access Point (HAP) transmits a carrier signal that is then leveraged by tags to power their sampling operation and T2T communications with a gateway. Specifically, tags first use the HAP's RF signals to operate their sensors. After that, they backscatter the HAP's RF signal to forward sampled data directly to the gateway or another tag. Emphasise that unlike works in Wireless Powered Communication Networks (WPCNs), in this network, passive tags *do not* have a battery/capacitor, meaning they can only carry out tasks when the HAP emits a signal.

Given the said network, the aim is to optimise its sensing and data transmission period in order to maximise the total samples collected by the gateway subject to *all* samples arriving at the gateway within a given time frame. The major challenge is to jointly determine the number of samples to collect and the links to activate in each time slot, where interfering links must be scheduled to transmit at different times. In this respect, a key consideration is that the transmit power of each tag is different, resulting in asymmetric communication links. Therefore, it is very important to consider the neighbours of each tag when scheduling links.

To illustrate the problem at hand, consider Figure 5.1. The HAP emits RF

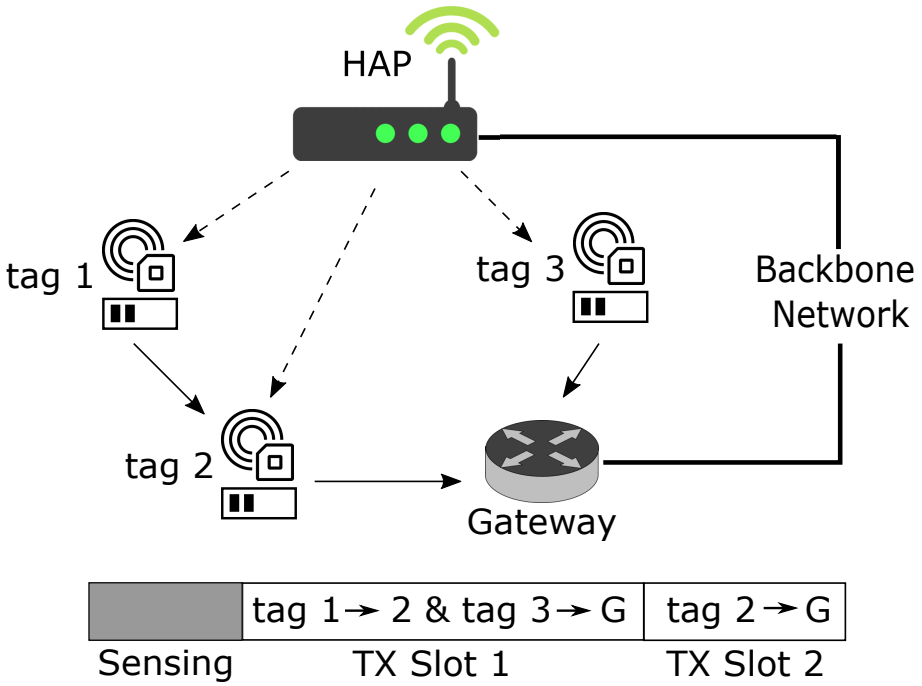

Figure 5.1: An example multi-hop backscatter IoT network.

signals (dashed arrows) in both the sensing and data transmission periods. Solid arrows represent backscattering of sensor data. Each tag has two samples after the sensing period, as indicated by the filled blocks. The schedule shows one sensing, and two data transmission periods. In this example, tag-2 and tag-3 are located within the backscatter transmission range of the gateway. Tag-1, however, cannot backscatter its samples directly to the gateway. Hence, tag-2 also works as the relay for tag-1. Thus, as shown in Figure 5.1, the HAP schedules two time slots for data transmissions. In time slot 1, the simultaneous backscatter links are $\{(\text{tag-1, tag-2}), (\text{tag-3, Gateway})\}$ and in time slot 2, the backscatter link is $\{(\text{tag-2, Gateway})\}$.

5.2 System model

Consider a wireless powered multi-hop tag-to-tag communications network with one HAP, denoted as h, a set of I tags and one gateway called s that receives data from tags. Tags have no energy storage and they are powered by the incident RF power

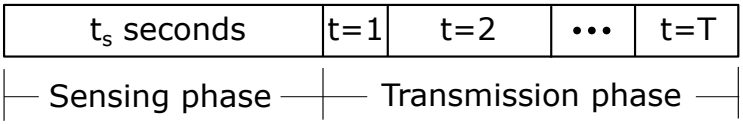

Figure 5.2: An example of a two-phase frame with a sensing and a transmission phase. The slots in the transmission phase have varying duration.

provided by the HAP. Specifically, the HAP h broadcasts RF signal to all tags, which in turn enables tags to gather and deliver sampled data to the gateway via multi-hop communications. Each tag has a built-in sensing module that enables data sensing and a backscatter transceiver for backscatter transmission and reception. Let $\mathcal{I}$ be the set of tags, which is indexed as $i \in \mathcal{I} = \{1, \ldots, I\}$.

Consider a two-phase frame with a fixed length of F seconds; see Figure 5.2. Note, if the system operates within an existing Wi-Fi network, the HAP will first send out a Clear-to-Send (CTS) message with the *Duration* field set to F seconds. It has a *sensing* phase with length t_s and a *transmission* phase with length $F - t_s$. In the *sensing* phase, the HAP h first broadcasts RF signal to all tags. This causes tags to enter sensing mode, which results in sampled data stored in the buffer of tags. In the *transmission* phase, each tag backscatters its sampled data to the gateway via multi-hop communications. There are also T transmission slots in the transmission phase. Each time slot is indexed by t, where $t \in \mathcal{T} = \{1, \ldots, T\}$. Each time slot t has duration $\hat{\tau}_t$, where the set of time slots satisfy $\sum_{t=1}^{T} \hat{\tau}_t = F - t_s$.

In each time slot t, the HAP schedules a set of links for backscatter transmissions. Define the set of links as a transmission set $\mathcal{L}(t)$ in time slot t. A transmission set contains M directed links that are activated simultaneously. Index each direction link as $m \in \{1, \ldots, M\}$. Let $(i_m, j_m)^t$ denote a directed link, i.e., transmission, from tag i_m to tag j_m in time slot t, where $i_m, j_m \in \mathcal{I}$. Therefore, $\mathcal{L}(t)$ can be represented as $\mathcal{L}(t) = \{(i_1, j_1)^t, \ldots, (i_M, j_M)^t\}$. The HAP also determines the duration $\hat{\tau}_t$ of time slot t, which is also the transmission time of set $\mathcal{L}(t)$.

5.2.1 Data sensing model

Use g_{hi} to indicate the channel coefficient between the HAP h and tag $i \in \mathcal{I}$ and it is given by [135],

$$g_{hi} = \kappa d_{hi}^{-\alpha}, \tag{5.1}$$

where d_{hi} is the distance from the HAP h to tag i, κ and α are the path loss and environment components, respectively. Hence, using (5.1), and assuming the HAP uses a transmit power of P_s, the incident RF power at tag i is,

$$\hat{p}_i = P_s \kappa d_{hi}^{-\alpha}, \tag{5.2}$$

Once the incident RF power at tag i is higher than the sensing circuit power P_c, tag i starts sampling. The sampling rate of each tag is δ kb per Joule of energy. Thus, the amount of sampled data generated by tag i during the sensing phase, denoted by $\hat{D}_i$, is thus,

$$\hat{D}_i = \delta P_s \kappa d_{hi}^{-\alpha} t_s. \tag{5.3}$$

5.2.2 Backscatter transmission model

A tag is able to transmit sampled data to another tag via backscattering. This backscattering communication is only enabled whenever there is an incident signal from the HAP [115]. As the power of the incident signal is different at each tag, the transmit power of tags is also different. When tag i is backscattering to tag j, the received power P_j at tag j is given as follows

$$P_j = \hat{p}_i \eta g_{ij}, \tag{5.4}$$

where g_{ij} is the channel coefficient between tag i and tag j as per Equ.(5.1). Let η denote the reflection coefficient [9] at each tag. Assume all tags have the same sensitivity P_{min}. Thus, P_j has to be greater than or equal to P_{min} to ensure data transmission. Therefore, it has

$$P_{min} \leq \frac{\hat{p}_i \eta \kappa}{d_{ij}^{\alpha}}, \tag{5.5}$$

where

$$d_{ij} \leq \sqrt[\alpha]{\frac{\hat{p}_i \eta \kappa}{P_{min}}}. \tag{5.6}$$

Note that, tag i can only backscatter to tag j when the distance between them is less than or equal to $\sqrt[\alpha]{\frac{\hat{p}_i \eta \kappa}{P_{min}}}$, which is defined as the backscatter communication range γ_i. Let $\mathcal{N}(i)$ contain the tags that are located within the backscatter communication range of tag i. Define $\mathcal{N}(i)$ the neighbour set of tag i. Formally,

$$\mathcal{N}(i) = \{j \mid j \in \mathcal{I}, d_{ij} \leq \gamma_i\}. \tag{5.7}$$

Therefore, tag i is able to transmit data to any tag j in its neighbour set, where $j \in \mathcal{N}(i)$, via backscattering. Under a given network topology, the incident power at each tag is a fixed value. Thus, the HAP is able to obtain the neighbour set $\mathcal{N}(i)$ for each tag i before scheduling transmissions.

Let the binary variable l_{ij}^t indicate whether link (i, j) is activated in time slot t. If $l_{ij}^t = 1$, then tag i is backscattering to tag j, and zero otherwise. Note that tags can only backscatter to or receive backscattered data from one tag at a time. Thus, it has,

$$\sum_{j \in \mathcal{N}(i)} (l_{ij}^t + l_{ji}^t) \leq 1, \quad \forall i \in \mathcal{I}, \forall t \in \mathcal{T}. \tag{5.8}$$

Let the binary variables b_i^t and r_i^t indicate whether tag i is in either of the

following modes: backscatter transmission (B-tx) or backscatter reception (B-rx). The corresponding binary indicator is set to one if a tag is in a given mode, and zero otherwise. Based on the indicator variable l_{ij}^t for link (i, j), b_i^t and r_i^t are set as follows,

$$b_i^t = \sum_{j \in \mathcal{N}(i)} l_{ij}^t, \tag{5.9}$$

and

$$r_i^t = \sum_{j \in \mathcal{N}(i)} l_{ji}^t. \tag{5.10}$$

In addition, a tag i experiences interference if any of its neighbours within $\mathcal{N}(i)$ is backscattering data. In other words, at most one tag $j \in \mathcal{N}(i)$ can backscatter at a time when $r_i^t = 1$. Formally,

$$r_i^t \sum_{j \in \mathcal{N}(i)} b_j^t \leq 1, \quad \forall i \in \mathcal{I}, \forall t \in \mathcal{T}. \tag{5.11}$$

Using (5.9) and (5.10), (5.11) can be rewritten as

$$\sum_{j \in \mathcal{N}(i)} l_{ji}^t \sum_{j \in \mathcal{N}(i)} \sum_{k \in \mathcal{N}(j)} l_{jk}^t \leq 1, \quad \forall i \in \mathcal{I}, \forall t \in \mathcal{T}. \tag{5.12}$$

5.2.3 Data storage and transmission model

Let D_i^t denote the amount of data samples in the buffer of tag i at the beginning of time slot t. Each tag has a uniform backscattering rate of R_b. Therefore, according to Equ. (5.3), D_i^t evolves as follows,

$$D_i^t = \hat{D}_i + R_b \sum_{\hat{t}=1}^{t-1} (r_i^{\hat{t}} - b_i^{\hat{t}}) \tau_{\hat{t}}, \quad \forall i \in \mathcal{I}, \forall t \in \mathcal{T}. \tag{5.13}$$

where ensuring the data buffer of tag i is non-negative. Formally,

$$0 \leq D_i^t, \quad \forall i \in \mathcal{I}, \forall t \in \mathcal{T}. \tag{5.14}$$

All data samples generated by tags are to be delivered to the gateway by the end of the transmission phase. Define l_{is}^t as the binary indicator for directed link from tag i to the gateway s, where $i \in \mathcal{N}(s)$. Note that the gateway can only receive backscattered data from one tag in a time slot. Thus, there are the following constraints,

$$\sum_{i \in \mathcal{N}(s)} l_{is}^t \leq 1, \quad \forall i \in \mathcal{I}, \forall t \in \mathcal{T}. \tag{5.15}$$

The gateway only receives data, and thus, the corresponding binary indicator r_s^t is given as follows,

$$r_s^t = \sum_{i \in \mathcal{N}(s)} l_{is}^t. \tag{5.16}$$

5.3 Problem statement and formulations

The problem is to maximise the number of sampled data collected by the gateway. To this end, this work jointly optimises (i) the time used during the sensing phase and the transmission phase, and (ii) the indicators l_{ij}^t of backscatter links to activate in each time slot and the duration of the time slot τ_t, which is also the activation time of the backscatter links.

First define D_s as the total amount of sampled data received by the gateway, which is given by,

$$D_s = R_b \sum_{t=1}^{T} r_s^t \tau_t. \tag{5.17}$$

The data transmission maximization problem is formulated as an Mixed Integer

Non-Linear Program (MINLP), which has the following objective function,

$$\max_{\{t_s, l_{ij}^t, \tau_t\}} D_s. \tag{5.18}$$

In Equ. (5.18), the aim is to maximise the total amount of sampled data transmitted to gateway s. Its decision variables are the optimal sensing time t_s, the binary indicator l_{ij}^t that shows which backscatter links to activate in each time slot as well as the activation time τ_t of these links.

The following constraints relate to the frame length, a tag's backscattering mode, data storage, multi-hop data flow and interference among tags. First, there is a constraint to ensure a frame is divided into a sensing and a transmission phase, which is given by,

$$F = t_s + \sum_{t=1}^{T} \tau_t. \tag{5.19}$$

Second, to ensure tag i can only be in either of the following modes: B-tx or B-rx, it has constraint Equ. (5.8). Third, constraint Equ. (5.14) is given that ensures the data buffer of tag i is always non-negative. Fourth, the sum of sampled data and the amount of data flows into a tag should equal to the amount of data flows out of the tag. Hence it has the following constraint,

$$\hat{D}_i + R_b \sum_{t=1}^{T} r_i^t \tau_t = R_b \sum_{t=1}^{T} b_i^t \tau_t, \quad \forall i \in \mathcal{I}. \tag{5.20}$$

Next, the following constraint is to ensure all data samples generated by tags during the sensing phase are transmitted to the gateway at the end of the transmission phase. Formally,

$$D_s = \sum_{i=1}^{I} \hat{D}_i. \tag{5.21}$$

Last, to ensure interference free transmission, there are constraints which are given

by Equ. (5.8), (4.6) and (5.15). According to Equ. (5.21), the proposed MINLP is represented as follows,

$$\max_{\{t_s, l_{ij}^t, \tau_t\}} \sum_{i=1}^{I} \hat{D}_i \tag{5.P1}$$

$$\text{s.t.} \quad (5.8), (4.6), (5.14), (5.15), (5.19), (5.20), (5.21)$$

The previous mathematical model is non-linear due to the terms $r_i^t \sum_{j\in\mathcal{N}(i)} b_j^t$, $r_i^t\tau_t$, $b_i^t\tau_t$ and $r_s^t\tau_t$ in constraints (4.6), (5.14), (5.20) and (5.21). The linearlization of the four terms is given as follows to form an MILP. Firstly, define $K_i^t = r_i^t \sum_{j\in\mathcal{N}(i)} b_j^t$, $M_i^t = r_i^t\tau_t$, $N_i^t = b_i^t\tau_t$ and $X_s^t = r_s^t\tau_t$. Therefore, constraints (4.6), (5.14), (5.20) and (5.21) are replaced respectively as follows,

$$K_i^t \leq 1, \tag{5.22}$$

$$0 \leq \hat{D}_i + R_b \sum_{\hat{t}=1}^{t-1} M_i^{\hat{t}} - R_b \sum_{\hat{t}=1}^{t-1} N_i^{\hat{t}}, \tag{5.23}$$

$$\hat{D}_i + R_b \sum_{t=1}^{T} M_i^t = R_b \sum_{t=1}^{T} N_i^t, \tag{5.24}$$

$$R_b \sum_{t=1}^{T} X_s^t = \sum_{i=1}^{I} \hat{D}_i. \tag{5.25}$$

The value of K_i^t is set as follows,

$$K_i^t \leq r_i^t I, \quad \forall i \in \mathcal{I}, \forall t \in \mathcal{T} \tag{5.26}$$

$$K_i^t \leq \sum_{j\in\mathcal{N}(i)} b_j^t, \quad \forall i \in \mathcal{I}, \forall t \in \mathcal{T} \tag{5.27}$$

$$K_i^t \geq \sum_{j\in\mathcal{N}(i)} b_j^t - (1 - r_i^t)I, \quad \forall i \in \mathcal{I}, \forall t \in \mathcal{T} \tag{5.28}$$

$$K_i^t \geq 0, \quad \forall i \in \mathcal{I}, \forall t \in \mathcal{T}, \tag{5.29}$$

where $K_i^t = \sum_{j\in\mathcal{N}(i)} b_j^t$ due to constraint (5.27) and (5.28) when $r_i^t = 1$. Besides, when $r_i^t = 0$, constraint (5.26) and (5.29) will force K_i^t to be zero. Similarly, the

value of M_i^t, N_i^t and X_s^t are given respectively as follows,

$$M_i^t \leq r_i^t F, \quad \forall i \in \mathcal{I}, \forall t \in \mathcal{T} \tag{5.30}$$

$$M_i^t \leq \tau_t, \quad \forall i \in \mathcal{I}, \forall t \in \mathcal{T} \tag{5.31}$$

$$M_i^t \geq \tau_t - (1 - r_i^t)F, \quad \forall i \in \mathcal{I}, \forall t \in \mathcal{T} \tag{5.32}$$

$$M_i^t \geq 0, \quad \forall i \in \mathcal{I}, \forall t \in \mathcal{T}, \tag{5.33}$$

$$N_i^t \leq b_i^t F, \quad \forall i \in \mathcal{I}, \forall t \in \mathcal{T} \tag{5.34}$$

$$N_i^t \leq \tau_t, \quad \forall i \in \mathcal{I}, \forall t \in \mathcal{T} \tag{5.35}$$

$$N_i^t \geq \tau_t - (1 - b_i^t)F, \quad \forall i \in \mathcal{I}, \forall t \in \mathcal{T} \tag{5.36}$$

$$N_i^t \geq 0, \quad \forall i \in \mathcal{I}, \forall t \in \mathcal{T}, \tag{5.37}$$

$$X_s^t \leq r_s^t F, \quad \forall t \in \mathcal{T} \tag{5.38}$$

$$X_s^t \leq \tau_t, \quad \forall t \in \mathcal{T} \tag{5.39}$$

$$X_s^t \geq \tau_t - (1 - r_s^t)F, \quad \forall t \in \mathcal{T} \tag{5.40}$$

$$X_s^t \geq 0, \quad \forall t \in \mathcal{T}. \tag{5.41}$$

Hence, it has the following MILP:

$$\max_{\{t_s, r_i^t, b_i^t, r_s^t, \tau_t\}} \sum_{i=1}^{I} \hat{D}_i. \tag{5.P2}$$

$$\text{s.t.} \quad (5.8), (5.15), (5.19), (5.22) - (5.41)$$

Note that the linearisation process from (5.P1) to (5.P2) has no loss of optimality. This is only mathematical manipulation. The product of a binary and a continuous variable can be linearised since the continuous variable is bounded below by zero and above by a Big M. In our case, the continuous variable is the duration

of a time slot, which is bounded by zero and a given time horizon. The previous MILP (**5.P2**) can be solved using any solvers; e.g., Gurobi [128][1]. However, it becomes computationally intractable for large problem instances. This is because in the transmission phase, the problem of determining the set of transmitting tags is equivalent to the classic NP-hard link scheduling problem [136, 137]. Specifically, assume that after the sensing phase there is a set of links with one or more samples. The problem at hand is to find the shortest link schedule such that all these links transmit their samples to their corresponding receiver. This is exactly the problem in [137]. However, unlike the work in [136, 137], the number of samples at each tag is affected by the link schedule in earlier time slots. This is because after a tag has transmitted its samples, it may receive more samples from its neighbours in later time slots. Next section presents a heuristic algorithm to determine the transmission set and duration of each time slot to optimise data collection at the gateway.

5.4 Maximum Link Scheduling (Max-L)

Max-L aims to maximise the number of simultaneous links in each time slot. This minimises the data transmission time used to send collected samples to gateway s, and allows for a longer sensing phase. Figure 5.3 depicts an overview of Max-L. It takes as inputs a constant sensing time t_0, buffer size D_i^t and neighbour set $\mathcal{N}(i)$ for each tag. It then proceeds to schedule links into each time slot; see Section 5.4.1. Max-L iteratively adds M simultaneous links into transmission set $\mathcal{L}(t)$. After that, Max-L calculates the transmission duration τ_t of time slot t according to the buffer size of backscatter transmitters in $\mathcal{L}(t)$, see Section 5.4.2. Next, Max-L updates the buffer size for all transmit-receiver pairs in $\mathcal{L}(t)$ to obtain D_i^{t+1}, see Section 5.4.3. It then repeats the previous steps for each subsequent time slot until all tags drain their buffer. Finally, given the initial sensing time and duration for each time slot, Max-L scales t_0 to t_s and τ_t to $\hat{\tau}_t$ proportionally such that $F = t_s + \sum \hat{\tau}_t$, see Section

[1]Note, Gurobi uses the branch-and-bound algorithm to solve MILP [129].

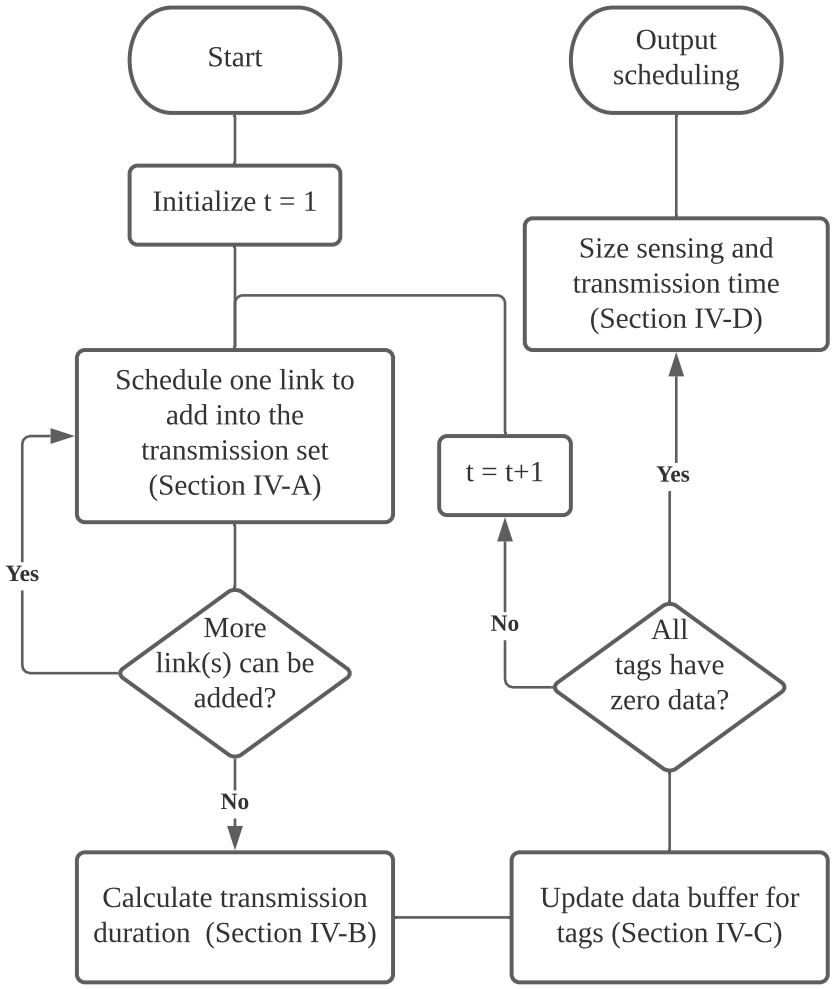

Figure 5.3: Flowchart of the proposed Max-L scheduling.

5.4.4. Max-L terminates and outputs the sensing duration, the transmission set as well as the transmission duration for each time slot.

Recall that the aim of Max-L is to optimize the trade-off between sensing and data transmission duration to acquire the maximum amount of data. At the same time, the algorithm should ensure all data is delivered to the gateway during the data transmission duration. Therefore, if a link has data, it is certainly to be scheduled for data transmission. The precedence of the scheduled links is not considered since it does not affect the data transmission duration. Furthermore, note that giving higher priority to tags with larger hop-count may not lead to more scheduled links in the next time slot. This is due to interference between scheduled links. The proposed

Max-L iteratively schedules links that interfere the least number of tags. Therefore, it maximizes the number of links in each time slot, and reduces the required time for data transmission.

5.4.1 Link Scheduling

Before outlining how Max-L selects links, this section first defines the *parent set* of each backscatter transmitter. Given the neighbour set $\mathcal{N}(i)$, the HAP determines the parents of tag i, denoted as $\mathcal{P}(i)$. Let μ_i be the number of hops from tag i to gateway s, where $\mu_s = 0$. Then it has

$$\mathcal{P}(i) = \{j \mid j \in \mathcal{N}(i), \mu_j = \mu_i - 1\}, \quad \forall i \in \mathcal{I}. \tag{5.42}$$

Note, as all nodes are connected, it has $\mathcal{P}(i) \neq \emptyset$ for each tag i in $\mathcal{I}$.

Max-L aims to construct a transmission set $\mathcal{L}(t)$ with as many links as possible. To do so, it iteratively adds one link into $\mathcal{L}(t)$. It stops when no more link could be added. A link $(i,j)^t$ cannot be added into $\mathcal{L}(t)$ if 1) tag i has no data, 2) the transmitting tag i interferes with the signal reception of any link(s) in $\mathcal{L}(t)$, or 3) at least one transmitting tag in $\mathcal{L}(t)$ interferes with the backscatter receiving at tag j.

Max-L first determines the set of tags $\hat{\mathcal{D}}^t$ with zero data at the beginning of time slot t, where

$$\hat{\mathcal{D}}^t = \{i \mid D_i^t = 0, \forall i \in \mathcal{I}\}. \tag{5.43}$$

Max-L adds the m-th link whereby the transmitter i_m is from the set $\mathcal{I} \setminus \hat{\mathcal{T}}^t(m)$, and the receiver j_m is from the set $\mathcal{P}(i_m) \setminus \hat{\mathcal{R}}^t(m)$. The set $\hat{\mathcal{T}}^t(m)$ contains all tags that have zero buffer size in time slot t as well as the tags in the neighbour set of all receiving tags in $\mathcal{L}(t)$. Thus, the tags in $\hat{\mathcal{T}}^t(m)$ cannot be scheduled as i_m. In addition, set $\hat{\mathcal{R}}^t(m)$ contains the tags in the neighbour set of all transmitting tags in $\mathcal{L}(t)$. Hence, Max-L always selects the receiving tag j_m from the parent set of i_m

and discards the tags in $\hat{\mathcal{R}}^t(m)$. The set $\hat{\mathcal{T}}^t(m)$ and $\hat{\mathcal{R}}^t(m)$ are defined as

$$\hat{\mathcal{T}}^t(m) = \begin{cases} \hat{\mathcal{D}}^t, & \text{if } m = 1, \\ \hat{\mathcal{D}}^t \cup \bigcup_{k=1}^{m-1} \mathcal{N}(j_k), & \text{if } m \geq 2, \end{cases} \tag{5.44}$$

$$\hat{\mathcal{R}}^t(m) = \begin{cases} \emptyset, & \text{if } m = 1, \\ \bigcup_{k=1}^{m-1} \mathcal{N}(i_k), & \text{if } m \geq 2. \end{cases} \tag{5.45}$$

From Equ. (5.44) and (5.45), it can be seen that $|\hat{\mathcal{T}}^t(m)|$ and $|\hat{\mathcal{R}}^t(m)|$ increase with the number of links in $\mathcal{L}(t)$. Let the m-th link in $\mathcal{L}(t)$ be $(i_m, j_m)^t$, then $|\hat{\mathcal{T}}^t(m+1)|$ and $|\hat{\mathcal{R}}^t(m+1)|$ are given as follows

$$\begin{aligned} |\hat{\mathcal{T}}^t(m+1)| &= |\hat{\mathcal{T}}^t(m)| + |\mathcal{N}(j_m) \setminus \hat{\mathcal{T}}^t(m)|, \\ |\hat{\mathcal{R}}^t(m+1)| &= |\hat{\mathcal{R}}^t(m)| + |\mathcal{N}(i_m) \setminus \hat{\mathcal{R}}^t(m)|. \end{aligned} \tag{5.46}$$

Observe that to maximise $|\mathcal{L}(t)|$, it needs to minimise $|\hat{\mathcal{T}}^t(m+1)|$ and $|\hat{\mathcal{R}}^t(m+1)|$; this gives Max-L more link choices it can select from in each time slot t. Therefore, Max-L chooses a transmitter i_m such that

$$i_m = \underset{k \in \mathcal{I} \setminus \hat{\mathcal{T}}^t(m)}{\arg\min} |\mathcal{N}(k) \setminus \hat{\mathcal{R}}^t(m)|, \tag{5.47}$$

and a receiver j_m that satisfies

$$j_m = \underset{k \in \mathcal{P}(i_m) \setminus \hat{\mathcal{R}}^t(m)}{\arg\min} |\mathcal{N}(k) \setminus \hat{\mathcal{T}}^t(m)|. \tag{5.48}$$

After that, Max-L updates transmission set $\mathcal{L}(t)$ by adding the new link $(i_m, j_m)^t$. It ends link scheduling when all M links are added into $\mathcal{L}(t)$, and thus it has $\mathcal{L}(t) = \{(i_1, j_1)^t, \ldots, (i_M, j_M)^t\}$.

5.4.2 Transmission Time

The next step is to calculate the transmission duration τ_t of transmission set $\mathcal{L}(t)$. Max-L sets τ_t to be equal to the required data transmission time for the link that carries the minimum number of samples. The reason for this is to avoid idle links; i.e., if it activates the link with the most samples instead, then links with fewer samples will complete their transmission earlier and thus remain idle until the end of the time slot.

To calculate τ_t, given the data buffer size D_i^t for all transmitting tags, where $i \in \{i_1, \ldots, i_M\}$ in $\mathcal{L}(t)$, it has

$$\tau_t = \min_{i \in \{i_1, \ldots, i_M\}} D_i^t / R_b. \tag{5.49}$$

5.4.3 Data buffer

At the end of each transmission time, Max-L updates the amount of data in each tag that belongs to $\mathcal{L}(t)$. Formally, for transmitter i_m and receiver j_m, in time slot $t+1$, they have

$$D_{i_m}^{t+1} = D_{i_m}^t - R_b \times \tau_t, \tag{5.50}$$

$$D_{j_m}^{t+1} = D_{j_m}^t + R_b \times \tau_t. \tag{5.51}$$

Note that the amount of data in tags that are neither in B-tx nor B-rx mode remain unchanged.

5.4.4 Sizing sensing and transmission time

In this last step, Max-L scales the initial sensing time t_0 to t_s and the transmission duration τ_t to $\hat{\tau}_t$ proportionally. This is to ensure that the sum of the scaled sensing time t_s and transmission time $\hat{\tau}_t$, where $t \in \{1, \ldots, T\}$, is the frame length F.

Note that sizing the sensing and transmission time does not affect the scheduled transmission set in each time slot. In particular, it has

$$t_s = t_0 \times \frac{F}{t_0 + \sum_{t=1}^{T} \tau_t}, \tag{5.52}$$

$$\hat{\tau}_t = \tau_t \times \frac{F}{t_0 + \sum_{t=1}^{T} \tau_t}, \quad \forall t \in \mathcal{T}. \tag{5.53}$$

5.4.5 Pseudocode

Algorithm 5.1 shows the details of Max-L. The inputs to Max-L are a constant sensing time, the buffer size and the neighbour set for each tag. Initially, Max-L obtains the parent set $\mathcal{P}(i)$ for each tag according to Equ. (5.42). In the first time slot, all tags have non-zero sampled data in their buffer, see line 1. Then, in each time slot, Max-L starts with the link scheduling process. It determines M simultaneous links in the transmission set; see line 4 to line 10. This process completes when no more tags can be scheduled as the transmitter or receiver, see line 5. After link scheduling, Max-L then determines the transmission time of time slot t; see line 12 and line 13. After that, Max-L updates the data buffer of all tags for the next time slot, see line 15 to line 16. It re-runs line 4 to line 18 to determine the links in all transmission sets as well as the duration of each time slot until the buffer of all tags is zero. The last step of Max-L is to size the sensing time and duration for each transmission slot so that their sum is equal to the frame length, see line 21 to line 24. Finally, Max-L outputs the sensing duration t_s, the transmission set $\{\mathcal{L}(t)\}$ as well as the duration $\{\hat{\tau}_t\}$ for each time slot.

To conclude this section, see the following proposition.

Proposition 5.1. *The run time complexity of Max-L scheduling is* $\mathcal{O}(TMI^2)$.

Proof. Max-L takes $\mathcal{O}(I)$ to determine the parent set of each tag, see line 1 in Algorithm 3.1. Next, in each time slot, it takes $\mathcal{O}(MI^2)$ to determine M simultaneous

Algorithm 5.1: Pseudocode of Max-L scheduling.

Input: t_0, $\{\hat{D}_i\}$, $\{\mathcal{N}(i)\}$
Output: t_s, $\{\hat{\tau}_t\}$, $\{\mathcal{L}(t)\}$

1 Obtain $\{\mathcal{P}(i)\}$ as per Equ. (5.42), set $t = 1$, $\hat{\mathcal{D}}^1 = \emptyset$
2 **while** $\hat{\mathcal{D}}^t \neq \mathcal{I}$ **do**
3 **** Link scheduling ****
4 Set $m = 1$, obtain i_1 and j_1 as per Equ. (5.47) and (5.48), obtain $\mathcal{L}(t) = \{l^t_{i_1 j_1}\}$, set $l^t_{i_1 j_1} = 1$
5 **while** $i_m \neq \emptyset$ *and* $j_m \neq \emptyset$ **do**
6 $m \leftarrow m + 1$
7 Obtain $\hat{\mathcal{T}}^t(m)$ and i_m as per Equ. (5.44) and (5.47)
8 Obtain $\hat{\mathcal{R}}^t(m)$ and j_m as per Equ. (5.45) and (5.48)
9 Update $\mathcal{L}(t)$ by adding $l^t_{i_m j_m}$ and set $l^t_{i_m j_m} = 1$
10 **end**
11 **** Transmission time ****
12 Set $M = m$, obtain $\{D^t_{i_m}\}, \forall m \in \{1, \ldots, M\}$
13 Calculate τ_t as per Equ. (5.49)
14 **** Data buffer ****
15 Obtain $D^{t+1}_{i_m}$ and $D^{t+1}_{j_m}$ as per Equ. (5.50) and (5.51)
16 $t \leftarrow t + 1$
17 Obtain $\hat{\mathcal{D}}^t$ as per Equ. (5.43)
18 **end**
19 Set $T = t$, obtain $\{\tau_t\}$ and $\mathcal{L}(t), \forall t \in \{1, \ldots, T\}$
20 **** Sizing sensing and transmission time ****
21 Obtain t_s as per Equ.(5.52)
22 **for** $t = 1, \ldots, T$ **do**
23 Obtain $\hat{\tau}_t$ as per Equ.(5.53)
24 **end**

links as shown from line 4 to line 10. It then takes $\mathcal{O}(M)$ to calculate the transmission time, see line 12 to line 13, and another $\mathcal{O}(2M)$ to update data buffer of both transmitting and receiving tags, see line 15 to line 18. Hence the total run time complexity of above steps for all T time slots is $\mathcal{O}(TM(I^2 + 3))$. Lastly, as shown from line 21 to line 24, Max-L takes $\mathcal{O}(T + 1)$ to size the sensing and transmission time into a frame length. Hence, the total run time complexity of Max-L scheduling is $\mathcal{O}(I + TM(I^2 + 3) + T + 1) = \mathcal{O}(TMI^2)$. □

Table 5.1: System Parameters

Parameter	**Symbol**	**Value (Unit)**
Path loss component [131]	κ	1
Environment component [131]	α	2
Frame length	F	100 (s)
HAP transmission power	P_S	100 (mW)
Sampling data generation rate [133]	δ	20 (kbpJ)
Backscatter data rate [130]	R_b	10 (kbps)
Backscatter transmission range [130]	γ_0	2 (m)
Number of tags for small-scale topologies	I	4
Number of tags for large-scale topologies	I	20

5.5 Evaluation

The simulations is conducted using Python 3.7 running on a laptop with an Intel Core i7 eight cores CPU @ 2.2GHz; see Table 5.1 for parameter values. In simulations, it is assumed each tag has a uniform backscatter communication range denoted as γ_0. Using the Gurobi [128] toolbox to solve the formulated MILP (**5.P2**). Tags and the gateway are randomly deployed on a 20×20 m^2 field. The HAP is located at the centre of the field. In each topology, it randomly places each tag within the transmission of the gateway or another tag to ensure connectivity to the gateway. The evaluation presents a comparison between the total amount of transmitted data and the number of required transmission sets used by Max-L and competing schedulers. It studies varying backscatter transmission range, number of tags and HAP transmission power. The results are an average over 1000 random topologies.

Note that the problem is new. Hence, there are no existing solutions that can be compared against fairly. To this end, a comparison of the proposed scheduler against upper and lower bound results is presented. Specifically, the upper bound is computed by relaxing the proposed MILP (**5.P2**), which is labeled as Relaxed-MILP. Specifically, it converts its binary variables b_i^t, r_i^t and r_s^t to real numbers. A called Single-link scheduler is proposed to obtain the lower bound. It randomly schedules one backscatter link in a transmission set, and sets the transmission duration to equal the time required to transmit all samples from the chosen link's transmitter.

It also compares the proposed Max-L scheduling with a random algorithm called Random scheduling. This scheduling algorithm first randomly schedules multiple backscatter links in a transmission set. If there is interference between any two selected links, the algorithm then randomly removes one link. After that, Random scheduling selects one backscatter link from the transmission set and determines the transmission time based on the data buffer of the backscatter transmitter.

5.5.1 Small random topologies

The evaluation firstly presents the total transmitted data of the proposed scheduling algorithms in small-scale random topologies with four tags. It varies the backscatter transmission range and HAP transmission power. Note, due to the complexity of the MILP, Gurobi was unable to obtain a solution when there are five tags and more.

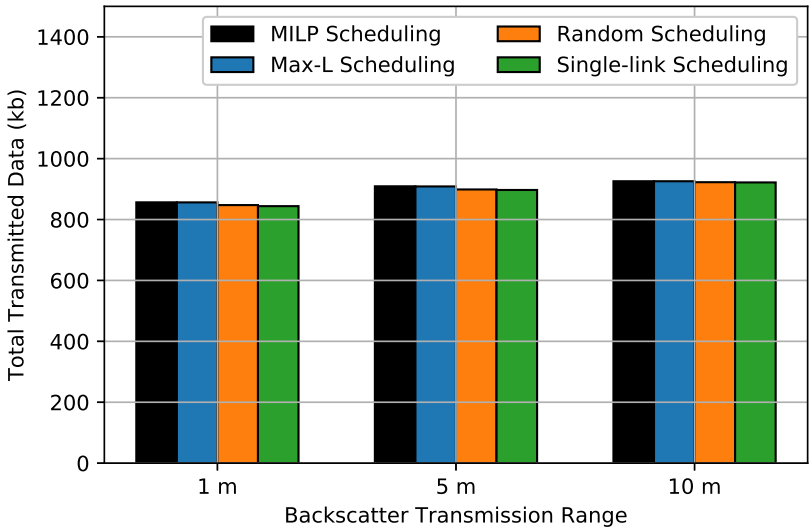

Figure 5.4: The total transmitted data versus backscatter transmission range for 4-tag small scale random topologies.

Referring to Figure 5.4 and 5.5, in both scenarios, Max-L scheduling achieves the same total transmitted data as the optimal result from MILP. Observe that Random achieves the same total transmitted data as single-link scheduling. Max-L outperforms Random and Single-link scheduling by 10 kb. This is because when the

number of tags is small, tags have small number of samples. Thus, there is little gap between the upper and lower bound of the scheduling algorithms.

As shown in Figure 5.4, when the backscatter transmission range increases from 1 to 5 meter and from 5 to 10 meter, the total transmitted data of Max-L increased by 50 kb and 20 kb, respectively. This is because with a larger backscatter transmission range, the number of hops from tags to the gateway reduces. This allows more data to be transmitted to the gateway. Note that if the backscatter transmission range continues to increase, then eventually all tags require only one hop to transmit data to the gateway, such as a star topology. In a star topology, tags upload their sampled data to the gateway in TDMA. Therefore, the total transmitted data achieved by Max-L, random and single-link scheduling equals to the optimal MILP.

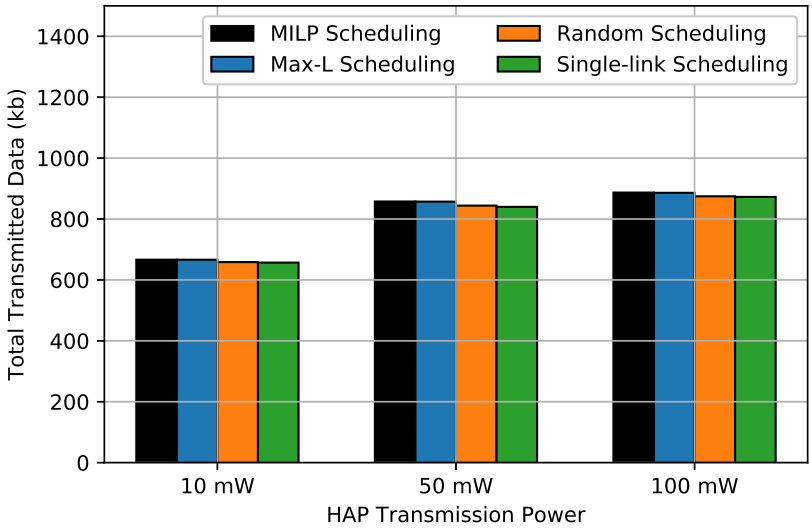

Figure 5.5: The total transmitted data versus backscatter HAP transmission power for 4-tag small scale random topologies.

Figure 5.5 shows that when the HAP transmission power increases from 10 to 50 mW and from 50 mW to 100 mW, the total transmitted data of Max-L increased by 200 kb and 30 kb, respectively. The reason is because the data sampling rate increases with the HAP transmission power, and thus, tags are able to transmit more data to the gateway with increased data transmission time. Therefore, when the HAP transmission power continues to increase, all scheduling algorithms will achieve

the maximum value in transmitted data. Note that the maximum transmitted data is limited by the backscatter transmission rate and fixed frame length.

5.5.2 Large random topologies

The next experiment evaluates the total transmitted data and the number of transmission sets under large random topologies where the network has more than 20 tags. Specifically, it conducts three experiments in terms of increasing backscatter transmission range, number of tags and HAP transmission power. It also shows a comparison against a new scheduler called Fixed Sensing (Fixed-S). Specifically, Fixed-S has a pre-determined sampling phase of $0.01 \times F$ seconds. Then in the transmission phase, it schedules backscatter links and transmission time in each slot using Random scheduling. Consequently, Fixed-S may not transmit all samples from tags to the gateway.

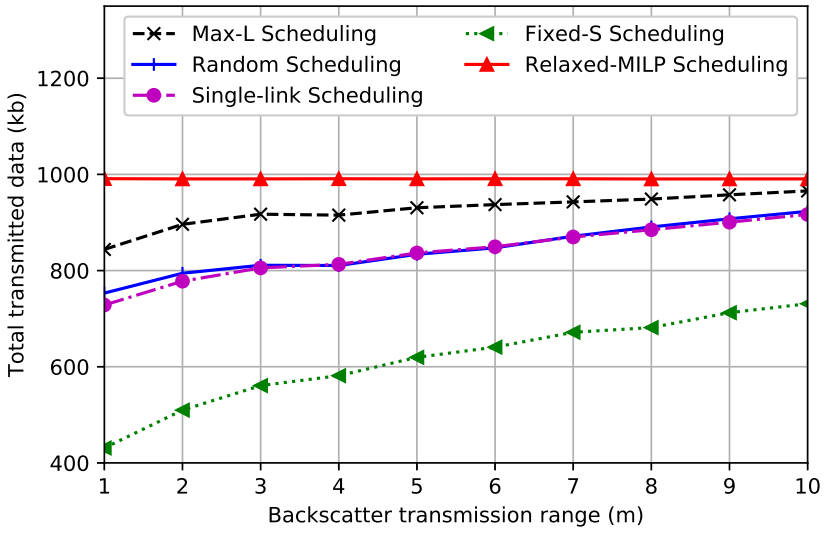

Figure 5.6: The total transmitted data versus backscatter transmission range over random topologies with 20 tags.

5.5.2.1 Varying backscatter transmission ranges

Figure 5.6 compares the total transmitted data using different scheduling algorithms over increasing backscatter transmission range. First, when the backscatter trans-

mission range is 1 meter, Max-L achieves a total transmitted data that is 85% of Relaxed-MILP. The total transmitted data of Max-L is also 12%, 15% and 64% higher than Random, Single-link and Fixed-S, respectively. Also note the gap between Random and Single-link is 30 kb when the backscatter transmission range is 1 meter. However, when the backscatter transmission range is 3 meter, the gap is only 5 kb. This is because when the backscatter transmission range is small, the interference among tags is limited. Hence, a transmission set contains more simultaneous links.

Similar to Figure 5.4, it can be observed that the total transmitted data of Max-L, Random, Single-link and Fixed-S increases with the backscatter transmission range. Specifically, the total transmitted data of Max-L Scheduling is increased by 12% and approaches the upper bound computed by Relaxed-MILP. In addition, in terms of total transmitted data, Random, Single-link and Fixed-S scheduling recorded an increase of 21%, 28% and 66% respectively. However, the total transmitted data of Relaxed-MILP scheduling remains the same at 990 kb over different backscatter transmission ranges. The reason is because when relaxing the binary indicators of B-tx and B-rx, tags are able to transmit and receive simultaneously in each time slot. Thus, a tag is able to accomplish multi-hop data flow and deliver data to the gateway in one time slot. Therefore, the backscatter transmission range does not affect the total transmitted data achieved by Relaxed-MILP.

Figure 5.7 compares the number of transmission sets over different backscatter transmission ranges. Note that Single-link has the largest number of transmission sets, which has the longest schedule among all schedulers. The reason is because it only selects one backscatter link in each transmission set. Furthermore, Max-L greedily includes as many backscatter links into each slot. Thus, Max-L achieves a shorter schedule with fewer transmission sets. However, it shows that Max-L has one more transmission set on average as compared to Random. This is because Max-L always selects the first transmitting tag that has the minimum number of neighbours. Once the tag receives data from other tags in a following slot, the

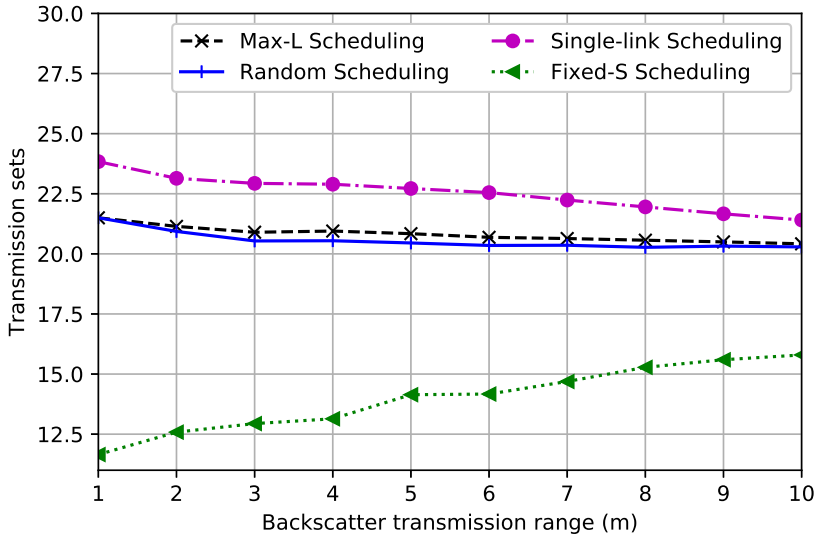

Figure 5.7: Transmission sets versus various backscatter transmission ranges over random topologies with 20 tags.

algorithm preferentially selects this tag.

From Figure 5.7, it also shows that the number of transmission sets for Max-L, Single-link and Random decreases with backscatter transmission range. Specifically, Single-link has 24 transmission sets when the backscatter transmission range is 1 meter. Besides, both Max-L and Random have 22 transmission sets. When the backscatter transmission range is 10 meters, the number of transmission sets for these scheduling algorithms is 22, 21 and 20, respectively. As explained in Section 5.5.1, when the backscatter transmission range increases, the number of hops between a tag and the gateway decreases accordingly. Hence, the number of transmission sets also decreases. It is worth mentioning that, if the backscatter transmission range continues to increase, the number of transmission sets will converge to 20.

When the backscatter transmission range increases from one to ten, on the contrary, Fixed-S has more transmission sets; it increases from 12 to 16 as shown in Figure 5.7. This is because the length of the data transmission phase is predetermined based on the value of β. When the backscatter transmission range is small, the tags located near the gateway accumulates data from the far away tags. As

a result, these tags require longer transmission time due to more sampled data in their buffer. Consequently, the transmission phase only contains a small number of transmission sets. However, when the backscatter transmission range is large, each tag is able to upload its own samples to the gateway directly. This decreases the required data transmission time for the tags that are near the gateway. Consequently, more transmission sets can be active in the transmission phase.

5.5.2.2 Varying number of tags

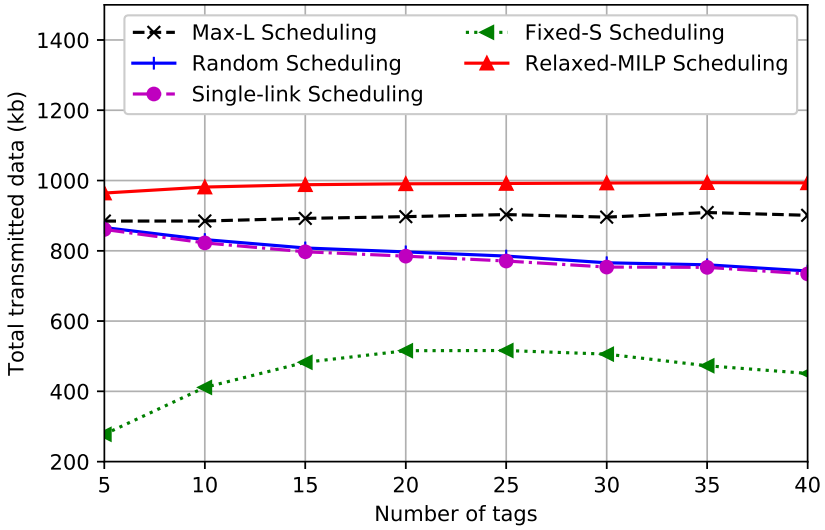

Figure 5.8: The total transmitted data versus number of tags of the proposed algorithms over random topologies.

Next, it increases the number of tags from five to 40 and investigate the total transmitted data and transmission sets. The backscatter transmission range is fixed to 2 meters. Note that when the number of tags increases, the network has a higher sampling rate. However, the required data transmission time increases with the number of tags, which yields less time for sampling. Therefore, there is a trade off between sampling rate and time. Hence, the amount of total transmitted data using Relaxed-MILP and Max-L scheduling algorithms converge to 990 and 900 kb, respectively, when there are 20 tags,

Figure 5.8 also shows that the total transmitted data of Random and Single-

link scheduling algorithms decreases with the number of tags. For example, when the number of tags increases from five to 40, the total transmitted data declined by 17%. This is because these two schedulers randomly select links in each transmission set. When the number of tags increases, these random scheduling algorithms are much less efficient in multi-hop transmission. As a result, the total transmitted data decreases with the number of tags regardless of the increased network sampling rate.

From Figure 5.8, it also shows that the total transmitted data using Fixed-S first increases from 280 to 520 kb when the number of tags increases from five to 20. It then slightly decreases from 520 to 450 kb, when the number of tags increases from 20 to 40. This is because when there is less than 20 tags, the network has a smaller amount of sampled data. Although Fixed-S is able to deliver all sampled data to the gateway, the total transmitted data is less than 520 kb. However, when the number of tags is more than 20, the network is unable to deliver all data to the gateway using Fixed-S. In addition, Fixed-S randomly schedules links in each transmission set. Hence, it is less efficient in delivering data to the gateway for larger networks. Therefore, the total transmitted data decreases with the number of tags.

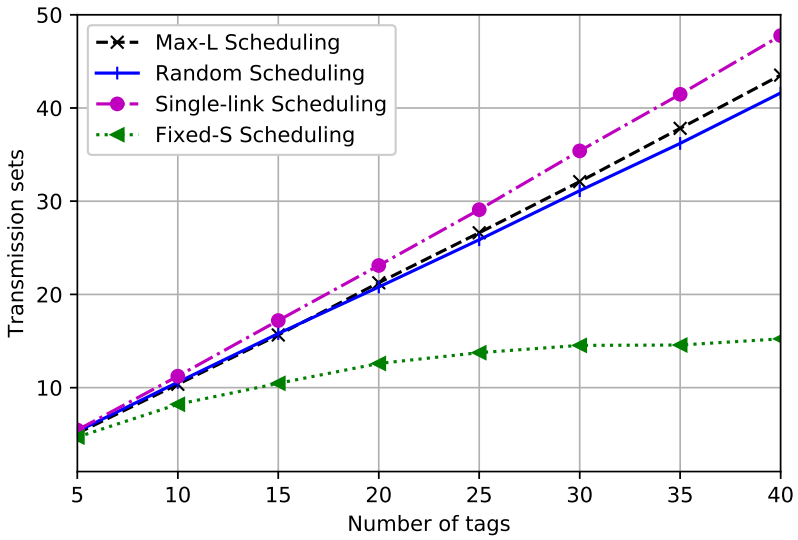

Figure 5.9: Transmission sets versus the number of tags over large-scale random topologies.

Figure 5.9 compares the number of transmission sets under different number of

tags. As it shows that the number of transmission sets increases with the number of tags. When the number of tags is less than 10, Max-L, Random and Single-link have the same number of transmission sets. This is because when number of tags is small, in most topologies, all tags are within the backscatter transmission range of the gateway. Thus, there is only one link in each transmission set. Then, when there are 40 tags, the number of transmission sets for Single-link, Max-L, Random and Fixed-S scheduling is 48, 43, 41 and 15, respectively. Similar to Figure 5.7, Single-link scheduling has the largest number of transmission sets because it uses transmission sets with only one link. In addition, note that Max-L has two more transmission sets than Random. The reason is because Max-L greedily first schedules the tag that has the minimum number of neighbours. Hence, if this tag is near the gateway, it will be scheduled in many transmission sets, to forward data for other tags.

From Figure 5.9, it also shows that Fixed-S has fewer transmission sets as compared to other algorithms. For example, when the number of tags is 40, Fixed-S only has 15 transmission sets while other algorithms have more than 40 transmission sets. This is because Fixed-S cannot deliver all sampled data from tags to the gateway. The number of transmission sets using Fixed-S first increases from five to 15. It then remains unchanged under different number of tags. This is because Fixed-S uses a constant transmission phase. As a result, the number of transmission set is determined by the number of samples at each tag. When there are only a few tags, the network requires a short transmission time to complete data transmission. Thus, the number of transmission sets first increases with the number of tags. However, due to the limited length of the transmission phase, the number of transmission sets converges to 15 when there are 30 tags.

5.5.2.3 Varying HAP transmit power

The last experiment aims to evaluate the total transmitted data and transmission sets when the HAP transmit power increases from 10 to 100 mW. Figure 5.10 com-

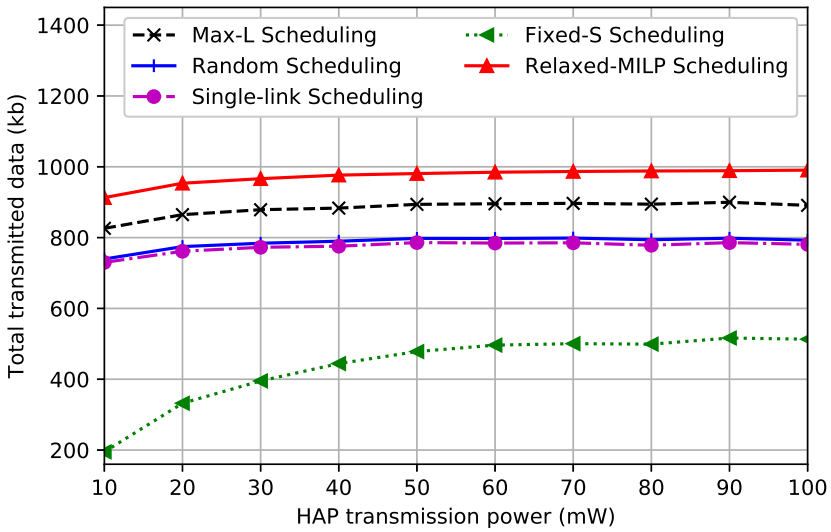

Figure 5.10: The total transmitted data versus HAP transmit power of the proposed algorithms over large-scale random topologies.

pares the total transmitted data under increasing HAP transmission power. As explained in Section 5.5.1, the total transmitted data of all scheduling algorithms increases with the HAP transmission power. Specifically, the amount of data downloaded by the gateway increased by 9%, 9%, 8%, 7% and 165% for Relaxed-MILP, Max-L, Random, Single-link and Fixed-S, respectively. Also note that when the HAP transmission power is larger than 60 mW, the total transmitted data has no further improvement for all scheduling algorithms. The reason is because although improving the HAP transmission power leads to a longer transmission time, it is still limited by the frame length F. Therefore, as it shows that, the total transmitted data of Relaxed-MILP converges to 990 kb, which is less than $R_b \times F$.

Figure 5.11 compares the number of transmission sets over different HAP transmission power. First, it shows that changing the HAP transmission power does not affect the number of transmission sets for Max-L, Random, and Single-link. This is because when the HAP has a higher transmit power, the sampled data at each tag increases accordingly. Thus, the required transmission time of each slot increases proportionally. However, the required number of transmission sets does not change with the amount of sampled data at each tag. For example, in a star topology with

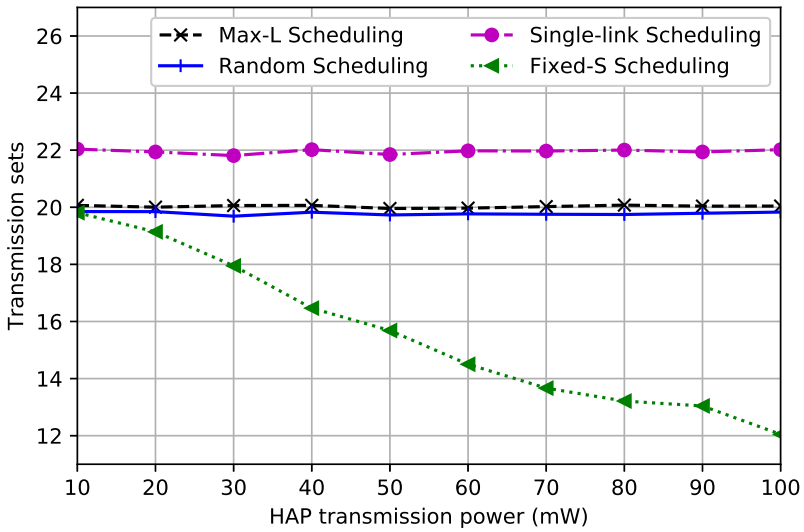

Figure 5.11: Number of transmission sets versus HAP transmission power over large-scale random topologies.

20 tags, there are 20 transmission sets since each transmission set has one tag. It also shows that the number of transmission sets for Fixed-S decreases significantly from 20 to 12 when the HAP has a higher transmit power. This is because the length of the transmission phase is predetermined based on β. When the HAP transmission power increases, a tag has more samples to transmit. Thus, the transmission time for each time slot increases accordingly, which reduces the number of transmission sets that are active in the transmission phase.

5.6 Conclusion

This chapter has considered sensing, link scheduling and routing in a novel IoT system whereby passive tags equipped with sensors are tasked with data collection and forwarding. The aim is to maximise the total sampled data collected by the tags. This chapter presents for the first time a MINLP formulation for the problem at hand. In addition, it proposes a heuristic called Max-L that maximises the number of links in each transmission set in order to reduce the required transmission time. The simulation results show that the proposed heuristic is able to achieve a total

transmitted data that is 64% higher than a single link scheduler. Furthermore, Max-L collects 85% of the optimal amount of samples.

Chapter 6

Conclusion

A challenging problem in WPCNs is to schedule uplink transmissions from multiple energy harvesting devices in order to maximise a system's sum-rate. In this respect, this thesis has investigated centralised link schedulers for uplink data transmissions in WPCNs. It takes NOMA and backscatter communications techniques into consideration to further improve system performance.

To date, in NOMA-WPCNs, no works have investigated link scheduling among energy harvesting devices to improve data collection at the HAP. Moreover, past works assume a HAP has perfect CSI to/from energy harvesting devices, and use this information to determine the optimal transmit power, transmission order or user groupings. Motivated by the lack of work on imperfect CSI, this thesis is the first to address the following research question: how to determine the optimal uplink transmission schedule for NOMA-WPCNs that yields the highest average sum-rate at the HAP, whereby the HAP has imperfect CSI?

To answer the previous research question, Chapter 3 proposes a discrete optimization approach to find the best schedule among all possible schedules. However, the number of schedules increases exponentially with the number of devices. Thus, it proposes a heuristic approach that allows the HAP to learn the best schedule iteratively. The simulation results show that both proposed solutions are able to find a

good schedule even though the HAP has imperfect CSI. Moreover, the results show that the heuristic approach is able to compute a solution for large-scale networks and has a near optimal solution as compared to the discrete optimization approach in small networks.

In backscatter assisted WPCNs, no prior works have addressed the energy trade-off between sampling and data transmissions. To this end, this thesis considers a novel AmBC assisted WPCNs, where hybrid devices have the ability to transmit data via their conventional radio or use AmBC. It takes advantage of AmBC to help sensor devices conserve energy, and thus leaving them with more energy to collect samples. Therefore, the second research problem investigates the operation mode of devices with the aim to maximise the number of samples uploaded by AmBC capable devices over multiple slots. A sub-problem is relay selection, where devices are able to forward its samples to intermediate relays using AmBC in order to maximise the number of samples. Chapter 4 formulates and solves the second research problem as an MILP. It also presents a heuristic approach called DWP to determine the operation mode of each device in each time slot over a given time horizon. Analytical and simulation results show that AmBC is able to improve the total samples uploaded to a HAP. Compared to the case without AmBC, the total data samples uploaded increased by 45% and 48% for MILP and the proposed heuristic protocol, respectively, when devices are AmBC capable.

Lastly, this thesis investigates data collection in a multi-hop T2T network, whereby passive tags equipped with sensors are tasked with data collection and forwarding to a gateway. Past works in on T2T communications mainly focus on hardware design to improve the transmission range or BER, as well as routing between two tags. However this thesis jointly considers sensing, link scheduling and routing. It proposes the third research question: how to schedule sensing and transmission time for each tag to maximise the total number of samples, while ensuring *all* samples, transmit to the gateway within a given time frame. Chapter 5 formulates for the first time a MINLP for the problem at hand. In addition, it outlines

a heuristic Max-L solution to generate transmission sets. Simulation results show that the following factors affect the amount of data collected by the gateway: (i) backscatter transmission range, (ii) number of tags, and (iii) HAP transmission power. Furthermore, simulation results show that the proposed heuristic is able to achieve a total transmitted data that is 64% higher than a single link scheduler.

In practical energy harvesting IoT sensing environment, it is always time and energy consuming to acquire the perfect channel state information. Random channel gains causes the harvested energy at IoT tags to vary. Hence. The amount of data collected by tags is always random. Therefore, a possible future work is to introduce randomness in the amount of data collected by tags. For example, using the tags to capture interesting events but the probability of an event occur is unknown. Another interest research direction is to apply modern machine learning technologies, such as deep learning and reinforcement learning, to cope with WPCNs with random environment. A major advantage of machine learning based schemes, e.g. deep neural network, is the efficient handling of data. It helps to find the rule in massive random data. For example, a machine learning based link scheduler is expected to achieve considerable performance with imperfect channel state information.

Bibliography

[1] T. Brito, A. I. Pereira, J. Lima, and A. Valente, "Wireless sensor network for ignitions detection: An IoT approach," *Electronics*, vol. 9, p. 893, May 2020.

[2] W. E. Chen, Y.-B. Lin, and L. X. Chen, "Pigtalk: an AI-based IoT platform for piglet crushing mitigation," *IEEE Trans. Ind. Informat.*, vol. 17, pp. 4345–4355, June 2021.

[3] T. Rault, A. Bouabdallah, and Y. Challal, "Energy efficiency in wireless sensor networks: A top-down survey," *Computer Networks*, vol. 67, pp. 104–122, Apr. 2014.

[4] W. R. Heinzelman, A. Chandrakasan, and H. Balakrishnan, "Energy-efficient communication protocol for wireless microsensor networks," in *33rd Annual Hawaii International Conference on System Sciences*, (Island of Maui), Jan 2000.

[5] S. Sudevalayam and P. Kulkarni, "Energy harvesting sensor nodes: survey and implications," *IEEE Commun. Surveys Tuts.*, vol. 13, pp. 443 – 461, Sept 2011.

[6] R. V. Prasad, S. Devasenapathy, V. S. Rao, and J. Vazifehdan, "Reincarnation in the ambiance: Devices and networks with energy harvesting," *IEEE Commun. Surveys Tuts.*, vol. 16, pp. 195–213, July 2014.

[7] M.-L. Ku, W. Li, Y. Chen, and K. J. R. Liu, "Advances in energy harvesting communications: Past, present, and future challenges," *IEEE Commun. Surveys Tuts.*, vol. 18, pp. 1384–1412, Nov. 2016.

[8] H. Ju and R. Zhang, "Throughput maximization for wireless powered communications networks," *IEEE Trans. Wireless Commun.*, vol. 13, no. 1, pp. 418–428, 2014.

[9] K. Han and K. Huang, "Wirelessly powered backscatter communication networks: Modeling, coverage, and capacity," *IEEE Trans. Wireless Commun.*, vol. 16, pp. 2548–2561, Apr. 2017.

[10] L. R. Varshney, "Transporting information and energy simultaneously," in *IEEE International Symposium on Information Theory*, (Toronto, Canada), pp. 1612–1616, July 2008.

[11] V. Liu, A. Parks, V. Talla, S. Gollakota, D. Wetherall, and J. R. Smith, "Ambient backscatter: wireless communication out of thin air," in *ACM SIGCOMM*, (Hong Kong, China), pp. 39–50, Aug 2013.

[12] S. M. R. Islam, N. Avazov, O. A. Dobre, and K. sup Kwak, "Power-domain non-orthogonal multiple access (NOMA) in 5G systems: Potentials and challenges," *IEEE Commun. Surveys Tuts.*, vol. 19, no. 2, pp. 721 – 742, 2017.

[13] C. R. Valenta, "Harvesting wireless power: Survey of energy-harvester conversion efficiency in far-field, wireless power transfer systems," *IEEE Microwave Magazine*, vol. 15, no. 4, pp. 108–120, 2014.

[14] X. Wei, Z. Wang, and H. Dai, "A critical review of wireless power transfer via strongly coupled magnetic resonances," *Energies*, vol. 7, pp. 4316–4341, July 2014.

[15] X. Lu, P. Wang, D. Niyato, D. I. Kim, and Z. Han, "Wireless charging tech-

nologies: Fundamentals, standards, and network applications," *IEEE Commun. Surveys Tuts.*, vol. 18, no. 2, pp. 1413–1452, 2016.

[16] S. Ho, J. Wang, W. Fu, and M. Sun, "A comparative study between novel witricity and traditional inductive magnetic coupling in wireless charging," *IEEE Trans. Magn.*, vol. 47, pp. 1522–1525, May 2011.

[17] G. A. Covic and J. T. Boys, "Inductive power transfer," *Proc. IEEE*, vol. 101, pp. 1276–1289, June 2013.

[18] T. Campi, S. Cruciani, F. Palandrani, V. De Santis, A. Hirata, and M. Feliziani, "Wireless power transfer charging system for AIMDs and pacemakers," *IEEE Trans. Microw. Theory Techn.*, vol. 64, pp. 633–642, Feb. 2016.

[19] Y. Do Chung, C. Y. Lee, D. W. Kim, H. Kang, Y. G. Park, and Y. S. Yoon, "Conceptual design and operating characteristics of multi-resonance antennas in the wireless power charging system for superconducting MAGLEV train," *IEEE Trans. Appl. Supercond.*, vol. 27, pp. 1–5, June 2017.

[20] J. H. Kim, B.-S. Lee, J.-H. Lee, S.-H. Lee, C.-B. Park, S.-M. Jung, S.-G. Lee, K.-P. Yi, and J. Baek, "Development of 1-MW inductive power transfer system for a high-speed train," *IEEE Trans. Ind. Electron.*, vol. 62, pp. 6242–6250, Oct. 2015.

[21] S. Raabe and G. A. Covic, "Practical design considerations for contactless power transfer quadrature pick-ups," *IEEE Trans. Ind. Electron.*, vol. 60, pp. 400–409, Jan. 2013.

[22] J. Shin, S. Shin, Y. Kim, S. Ahn, S. Lee, G. Jung, S.-J. Jeon, and D.-H. Cho, "Design and implementation of shaped magnetic-resonance-based wireless power transfer system for roadway-powered moving electric vehicles," *IEEE Trans. Ind. Electron.*, vol. 61, pp. 1179–1192, Mar. 2014.

[23] S. Hui, "Planar wireless charging technology for portable electronic products and Qi," *Proc. IEEE*, vol. 101, pp. 1290–1301, June 2013.

[24] T. Wang, C. Jiang, and Y. Ren, "Access points selection in super wifi network powered by solar energy harvesting," in *2016 IEEE Wireless Communications and Networking Conference*, (Doha, Qatar), pp. 1–5, Apr. 2016.

[25] A. B. Kurs, "Resonator coil," July 21 2015. US Patent D734,731.

[26] P. A. Abetti, "Wireless charging of mobile phones: Powerkiss and powermat (2007-2014)," *International Journal of Technology Management*, vol. 70, no. 2-3, pp. 218–238, 2016.

[27] P. Jung, I. Kunath, H. Petzold, and M. Stratmann, "Inductive charger for hand held appliances," May 2016. US Patent 9,337,675.

[28] P. G. Nazaroff, P. L. Shreve, A. K. Johnson, C. H. Li, and W. H. R. Lo, "Rinsing glass and charger combination for a power toothbrush," May 2016. US Patent 9,356,465.

[29] J. Smeets, T. Overboom, J. Jansen, and E. Lomonova, "Comparison of position-independent contactless energy transfer systems," *IEEE Trans. Power Electron.*, vol. 28, pp. 2059–2067, Apr. 2013.

[30] L. Xie, Y. Shi, Y. T. Hou, and A. Lou, "Wireless power transfer and applications to sensor networks," *IEEE Wireless Communications*, vol. 20, pp. 140–145, Aug. 2013.

[31] A. Mittleider, B. Griffin, and C. Detweiler, "Experimental analysis of a UAV-based wireless power transfer localization system," in *Experimental Robotics*, pp. 357–371, Springer International Publishing, 2016.

[32] X. Lu, P. Wang, D. Niyato, D. I. Kim, and Z. Han, "Wireless networks with rf energy harvesting: A contemporary survey," *IEEE Commun. Surveys Tuts.*, vol. 17, pp. 757–789, Nov. 2015.

[33] "Apple joins wireless power consortium, charging up iphone 8 rumor." AreteSolutions-http://www.aretesolutions.com.au.

[34] S. Y. R. Hui, W. Zhong, and C. K. Lee, "A critical review of recent progress in mid-range wireless power transfer," *IEEE Trans. Power Electron.*, vol. 29, pp. 4500–4511, Sept. 2014.

[35] J. M. Miller, O. C. Onar, C. White, S. Campbell, C. Coomer, L. Seiber, R. Sepe, and A. Steyerl, "Demonstrating dynamic wireless charging of an electric vehicle: The benefit of electrochemical capacitor smoothing," *IEEE Power Electronics Magazine*, vol. 1, pp. 12–24, Mar. 2014.

[36] S. Jeong, Y. J. Jang, and D. Kum, "Economic analysis of the dynamic charging electric vehicle," *IEEE Trans. Power Electron.*, vol. 30, pp. 6368–6377, Nov. 2015.

[37] S. Li and C. C. Mi, "Wireless power transfer for electric vehicle applications," *IEEE Trans. Emerg. Sel. Topics Power Electron.*, vol. 3, pp. 4–17, Mar. 2015.

[38] J. Sanz, J. Villa, J. Sallan, J. Perie, and L. G. Duarte, "UNPLUGGED project: development of a 50 kW inductive electric vehicle battery charge system," in *Electric Vehicle Symposium and Exhibition (EVS27), 2013 World*, (Barcelona, Spain), pp. 1–7, Nov. 2013.

[39] H. Ju and R. Zhang, "Throughput maximization in wireless powered communication networks," *IEEE Trans. Wireless Commun.*, vol. 13, pp. 418–428, Jan 2014.

[40] N. Van Huynh, D. T. Hoang, X. Lu, D. Niyato, P. Wang, and D. I. Kim, "Ambient backscatter communications: A contemporary survey," *IEEE Commun. Surveys Tuts.*, vol. 20, pp. 2889–2922, Fourthquarter 2018.

[41] B. Kellogg, A. Parks, S. Gollakota, J. R. Smith, and D. Wetherall, "Wi-Fi

backscatter: Internet connectivity for RF-powered devices," in *ACM SIGCOMM*, (Chicago, USA), Aug. 2014.

[42] M. Buettner, B. Greenstein, A. Sample, J. R. Smith, and D. Wetherall, "Revisiting smart dust with RFID sensor networks," in *Seventh ACM Workshop on Hot Topics in Networks (HotNets-VII)*, (Alberta, Canada), pp. 1–6, Oct. 2008.

[43] X. Lu, D. Niyato, H. Jiang, D. I. Kim, Y. Xiao, and Z. Han, "Ambient backscatter assisted wireless powered communications," *IEEE Wireless Communications*, vol. 25, pp. 170–177, Apr. 2018.

[44] P. V. Nikitin, S. Ramamurthy, R. Martinez, and K. S. Rao, "Passive tag-to-tag communication," in *IEEE Intl. Conf. on RFID*, (Orlando, USA), Apr. 2012.

[45] D. Tse and P. Viswanath, *Fundamentals of wireless communication*. Cambridge university press, 2005.

[46] Y. Saito, Y. Kishiyama, A. Benjebbour, T. Nakamura, A. Li, and K. Higuchi, "Non-orthogonal multiple access (NOMA) for cellular future radio access," in *2013 IEEE 77th vehicular technology conference (VTC Spring)*, (Dresden, Germany), pp. 1–5, June 2013.

[47] L. Dai, B. Wang, Y. Yuan, S. Han, I. Chih-Lin, and Z. Wang, "Non-orthogonal multiple access for 5G: solutions, challenges, opportunities, and future research trends," *IEEE Communications Magazine*, vol. 53, pp. 74–81, Sept. 2015.

[48] J. Yang and S. Ulukus, "Optimal packet scheduling in an energy harvesting communication system," *IEEE Trans. Commun.*, vol. 60, pp. 220–230, Jan. 2012.

[49] K. Tutuncuoglu and A. Yener, "Optimum transmission policies for battery limited energy harvesting nodes," *IEEE Trans. Wireless Commun.*, vol. 11, pp. 1180–1189, Mar. 2012.

[50] O. Ozel, K. Tutuncuoglu, J. Yang, S. Ulukus, and A. Yener, "Transmission with energy harvesting nodes in fading wireless channels: Optimal policies," *IEEE J. Sel. Areas Commun.*, vol. 29, pp. 1732–1743, Sept. 2011.

[51] F. M. Ozcelik, G. Uctu, and E. Uysal-Biyikoglu, "Minimization of transmission duration of data packets over an energy harvesting fading channel," *IEEE Commun. Lett.*, vol. 16, pp. 1968–1971, Dec. 2012.

[52] C. K. Ho and R. Zhang, "Optimal energy allocation for wireless communications with energy harvesting constraints," *IEEE Trans. Signal Process.*, vol. 60, pp. 4808–4818, Sept. 2012.

[53] P. He, L. Zhao, S. Zhou, and Z. Niu, "Recursive waterfilling for wireless links with energy harvesting transmitters," *IEEE Trans. Veh. Technol.*, vol. 63, pp. 1232–1241, Mar. 2014.

[54] P. Blasco, D. Gunduz, and M. Dohler, "A learning theoretic approach to energy harvesting communication system optimization," *IEEE Trans. on Wirel. Commun.*, vol. 12, pp. 1872–1882, Apr. 2013.

[55] Y. Xiao, Z. Han, D. Niyato, and C. Yuen, "Bayesian reinforcement learning for energy harvesting communication systems with uncertainty," in *IEEE ICC*, (London, UK), pp. 5398–5403, June 2015.

[56] A. Ortiz, H. Al-Shatri, X. Li, T. Weber, and A. Klein, "Reinforcement learning for energy harvesting point-to-point communications," in *IEEE ICC*, (Kuala Lumpur, Malaysia), pp. 1–6, May 2016.

[57] F. Iannello, O. Simeone, and U. Spagnolini, "Dynamic framed-ALOHA for energy-constrained wireless sensor networks with energy harvesting," in *IEEE GLOBECOM*, (Miami, FL, USA), pp. 1–6, Dec. 2011.

[58] F. Iannello, O. Simeone, and U. Spagnolini, "Medium access control protocols

for wireless sensor networks with energy harvesting," *IEEE Trans. Commun.*, vol. 60, pp. 1381–1389, May 2012.

[59] F. Vázquez-Gallego, J. Alonso-Zarate, and L. Alonso, "Reservation dynamic frame slotted-ALOHA for wireless M2M networks with energy harvesting," in *IEEE ICC*, (London, UK), pp. 5985–5991, June 2015.

[60] Y. L. Che, L. Duan, and R. Zhang, "Spatial throughput maximization of wireless powered communication networks," *IEEE J. Sel. Areas Commun.*, vol. 33, pp. 1534–1548, Aug. 2015.

[61] L. Liu, R. Zhang, and K.-C. Chua, "Multi-antenna wireless powered communication with energy beamforming," *IEEE Trans. on Comms.*, vol. 62, pp. 4349–4361, Dec. 2014.

[62] H. Lee, K.-J. Lee, H.-B. Kong, and I. Lee, "Sum-rate maximization for multiuser MIMO wireless powered communication networks," *IEEE Trans. Veh. Technol.*, vol. 65, pp. 9420–9424, Nov. 2016.

[63] D. Hwang, D. I. Kim, and T.-J. Lee, "Throughput maximization for multiuser MIMO wireless powered communication networks," *IEEE Trans. Veh. Technol.*, vol. 65, pp. 5743–5748, July 2016.

[64] H. Ju and R. Zhang, "User cooperation in wireless powered communication networks," in *IEEE Globecom*, (Austin, USA), pp. 1430–1435, Dec. 2014.

[65] H. Chen, Y. Li, J. L. Rebelatto, B. F. Uchoa-Filho, and B. Vucetic, "Harvest-then-cooperate: Wireless-powered cooperative communications," *IEEE Trans. Signal Process.*, vol. 63, pp. 1700–1711, Apr. 2015.

[66] K.-H. Liu and T.-L. Kung, "Performance improvement for rf energy-harvesting relays via relay selection," *IEEE Trans. Veh. Technol.*, vol. 66, pp. 8482–8494, Sept. 2017.

[67] L. P. Qian, G. Feng, and V. C. M. Leung, "Optimal transmission policies for relay communication networks with ambient energy harvesting relays," *IEEE J. Sel. Areas Commun.*, vol. 34, pp. 3754–3768, Dec. 2016.

[68] Y. Huang and B. Clerckx, "Relaying strategies for wireless-powered MIMO relay networks," *IEEE Trans. Wireless Commun.*, vol. 15, pp. 6033–6047, Sept. 2016.

[69] S. Lee, R. Zhang, and K. Huang, "Opportunistic wireless energy harvesting in cognitive radio networks," *IEEE Trans. Wireless Commun.*, vol. 12, pp. 4788–4799, Sept. 2013.

[70] D. T. Hoang, D. Niyato, P. Wang, and I. K. Dong, "Opportunistic channel access and RF energy harvesting in cognitive radio networks," *IEEE J. Sel. Areas Commun.*, vol. 32, pp. 2039–2052, Nov. 2014.

[71] D. T. Hoang, D. Niyato, P. Wang, and I. K. Dong, "Performance optimization for cooperative multiuser cognitive radio networks with RF energy harvesting capability," *IEEE Trans. Wireless Commun.*, vol. 14, pp. 3614–3629, July 2015.

[72] W. Liu, X. Zhou, S. Durrani, and P. Popovski, "Secure communication with a wireless-powered friendly jammer," *IEEE Trans. Wireless Commun.*, vol. 15, pp. 401–415, Jan. 2016.

[73] P. D. Diamantoulakis, K. N. Pappi, Z. Ding, and G. K. Karagiannidis, "Optimal design of non-orthogonal multiple access with wireless power transfer," in *IEE ICC*, (Kuala Lumpur, Malaysia), pp. 1–6, May 2016.

[74] P. D. Diamantoulakis, K. N. Pappi, Z. Ding, and G. K. Karagiannidis, "Wireless powered communications with NOMA," *IEEE Trans. Wireless Commun.*, vol. 15, pp. 8422–8436, Dec. 2016.

[75] H. Chingoska, Z. Hadzi-Velkov, I. Nikoloska, and N. Zlatanov, "Resource allocation in wireless powered communication networks with non-orthogonal multiple access," *IEEE Commun. Lett.*, vol. 5, pp. 684–687, Dec. 2016.

[76] M. A. Abd-Elmagid, A. Biason, T. ElBatt, K. G. Seddik, and M. Zorzi, "Non-orthogonal multiple access schemes in wireless powered communication networks," in *IEEE ICC*, (Paris, France), pp. 1–6, May 2017.

[77] M. M. Aboelwafa, M. A. Abd-Elmagid, A. Biason, K. G. Seddik, T. ElBatt, and M. Zorzi, "Towards optimal resource allocation in wireless powered communication networks with non-orthogonal multiple access," *Elsevier Ad Hoc Networks*, vol. 85, pp. 1–10, Mar. 2019.

[78] Y. Yuan and Z. Ding, "The application of non-orthogonal multiple access in wireless powered communication networks," in *IEEE 17th International Workshop on Signal Processing Advances in Wireless Communications (SPAWC)*, (Edinburgh, UK), pp. 1–5, July 2016.

[79] T. A. Zewde and M. C. Gursoy, "NOMA-based energy-efficient wireless powered communications," *IEEE Trans. Green Commun. Netw.*, vol. 2, pp. 679–692, Sept. 2018.

[80] Q. Wu, W. Chen, D. W. K. Ng, and R. Schober, "Spectral and energy-efficient wireless powered iot networks: NOMA or TDMA?," *IEEE Trans. on Veh. Tech.*, vol. 67, pp. 6663–6667, July 2018.

[81] M. Lei, X. Zhang, T. Zhang, L. Lei, Q. He, and D. Yuan, "Successive interference cancellation for throughput maximization in wireless powered communication networks," in *IEEE VTC*, (Montreal, QC, Canada), pp. 1–6, Sept. 2016.

[82] G. Yang, C. K. Ho, R. Zhang, and Y. L. Guan, "Throughput optimization for

massive MIMO systems powered by wireless energy transfer," *IEEE J. Sel. Areas Commun.*, vol. 33, pp. 1640–1650, Aug. 2015.

[83] Z. Chang, Z. Wang, X. Guo, Z. Han, and T. Ristaniemi, "Energy-efficient resource allocation for wireless powered massive MIMO system with imperfect CSI," *IEEE Trans. Green Commun. Netw.*, vol. 1, pp. 121–130, June 2017.

[84] E. Boshkovska, D. W. K. Ng, N. Zlatanov, A. Koelpin, and R. Schober, "Robust resource allocation for MIMO wireless powered communication networks based on a non-linear EH model," *IEEE Trans. Commun.*, vol. 65, pp. 1984–1999, May 2017.

[85] J. Zhang and G. Pan, "Outage analysis of wireless-powered relaying MIMO systems with non-linear energy harvesters and imperfect CSI," *IEEE Access*, vol. 4, pp. 7046–7053, Nov. 2016.

[86] J. Ye, H. Lei, Y. Liu, G. Pan, D. B. da Costa, Q. Ni, and Z. Ding, "Cooperative communications with wireless energy harvesting over nakagami-m fading channels," *IEEE Trans. Commun.*, vol. 65, pp. 5149–5164, Dec. 2017.

[87] Y. Wu, X. Chen, C. Yuen, and C. Zhong, "Robust resource allocation for secrecy wireless powered communication networks," *IEEE Commun. Lett.*, vol. 20, pp. 2430–2433, Dec. 2016.

[88] G. Pan, H. Lei, Y. Deng, L. Fang, J. Yang, Y. Chen, and Z. Ding, "On secrecy performance of MISO SWIPT systems with TAS and imperfect CSI," *IEEE Trans. Commun.*, vol. 64, pp. 3831 – 3843, Sept. 2016.

[89] X. Liu, Y. Gao, M. Guo, and N. Sha, "Secrecy throughput optimization for the WPCNs with non-linear EH model," *IEEE Access*, vol. 7, pp. 59477–59490, May 2019.

[90] B. Lyu, C. You, Z. Yang, and G. Gui, "The optimal control policy for rf-

powered backscatter communication networks," *IEEE Trans. Veh. Technol.*, vol. 67, pp. 2804–2808, Mar. 2018.

[91] D. Li, W. Peng, and Y.-C. Liang, "Hybrid ambient backscatter communication systems with harvest-then-transmit protocols," *IEEE Access*, vol. 6, pp. 45288–45298, Aug. 2018.

[92] X. Liu, Y. Gao, and F. Hu, "Optimal time scheduling scheme for wireless powered ambient backscatter communications in IoT networks," *IEEE Internet Things J.*, vol. 6, pp. 2264–2272, Apr. 2019.

[93] B. Lyu, Z. Yang, G. Gui, and H. Sari, "Optimal time allocation in backscatter assisted wireless powered communication networks," *Sensors*, vol. 17, p. 1258, June 2017.

[94] N.-T. Nguyen, N. Van Huynh, D. T. Hoang, D. N. Nguyen, N.-H. Nguyen, Q.-T. Nguyen, and E. Dutkiewicz, "Energy management and time scheduling for heterogeneous iot wireless-powered backscatter networks," in *IEEE International Conference on Communications (ICC)*, (Shanghai,China), pp. 1–6, May 2019.

[95] D. Li, W. Peng, and F. Hu, "Capacity of backscatter communication systems with tag selection," *IEEE Trans. Veh. Technol.*, vol. 68, pp. 10311–10314, Oct. 2019.

[96] D. Li, "Fairness-based multiuser scheduling for ambient backscatter communication systems," *IEEE Commun. Lett.*, Mar. 2020.

[97] Y. Zhang, B. Li, F. Gao, and Z. Han, "A robust design for ultra reliable ambient backscatter communication systems," *IEEE Internet Things J.*, vol. 6, pp. 8989–8999, Oct. 2019.

[98] B. Lyu, Z. Yang, G. Gui, and Y. Feng, "Wireless powered communication net-

works assisted by backscatter communication," *IEEE Access*, vol. 5, pp. 7254–7262, Mar. 2017.

[99] G. Yang, D. Yuan, Y.-C. Liang, R. Zhang, and V. C. Leung, "Optimal resource allocation in full-duplex ambient backscatter communication networks for wireless-powered IoT," *IEEE Internet Things J.*, vol. 6, pp. 2612–2625, Apr. 2019.

[100] S. H. Kim and D. I. Kim, "Hybrid backscatter communication for wireless powered communication networks," in *International Symposium on Wireless Communication Systems (ISWCS)*, (Poznan, Poland), pp. 265–269, Sept. 2016.

[101] S. H. Kim and D. I. Kim, "Hybrid backscatter communication for wireless-powered heterogeneous networks," *IEEE Trans. Wireless Commun.*, vol. 16, pp. 6557–6570, Oct. 2017.

[102] D. T. Hoang, D. Niyato, P. Wang, D. I. Kim, and L. B. Le, "Optimal data scheduling and admission control for backscatter sensor networks," *IEEE Trans. Commun.*, vol. 65, pp. 2062–2077, May 2017.

[103] D. T. Hoang, D. Niyato, P. Wang, D. I. Kim, and Z. Han, "Ambient backscatter: A new approach to improve network performance for RF-powered cognitive radio networks," *IEEE Trans. Commun.*, vol. 65, pp. 3659–3674, Sept. 2017.

[104] R. Kishore, S. Gurugopinath, P. C. Sofotasios, S. Muhaidat, and N. Al-Dhahir, "Opportunistic ambient backscatter communication in rf-powered cognitive radio networks," *IEEE Trans. Cogn. Commun. Netw.*, vol. 5, pp. 413–426, June 2019.

[105] Y. Zhuang, X. Li, H. Ji, H. Zhang, and V. C. Leung, "Optimal resource allocation for rf-powered underlay cognitive radio networks with ambient backscatter communication," *IEEE Trans. Veh. Technol.*, Dec. 2020.

[106] S. Gong, L. Gao, J. Xu, Y. Guo, D. T. Hoang, and D. Niyato, "Exploiting backscatter-aided relay communications with hybrid access model in device-to-device networks," *IEEE Trans. Cogn. Commun. Netw.*, vol. 5, pp. 835–848, Dec. 2019.

[107] S. Gong, X. Huang, J. Xu, W. Liu, P. Wang, and D. Niyato, "Backscatter relay communications powered by wireless energy beamforming," *IEEE Trans. Commun.*, vol. 66, pp. 3187–3200, July 2018.

[108] J. Xu, J. Li, S. Gong, K. Zhu, and D. Niyato, "Passive relaying game for wireless powered internet of things in backscatter-aided hybrid radio networks," *IEEE Internet Things J.*, vol. 6, pp. 8933–8944, Oct. 2019.

[109] T. T. Anh, N. C. Luong, and D. Niyato, "A deep reinforcement learning approach for backscatter-assisted relay communications," *IEEE Commun. Lett.*, vol. 10, pp. 166–169, Jan. 2021.

[110] B. Lyu, Z. Yang, H. Guo, F. Tian, and G. Gui, "Relay cooperation enhanced backscatter communication for internet-of-things," *IEEE Internet Things J.*, vol. 6, pp. 2860–2871, Apr. 2019.

[111] X. Lu, D. Niyato, H. Jiang, E. Hossain, and P. Wang, "Ambient backscatter-assisted wireless-powered relaying," *IEEE Trans. Green Commun. Netw.*, vol. 3, pp. 1087–1105, Dec. 2019.

[112] C. Yang, X. Wang, and K.-W. Chin, "On max-min throughput in backscatter-assisted wirelessly powered iot," *IEEE Internet Things J.*, vol. 7, pp. 137 – 147, Jan. 2020.

[113] J. Ryoo, J. Jian, A. Athalye, S. R. Das, and M. Stanaćević, "Design and evaluation of BTTN: A backscattering tag-to-tag network," *IEEE Internet Things J.*, vol. 5, pp. 2844–2855, Aug. 2018.

[114] A. Y. Majid, M. Jansen, G. O. Delgado, K. S. Ytidtnm, and P. Pawetczak, "Multi-hop backscatter tag-to-tag networks," in *IEEE INFOCOM*, (Paris, France), Apr. 2019.

[115] J. Zhao, W. Gong, and J. Liu, "X-tandem: Towards multi-hop backscatter communication with commodity WiFi," in *ACM Mobicom*, (New Delhi, India), Oct. 2018.

[116] H. Niu and S. Jagannathan, "A cross layer routing scheme for passive RFID tag-to-tag communication," in *IEEE LCN*, (Edmonton, Canada), Sept. 2014.

[117] C. Liu, Z. J. Haas, and Z. Tian, "On the design of multi-hop tag-to-tag routing protocol for large-scale networks of passive tags," *IEEE Open J. Commun. Soc.*, vol. 1, pp. 1035–1055, July 2020.

[118] S. Verdu, *Multiuser Detection*. Cambridge University Press, 1998.

[119] C. Song, Y. Huang, J. Zhou, J. Zhang, S. Yuan, and P. Carter, "A high-efficiency broadband rectenna for ambient wireless energy harvesting," *IEEE Trans. on Antennas Propag.*, vol. 63, pp. 3486–3495, Aug. 2015.

[120] Y. Luo, L. Pu, Y. Zhao, W. Wang, Q. Yang, and Z. Peng, "Revisiting transmission scheduling in RF energy harvesting wireless communications," in *ACM MobiHOC*, (Los Angeles, CA, USA), pp. 314–315, Feb. 2018.

[121] J. Xu and R. Zhang, "Throughput optimal policies for energy harvesting wireless transmitters with non-ideal circuit power," *IEEE J. Sel. Areas Commun.*, vol. 32, pp. 322–332, Feb. 2016.

[122] M. Lei, X. Zhang, T. Zhang, L. Lei, Q. He, and D. Yuan, "Successive interference cancellation for throughput maximization in wireless powered communication networks," in *Vehicular Technology Conference*, (Sydney, Australia), pp. 1–6, June 2017.

[123] M. Kontik and S. C. Ergen, "Scheduling in successive interference cancellation based wireless ad hoc networks," *IEEE Commun. Lett.*, vol. 19, pp. 1524–1527, Sept. 2015.

[124] S. Andradóttir, "A global search method for discrete stochastic optimization," *SIAM J. on Optim.*, vol. 6, pp. 513–530, Feb. 1996.

[125] J. Fei, K.-W. Chin, C. Yang, and M. Ros, "Charge-and-activate policies for targets monitoring in rf-harvesting sensor networks," *IEEE Transactions on Vehicular Technology*, vol. 69, pp. 7835–7846, July 2020.

[126] T. S. Rappaport *et al.*, *Wireless communications: principles and practice*, vol. 2. prentice hall PTR New Jersey, 1996.

[127] M. Elsaadany, A. Ali, and W. Hamouda, "Cellular LTE-A technologies for the future internet-of-things: Physical layer features and challenges," *IEEE Commun. Surveys Tuts.*, vol. 19, pp. 2544–2572, Fourthquarter 2017.

[128] "Gubobi official site." http://www.gurobi.com, 2019.

[129] J. Kronqvist, D. E. Bernal, A. Lundell, and I. E. Grossmann, "A review and comparison of solvers for convex MINLP," *Optimization and Engineering*, vol. 20, pp. 397–455, June 2019.

[130] D. Bharadia, K. R. Joshi, M. Kotaru, and S. Katti, "Backfi: High throughput wifi backscatter," *ACM SIGCOMM Computer Communication Review*, vol. 45, pp. 283–296, Aug. 2015.

[131] H. Sun, Y.-x. Guo, M. He, and Z. Zhong, "A dual-band rectenna using broadband yagi antenna array for ambient rf power harvesting," *IEEE Antennas Wireless Propag. Lett.*, vol. 12, pp. 918–921, July 2013.

[132] I. Mahgoub and M. Ilyas, *Sensor network protocols*. CRC press, 2018.

[133] I. Stoianov, L. Nachman, S. Madden, T. Tokmouline, and M. Csail, "Pipenet: A wireless sensor network for pipeline monitoring," in *IEEE IPSN*, (Cambridge, USA), pp. 264–273, Apr. 2007.

[134] "802.15.4-2020 - IEEE approved draft standard for low-rate wireless networks." https://standards.ieee.org/standard/802_15_4-2020.html.

[135] S. Guo, F. Wang, Y. Yang, and B. Xiao, "Energy-efficient cooperative transmission for simultaneous wireless information and power transfer in clustered wireless sensor networks," *IEEE Trans. on Commun.*, vol. 63, pp. 4405–4417, Nov. 2015.

[136] M. Andrews and M. Dinitz, "Maximizing capacity in arbitrary wireless networks in the SINR model: Complexity and game theory," in *IEEE INFOCOM*, (Rio de Janeiro, Brazil), Apr. 2009.

[137] V. Angelakis, A. Ephremides, Q. He, and D. Yuan, "Minimum-time link scheduling for emptying wireless systems: Solution characterization and algorithmic framework," *IEEE Trans. Inf. Theory*, vol. 60, pp. 1083–1100, Feb. 2014.